RL-TR-93-258, Vol I (of two)
Final Technical Report
December 1993

INVESTIGATION AND SIMULATION OF NONLINEAR PROCESSORS FOR SPREAD SPECTRUM RECEIVERS

Illinois Institute of Technology

Donald R. Ucci, William Jacklin, and Jimm Grimm

APPROVED FOR PUBLIC RELEASE; DISTRIBUTION UNLIMITED.

Rome Laboratory
Air Force Materiel Command
Griffiss Air Force Base, New York

This report has been reviewed by the Rome Laboratory Public Affairs Office (PA) and is releasable to the National Technical Information Service (NTIS). At NTIS it will be releasable to the general public, including foreign nations.

Although this report references * limited documents listed on page R-1, no limited information has been extracted.

RL-TR-93-258, Vol I (of two) has been reviewed and is approved for publication.

APPROVED:

JOHN J. PATTI
Project Engineer

FOR THE COMMANDER

JOHN A. GRANIERO
Chief Scientist for C3

If your address has changed or if you wish to be removed from the Rome Laboratory mailing list, or if the addressee is no longer employed by your organization, please notify RL (C3BB) Griffiss AFB NY 13441. This will assist us in maintaining a current mailing list.

Do not return copies of this report unless contractual obligations or notices on a specific document require that it be returned.

REPORT DOCUMENTATION PAGE

Form Approved
OMB No. 0704-0188

1. AGENCY USE ONLY (Leave Blank)	2. REPORT DATE	3. REPORT TYPE AND DATES COVERED
	December 1993	Final Feb 92 - Aug 93

4. TITLE AND SUBTITLE
INVESTIGATION AND SIMULATION OF NONLINEAR PROCESSORS FOR SPREAD SPECTRUM RECEIVERS

5. FUNDING NUMBERS
C - F30602-92-C-0039
PE - 62702F
PR - 4519
TA - 42
WU - PA

6. AUTHOR(S)
Donald R. Ucci, William Jacklin, and Jimm Grimm

7. PERFORMING ORGANIZATION NAME(S) AND ADDRESS(ES)
Illinois Institute of Technology
Electrical and Computer Engineering Department
Chicago IL 60616-3793

8. PERFORMING ORGANIZATION REPORT NUMBER
N/A

9. SPONSORING/MONITORING AGENCY NAME(S) AND ADDRESS(ES)
Rome Laboratory (C3BB)
525 Brooks Road
Griffiss AFB NY 13441-4505

10. SPONSORING/MONITORING AGENCY REPORT NUMBER
RL-TR-93-258, Vol I (of two)

11. SUPPLEMENTARY NOTES
Rome Laboratory Project Engineer: John J. Patti/C3BB/(315) 330-3615

12a. DISTRIBUTION/AVAILABILITY STATEMENT
Approved for public release; distribution unlimited.

12b. DISTRIBUTION CODE

13. ABSTRACT (Maximum 200 words)
The objective of the recent research effort was to investigate and determine the viability of utilizing Locally Optimal (LO) nonlinear processing to mitigate non-Gaussian interfering signals in a Direct Sequence (DS) SS communications system. The effort centered on the use of memoryless techniques, as well as techniques employing memory, and performance comparisons of many receiver and nonlinear processor configurations. The approach used included the analysis and evaluation of several implementation of the various nonlinear processing algorithms. The analysis included the study of well known techniques, as well as newly developed methods. Evaluation was accomplished through the development of software simulations designed to test the algorithms in various signalling scenarios. The results illustrate the tradeoffs of each nonlinear processor algorithm for use in a spread spectrum receiver. This knowledge can be used to determine the most effective processor for a given interference scenario. The work presented in this report is directly in line with the mission of Rome Laboratory (RL) to provide secure, reliable communications to the United States Air Force.

14. SUBJECT TERMS
Adaptive Filtering, Nonlinear Processing, Spread Spectrum

15. NUMBER OF PAGES
116

16. PRICE CODE

17. SECURITY CLASSIFICATION OF REPORT	18. SECURITY CLASSIFICATION OF THIS PAGE	19. SECURITY CLASSIFICATION OF ABSTRACT	20. LIMITATION OF ABSTRACT
UNCLASSIFIED	UNCLASSIFIED	UNCLASSIFIED	UL

TABLE OF CONTENTS

Volume I

1. INTRODUCTION

Most modern military communication is performed using Spread Spectrum (SS) systems techniques because of their relative robustness in jamming environments. Despite this resistance to interfering signals, SS systems can undergo performance degradation when subjected to severe jamming [Haze88, Drap89]. The primary reason for this is that, although SS techniques can provide some immunity to jammers, the reception of the SS signal is still accomplished using linear receivers. The linear receiver is only optimal in the case of Gaussian channel noise and jamming signals are, by design, non-Gaussian.

It has long been known that the optimal and quasi-optimal receivers for such scenarios are nonlinear processors [Drap85, Higb88, Midd66, Spau85]. These processors have, in the past, been difficult to implement in available hardware. Today's technology has opened a window of opportunity to solving the problem of rejecting interfering signals in such situations because of advances in high speed digital signal processors.

The objective of the recent research effort was to investigate and determine the viability of utilizing Locally Optimal (LO) nonlinear processing to mitigate non-Gaussian interfering signals in a Direct Sequence (DS) SS communications system. The effort centered on the use of memoryless techniques, as well as techniques employing memory, and performance comparisons of many receiver and nonlinear processor configurations.

The approach used included the analysis and evaluation of several implementations of the various nonlinear processing algorithms. The analysis included the study of well known techniques as well as newly developed methods. Evaluation was accomplished through the development of software simulations designed to test the algorithms in various signalling scenarios.

The results illustrate the tradeoffs of each nonlinear processor algorithm for use in a spread spectrum receiver. This knowledge can be used to determine the most effective processor for a given interference scenario. The work presented in this report is directly in line with the mission of Rome Laboratories (RL) to provide secure, reliable communications to the United States Air Force.

1.1 Problem Statement and Formulation

The design and development of a digital communications system which exhibits a low probability of error (P_e) in a variety of jamming scenarios is of paramount importance in military applications. To attain this goal, it is necessary to design a receiver which will mitigate the effects of the interference and thereby facilitate the correct demodulation of the transmitted signal. For many practical applications in which the interference is thermal (Gaussian[1]) noise, the optimum receiver is a linear processor which incorporates the use of a matched filter for signal recovery. The matched filter impulse response is:

$$h(t)=ks(T-t) \tag{1-1}$$

where $h(t)$ is the matched filter impulse response, $s(t)$ is the real transmitted signal waveform, T is the sampling time of the matched filter (equal to the period of the transmitted waveform), and k is an arbitrary constant.

Alternately, a time correlator realization of the matched filter can be used for signal recovery. The time correlator produces an output exactly equal to that of the matched filter at

---

[1] Thermal noise can be modelled using the Gaussian Probability Density Function (PDF) given by: $f_N(n)=\frac{1}{\sqrt{2\pi\sigma^2}}e^{\frac{(n-\mu)^2}{2\sigma^2}}$, where N is the Gaussian random variable, μ is the mean, and σ^2 is the variance.

the sample time T, and can be written as:

$$z=\int_0^T r(t)s(t)dt \tag{1-2}$$

where z is the output of the correlator sampled at time T, $r(t)$ is the received signal, and $s(t)$ is the transmitted signal waveform. In most digital communications systems, the received signal is sampled and discrete-time processing is used. Therefore, Eq. (1-2) becomes

$$z_m=\sum_{k=1}^{N} r_k s_{mk} \ , \quad m=1,\ldots,M \tag{1-3}$$

where z_m is the correlator output corresponding to the m^{th} possible transmitted signal, r_k is the k^{th} sample of the received signal, s_{mk} is the k^{th} sample of the m^{th} possible transmitted signal, N is the number of samples (elements) per signal vector, and M is the total number of possible signals. As may be seen, Eq. (1-3) is a linear function of the received samples, and hence is termed a *linear receiver*. Note that when the communications system employs two-dimensional signalling, the operations of Eqs. (1-1) to (1-3) must be performed on both the In-phase (I) and Quadrature (Q) channels.

In a jamming environment, however, a digital communications system that employs a linear receiver experiences a performance degradation due to the highly non-Gaussian nature of the jammer. Therefore, communications systems subjected to large jamming signals require other (nonlinear) processing methods for signal recovery. Furthermore, the receiver must be adaptive since in hostile situations the jamming statistics will often be nonstationary.

The nonlinearity needed can be derived from the likelihood function of statistical decision theory [Midd66,Spau85]. In the classical approach two methods are discussed: they are the Globally Optimal (GO) and the Locally Optimal (LO) demodulators. The GO demodulator provides more robust performance whereas the LO demodulator is much simpler to implement

[Haze88]. The former is obtained directly from the likelihood function whereas the latter is an alternate form obtained from a Taylor series approximation and yields near-optimal performance for large Jammer-to-Signal (*J/S*) ratios. The likelihood function is generated from the PDF of the incoming signal.

The memoryless two-dimensional GO demodulator decision rule is formulated in the following manner.

For a received signal vector pair $(\overline{r_I}, \overline{r_Q})$:

Choose $(\overline{s_{I_m}}, \overline{s_{Q_m}})$ which maximizes

$$z_m = \sum_{k=1}^{N} \ln\left[f_{N_I N_Q}(r_{I_k} - s_{I_{mk}}, r_{Q_k} - s_{Q_{mk}})\right] \tag{1-4}$$

where $(\overline{s_{I_m}}, \overline{s_{Q_m}})$ is the m^{th} of M possible transmitted signal vector pairs with components $(s_{I_{mk}}, s_{Q_{mk}})$, (r_{I_k}, r_{Q_k}) is the k^{th} sample pair of the received signal vector pair, $\overline{N}_I$ and $\overline{N}_Q$ are the I and Q random noise vectors, and $f_{N_I N_Q}(\cdot)$ is the noise PDF.

The memoryless two-dimensional LO demodulator is obtained from the GO demodulator through a Taylor Series expansion around the signalling point. The resulting decision rule is:

Choose $(\overline{s_{I_m}}, \overline{s_{Q_m}})$ which maximizes:

$$l_m = \sum_{k=1}^{N} \left\{ s_{I_{mk}}\, g(r_k) \cos\theta_k + s_{Q_{mk}}\, g(r_k) \sin\theta_k \right\} \tag{1-5}$$

where $r_k = \sqrt{r_{I_k}^2 + r_{Q_k}^2}$ is the envelope of the received signal sample pair, $\theta_k = \tan^{-1}\left[\frac{r_{Q_k}}{r_{I_k}}\right]$ is the phase, $f_R(r_k)$ is the received envelope PDF, and

$$g(r_k) = -\frac{\frac{d}{dr_k} f_R(r_k)}{f_R(r_k)} + \frac{1}{r_k} \qquad \text{(1-6)}$$

is the LO Memoryless Nonlinear Transform (MNT).

Both the GO and LO demodulators require knowledge of the received signal PDF. In addition, the LO demodulator uses the derivative of the received signal PDF. Thus, both receivers need a mechanism to derive (an estimate of) the PDF from the input. Historically, experimental PDFs have been estimated using histograms with bins of equal width. One modification, called the Equi-probable Bin Histogram (EBH) method [Haze88], uses bins containing equal numbers of samples.

One major drawback inherent to the histogram methods of estimating the received signal PDF is that they produce discrete approximations of the actual continuous PDF. The error associated with these approximations is further amplified by the differentiation process required to produce the LO MNT. Thus, a means of constructing a continuous estimate of the received signal PDF would be beneficial. One such method which provides a piecewise continuous approximation is the M-Interval Polynomial Approximation (MIPA) [Haze88]. However, this approximation still has discontinuities at the breakpoints where adjacent approximating polynomials meet. The Fourier Series Approximation (FSA) approach, on the other hand, provides an estimate of the PDF, using the Fourier series expansion, which is continuous throughout its entire domain.

The derivation and performance evaluation of the EBH and the FSA memoryless LO processor implementations have comprised a major portion of the recent research effort. The simulation of both memoryless methods in a standard communications system and also a spread spectrum system provided valuable insight into the LO processor's performance characteristics.

Also, the performance of FSA and EBH LO processing in a spread spectrum system was compared to the performance associated with standard histogram and MIPA processing. Finally, LO processing with memory was examined, with emphasis on the methodology incorporated in the Robust Digital Adaptive Transceiver [Drap89].

1.2 Development of the Memoryless Locally Optimal (LO) Maximum Likelihood (ML) Function for Two-Dimensional Signalling

A brief derivation of the memoryless GO and LO detectors is presented in this subsection.

Let the transmitter be a two-dimensional M-ary signal source represented by a random vector pair with an I component $\overline{S}_I$ taking on a value $\overline{s}_{I_m}$, and a Q component $\overline{S}_Q$ taking on a value $\overline{s}_{Q_m}$. Here $(\overline{s}_{I_m}, \overline{s}_{Q_m})$ represents the m^{th} of M possible signal pairs. For the received signal, the I component is $\overline{R}_I$ with value $\overline{r}_I$ and the Q component is $\overline{R}_Q$ with value $\overline{r}_Q$. Finally the interference (thermal noise and jammer) is characterized by an I component $\overline{N}_I$ having a value $\overline{n}_I$ and a Q component $\overline{N}_Q$ having a value $\overline{n}_Q$. The relationship between the transmitted and received signals is given by:

$$\overline{R}_I = \overline{S}_I + \overline{N}_I \quad , \quad \overline{R}_Q = \overline{S}_Q + \overline{N}_Q \tag{1-7}$$

The Maximum Likelihood (ML) detection algorithm at the receiver is implemented as:

Choose the possible signal pair, $(\overline{s}_{I_m}, \overline{s}_{Q_m})$, which maximizes:

$$z_m = f_{\overline{R}_I \overline{R}_Q}(\overline{r}_I, \overline{r}_Q \mid \overline{s}_{I_m}, \overline{s}_{Q_m}) \tag{1-8}$$

which is the PDF of the received signal conditioned on the m^{th} transmitted signal pair. The variable z_m is called the ML decision statistic. Using the relationship defined in Eq. (1-7) and assuming statistical independence of the signal and interference, Eq. (1-8) becomes:

$$z_m = f_{\overline{N}_I \overline{N}_Q}(\overline{r}_I - \overline{s}_{I_m}, \overline{r}_Q - \overline{s}_{Q_m}) \tag{1-9}$$

where $f_{\overline{N}_I \overline{N}_Q}(\cdot)$ is the joint interference PDF. Next, if the elements of both the I and the Q received vectors are assumed to be Independent and Identically Distributed (IID)[2], Eq. (1-9) becomes

$$z_m = \prod_{k=1}^{N} f_{N_I N_Q}(r_{I_k} - s_{I_{mk}}, r_{Q_k} - s_{Q_{mk}}) \tag{1-10}$$

where (r_{I_k}, r_{Q_k}) is the k^{th} received signal sample pair, and $(s_{I_{mk}}, s_{Q_{mk}})$ is the k^{th} sample pair of the m^{th} possible source signal. Since the logarithm is a monotonically increasing function, the natural logarithm of Eq. (1-10) is used to simplify calculations [Mels78]. This results in the GO ML decision statistic of Eq.(1-4), repeated here for convenience:

Choose $(\overline{s}_{I_m}, \overline{s}_{Q_m})$ which maximizes:

$$z_m = \sum_{k=1}^{N} \ln\left[f_{N_I N_Q}(r_{I_k} - s_{I_{mk}}, r_{Q_k} - s_{Q_{mk}})\right] \tag{1-11}$$

---

[2] The resulting GO and LO processors are memoryless due to the IID assumption.

For a large *J/S* ratio[3], a first-order two-dimensional Taylor Series expansion around the received signal point can be used to approximate the interference PDF. The expansion is valid under the assumption that the deviation of the interference from the received signal point is minimal for a large *J/S*. Also, in this case the interference PDF may be approximated by the received signal PDF, $f_{R_I R_Q}(\cdot)$. These simplifications result in the LO ML decision statistic [Illi91]:

Choose $(\overline{s}_{I_m}, \overline{s}_{Q_m})$ which maximizes:

$$l_m = -\sum_{k=1}^{N} \left\{ s_{I_m} \frac{\frac{\partial}{\partial r_{I_k}} f_{R_I R_Q}(r_{I_k}, r_{Q_k})}{f_{R_I R_Q}(r_{I_k}, r_{Q_k})} + s_{Q_m} \frac{\frac{\partial}{\partial r_{Q_k}} f_{R_I R_Q}(r_{I_k}, r_{Q_k})}{f_{R_I R_Q}(r_{I_k}, r_{Q_k})} \right\} \tag{1-12}$$

However, determination of the received signal joint PDF is a difficult process, and determination of the partial derivatives even more so. To reduce the complexity of the likelihood function, bivariate radial symmetry of the received signal PDF is assumed. Under this assumption, the received signal PDF is given by:

$$f_{R_I R_Q}(r_I, r_Q) = \begin{cases} \dfrac{f_R(r)}{2\pi r}, & 0 < \theta < 2\pi \\ 0, & \textit{elsewhere} \end{cases} \tag{1-13}$$

where $f_R(r)$ is the received envelope PDF, $r = \sqrt{r_I^2 + r_Q^2}$ is the received magnitude, and $\theta = \tan^{-1}(r_Q / r_I)$ is the received phase angle. The radial symmetry assumption is valid for

[3] A typical jammer is usually at least 20 dB greater than the transmitted signal. Therefore, for a signal environment where jammers are present, a large *J/S* assumption is valid.

interference sources of interest as they will have random phase angles. Even a constant-frequency waveform will have a vector that rotates at a uniform rate and is therefore equally likely at any angle [Higb88]. With this assumption the LO ML decision statistic of Eq. (1-12) reduces to Eqs. (1-5) and (1-6), repeated here for convenience:

Choose $(\overline{s_{I_m}}, \overline{s_{Q_m}})$ which maximizes:

$$l_m = \sum_{k=1}^{N} \left\{ s_{I_m}\, g(r_k) \cos\theta_k + s_{Q_m}\, g(r_k) \sin\theta_k \right\} \tag{1-14}$$

where

$$g(r_k) = -\frac{\frac{d}{dr_k} f_R(r_k)}{f_R(r_k)} + \frac{1}{r_k} \tag{1-15}$$

is the LO MNT.

2. MEMORYLESS LOCALLY OPTIMAL PROCESSOR ALGORITHMS

The memoryless LO receiver derived in Section 1.2 requires the PDF of the received signal to generate the LO MNT used in detection of the transmitted signal. However, in practice a priori knowledge concerning the received signal PDF is not available. Instead, an approximation must be made based on the information, usually the received signal samples, available at the receiver. This section presents two methods of estimating the required PDF.

The Equiprobable Bin Histogram (EBH) method is an extension of the traditional histogram method [Krey88] of estimating PDFs. In this method, the histogram bins are chosen to have equal probability rather than equal width as is the usual case. Thus, the width of the bins is allowed to vary, while the height of each bin is constrained so that the area under the PDF approximation is equal to one. This provides an improved resolution over the traditional histogram method in regions where there are a large number of samples.

The next method discussed is the Fourier Series Approximation (FSA) which utilizes a Fourier series to estimate the received signal PDF. This algorithm, in contrast to the EBH method, produces an approximation of the PDF which is continuous and has continuous derivatives throughout its entire domain. This is extremely useful since the LO MNT requires the derivative of the received signal PDF, and the differentiation process tends to increase the error associated with the discrete approximations generated by the histogram methods.

2.1 Equiprobable Bin Histogram (EBH)

A standard histogram has bins of equal width, and provides equal resolution over the entire range of interest. Intuitively it seems better if more resolution could be given to the intervals of data corresponding to higher probabilities. One method of achieving this is to constrain the bins to have equal probability rather than equal width. The probability of a random sample falling in a given bin is the area of the bin, so the bins must have equal area to be equiprobable. For a given data sequence this may be accomplished by assigning an equal number of samples to each bin. A histogram with these constraints is known as an Equiprobable Bin Histogram (EBH), and unlike a standard histogram, both the height *and* the width of the EBH bins vary.

An EBH is constructed by sorting the data in ascending order and assigning an equal number of data points to each bin. Figure (2-1) is a five bin (B=5) EBH for an arbitrary data sequence. The data point with the largest value in the i^{th} bin is called the i^{th} breakpoint and is denoted X_i. The zeroth breakpoint, X_0, is the minimum value of all data points. The height of each bin, Y_i, is determined from the constraints described above: the width times the height of each bin must be equal and the total area of all bins must equal one. Thus, $Y_i=(X_i-X_{i-1})/B$.

Five Bin EBH

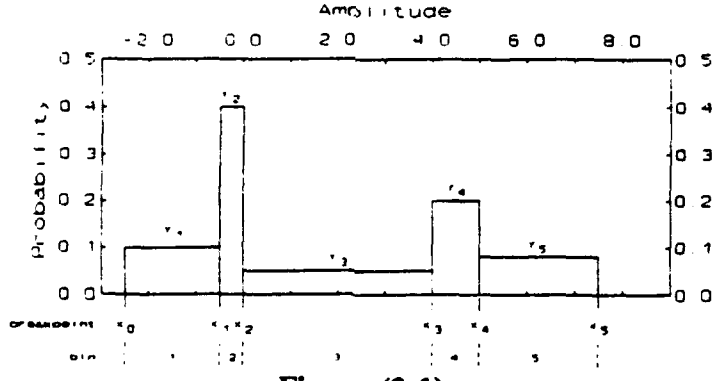

Figure (2-1)

Several examples demonstrate the differences between a standard histogram, an EBH, and the ideal PDF. A 6 dB Binary Phase Shift Keying (BPSK) signal added to 0 dB Gaussian noise is shown in Fig. (2-2). Figure (2-3) shows the corresponding 10 bin histogram and 10 bin EBH. As may be seen in the figure, both histogram methods provide an approximation that is reasonably close to the ideal PDF, represented by the smooth non-boldface line. The same analysis for a 26 dB BPSK signal added to 0 dB Gaussian noise is shown in Fig. (2-4). In this case there are two regions of high probability, namely at amplitudes of -20 and 20. It may be seen that the standard histogram gives equal resolution to the entire range of the PDF, while the EBH focuses on the areas of high probability and provides a representation that is closer to the ideal PDF.

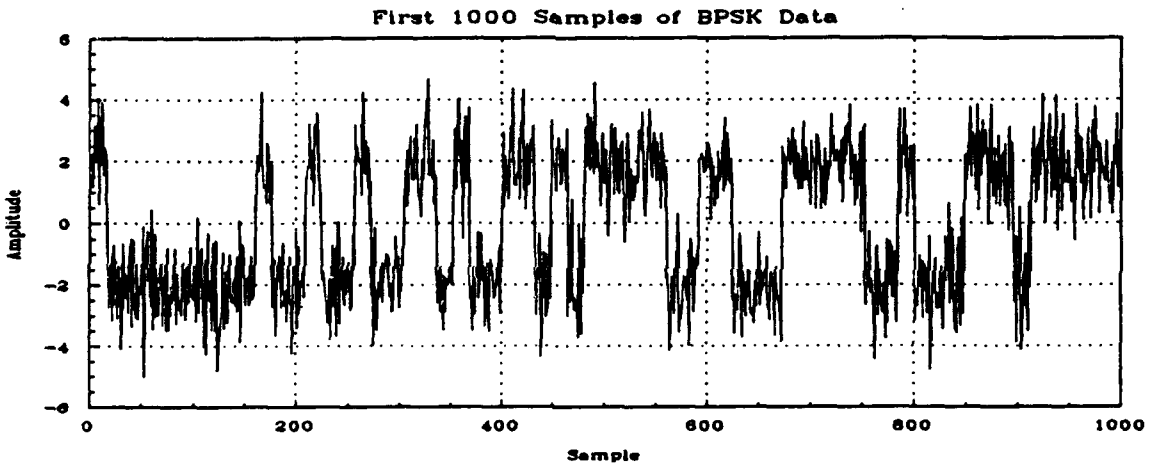

Figure (2-2)

It should be noted that the magnitude PDFs of the jamming scenarios in this report have a single region of high probability, and the performance of the EBH offers little or no improvement over the standard histogram. However, for future jamming scenarios the EBH may be of greater value.

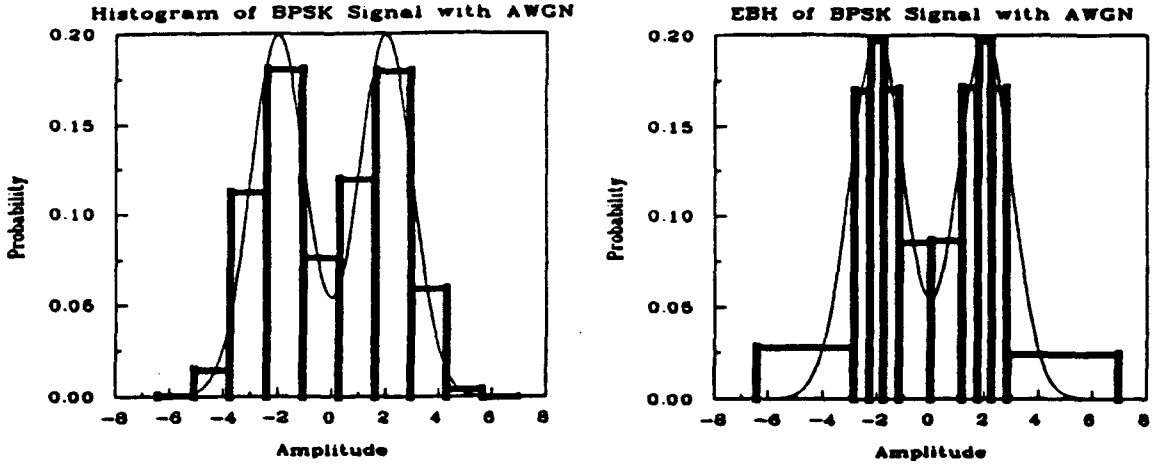

Figure (2-3)

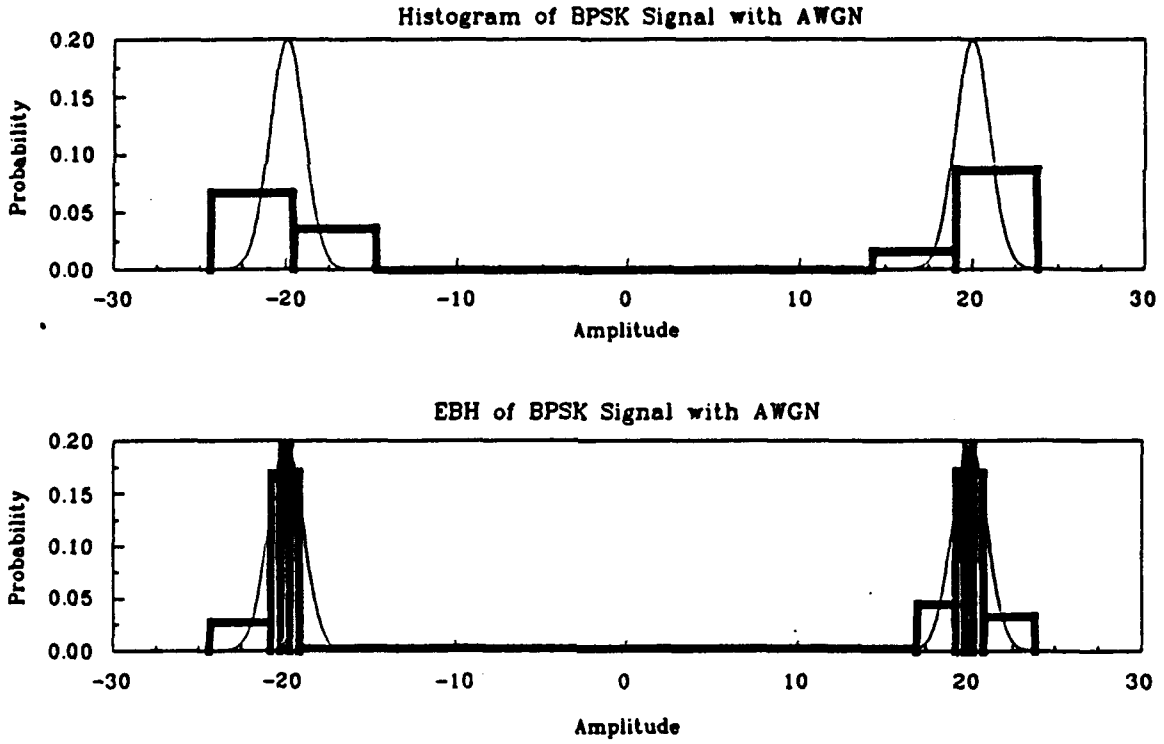

Figure (2-4)

2.2 The Fourier Series Approximation (FSA) Algorithm

A novel method of generating a *continuous* LO MNT using the Fourier series has been derived and simulated. The Fourier Series Approximation (FSA) is a method of generating a continuous estimation of the PDF of a random variable. This method is extremely useful for LO processing since the LO MNT requires the derivative of the received signal PDF, and the differentiation process amplifies the error associated with discrete histogram approximation methods. This section presents the derivation of the FSA algorithm, a method of implementation based on a histogram approach, and a direct parametric implementation of the FSA algorithm.

2.2.1 Derivation of the FSA Algorithm

Given the received signal magnitude, r, the envelope PDF, $f_R(r)$, is approximated by the following expression:

$$\hat{f}_R(r) = \frac{a_0}{2} + \sum_{n=1}^{p} a_n \cos(n\omega_0 r) + \sum_{n=1}^{p} b_n \sin(n\omega_0 r) \qquad \text{(2-1)}$$

where $\omega_0 = \dfrac{2\pi}{r_{max} - r_{min}} = \dfrac{2\pi}{T}$, r_{max} is the maximum value of the received signal set being processed, r_{min} is the minimum value of the received signal set, and p is the order of the FSA. The coefficients $\{a_n\}$ and $\{b_n\}$ are determined by minimizing the following error criterion:

$$e(r) = \int_{r_{min}}^{r_{max}} [f_R(r) - \hat{f}_R(r)]^2 dr$$
$$= \int_{r_{min}}^{r_{max}} [f_R(r) - \frac{a_0}{2} - \sum_{n=1}^{p} a_n \cos(n\omega_0 r) - \sum_{n=1}^{p} b_n \sin(n\omega_0 r)]^2 dr \quad \text{(2-2)}$$

Differentiating Eq. (2-2) with respect to a_0 and equating to zero yields the following expression:

$$\int_{r_{min}}^{r_{max}} \left[\frac{a_0}{2} + \sum_{n=1}^{p} a_n \cos(n\omega_0 r) + \sum_{n=1}^{p} b_n \sin(n\omega_0 r) \right] dr = \int_{r_{min}}^{r_{max}} f_R(r) dr \quad \text{(2-3)}$$

By noting that the integration of the sine and cosine functions over an integer multiple of their period is equal to zero and that $\int_{r_{min}}^{r_{max}} f_R(r) dr = 1$, Eq. (2-3) becomes

$$a_0 = \frac{2}{r_{max} - r_{min}} \quad \text{(2-4)}$$

To find the coefficients $\{a_n\}$, differentiation is performed with respect to a_k and the result is equated to zero. This gives the following equation:

$$\int_{r_{min}}^{r_{max}} \cos(k\omega_0 r) \left[f_R(r) - \frac{a_0}{2} - \sum_{n=1}^{p} a_n \cos(n\omega_0 r) - \sum_{n=1}^{p} b_n \sin(n\omega_0 r) \right] dr = 0 \quad \text{(2-5)}$$

After some manipulation, the expression for a_k is found to be

$$a_k = \frac{2}{r_{max} - r_{min}} \int_{r_{min}}^{r_{max}} \cos(k\omega_0 r) f_R(r) dr, \quad k = 1, \ldots, p \quad \text{(2-6)}$$

Similarly, the coefficients $\{b_n\}$ are found by differentiating Eq. (2-2) with respect to b_k and equating to zero, resulting in the expression:

$$\int_{r_{min}}^{r_{max}} \sin(k\omega_0 r)\left[f_R(r) - \frac{a_0}{2} - \sum_{n=1}^{p} a_n \cos(n\omega_0 r) - \sum_{n=1}^{p} b_n \sin(n\omega_0 r)\right] dr = 0 \qquad \textbf{(2-7)}$$

Again, after some manipulation, the expression for b_k is found to be

$$b_k = \frac{2}{r_{max} - r_{min}} \int_{r_{min}}^{r_{max}} \sin(k\omega_0 r) f_R(r) dr, \quad k = 1, \ldots, p \qquad \textbf{(2-8)}$$

Finally, the LO MNT function is given by:

$$g(r) = -\frac{\frac{d}{dr} f_R(r)}{f_R(r)} + \frac{1}{r} \qquad \textbf{(2-9)}$$

and its FSA derived estimate, $\hat{g}(r)$, is

$$\hat{g}(r) = \frac{\sum_{n=1}^{p} a_n n\omega_0 \sin(n\omega_0 r) - \sum_{n=1}^{p} b_n n\omega_0 \cos(n\omega_0 r)}{\frac{a_0}{2} + \sum_{n=1}^{p} a_n \cos(n\omega_0 r) + \sum_{n=1}^{p} b_n \sin(n\omega_0 r)} + \frac{1}{r} \qquad \textbf{(2-10)}$$

Equations (2-1), (2-4), (2-6), (2-8), and (2-10) specify the FSA algorithm completely.

2.2.2 The Histogram-based Implementation of the FSA Algorithm

One method of implementing the FSA algorithm involves using the FSA to approximate a histogram estimate of the PDF. The coefficients $\{a_n\}$ and $\{b_n\}$ are approximated by evaluating Eqs. (2-6) and (2-8) using rectangular numerical integration [Krey88], with $f_R(r)$ replaced by a

histogram approximation of the received signal envelope PDF. The resulting approximations for the FSA coefficients are:

$$\hat{a}_n = \frac{2\Delta}{r_{max} - r_{min}} \sum_{i=0}^{B-1} y_i \cos(n \frac{2\pi}{r_{max} - r_{min}} x_i) \qquad \textbf{(2-11)}$$

$$\hat{b}_n = \frac{2\Delta}{r_{max} - r_{min}} \sum_{i=0}^{B-1} y_i \sin(n \frac{2\pi}{r_{max} - r_{min}} x_i) \qquad \textbf{(2-12)}$$

where y_i is the value of the i^{th} histogram bin of the PDF, x_i is the received signal value corresponding to the i^{th} histogram bin, B is the number of histogram bins, and Δ is the bin width.

The LO MNT is then estimated using the following algorithm:

1. Let $N_1 = N_2 = D_2 = 0$ and let $D_1 = \frac{a_0}{2}$: (INITIALIZATION)

2. For $n = 1$ to p : (ITERATION)

{

$$N_1 = N_1 + \hat{a}_n n\omega_0 \sin(n\omega_0 r)$$

$$N_2 = N_2 - \hat{b}_n n\omega_0 \cos(n\omega_0 r)$$

$$D_1 = D_1 + \hat{a}_n \cos(n\omega_0 r)$$

$$D_2 = D_2 + \hat{b}_n \sin(n\omega_0 r)$$

}

3. $\hat{g}(r) = \frac{N_1 + N_2}{D_1 + D_2} + \frac{1}{r}$: (COMPUTATION)

2.2.3 Parametric Implementation of the FSA Algorithm

The expectation of a function $h(X)$ of a random variable X having a PDF $f_X(x)$ is defined as

$$E\{h(X)\} = \int_{-\infty}^{\infty} h(x) f_X(x)\, dx \tag{2-13}$$

Using this definition, Eqs. (2-6) and (2-8) may be rewritten as

$$a_n = \frac{2}{r_{max} - r_{min}} E\{\cos(n\omega_0 R)\}, \quad n=1,\ldots,p \tag{2-14}$$

and

$$b_n = \frac{2}{r_{max} - r_{min}} E\{\sin(n\omega_0 R)\}, \quad n=1,\ldots,p \tag{2-15}$$

Equations (2-14) and (2-15) can be approximated using a sample average of the form

$$a_n = \frac{2}{r_{max} - r_{min}} \frac{1}{N} \sum_{k=1}^{N} \cos(n\omega_0 r_k) \tag{2-16}$$

and

$$b_n = \frac{2}{r_{max} - r_{min}} \frac{1}{N} \sum_{k=1}^{N} \sin(n\omega_0 r_k) \tag{2-17}$$

where r_k is the k^{th} sample of the random variable R, and N is the total number of available samples.

The parametric implementation of the FSA has an advantage over the histogram-based method in that the parametric method does not require the intermediate stage of approximating

the PDF with a histogram. However, the parametric form has the disadvantage of added complexity since the sample averages of Eqs. (2-16) and (2-17) require calculation of $2Np$ trigonometric functions, where p and N can both be large.

3. SIMULATION OF THE MEMORYLESS LOCALLY OPTIMAL PROCESSOR ALGORITHMS

Software simulation was the method chosen to characterize the performance of each memoryless LO receiver implementation. For most types of jammers, determining the theoretical performance of the LO receiver is a mathematically intractable problem. Simulation provides a means of determining the types of performance gains incurred in a variety of jamming scenarios.

Two types of communications systems were simulated using the Signal Processing Worksystem™ (SPW) by Comdisco Systems, Inc. The first was a conventional Quadrature Phase Shift Keying (QPSK) communications system. This simulation was used to isolate the performance gain associated with the LO processor. The second simulation configuration was a QPSK DSSS system which was used to determine the performance characteristics of the LO processor in a spreading environment. By using both simulations, it is possible to determine scenarios in which the LO processor improves overall system performance.

This section provides an introduction and overview of the SPW simulation package. The conventional QPSK and QPSK DSSS simulations are also presented.

3.1 Introduction to the SPW Environment

The Signal Processing Worksystem™ (SPW) from Comdisco Systems, Inc. is the simulation platform of choice. It consists of several modules which aid in the different design phases of communication systems. These include: the Block Diagram Editor (BDE), the Signal Display Editor (SDE), the Filter Design System (FDS), and the Code Generation System (CGS) [Comd91].

The BDE is a graphical, block oriented environment in which communication systems can be readily implemented and simulated. Each system component is represented as a graphical block. The blocks provided in SPW are very general, allowing use in a wide variety of applications. Over 150 library blocks are provided in the BDE, including:

- modulators / demodulators such as Binary Phase Shift Keying (BPSK), Quadrature Phase Shift Keying (QPSK), and Minimum Shift Keying (MSK)
- encoders / decoders such as Hamming, Reed-Solomon, convolutional
- mathematical functions, including simple arithmetic, trigonometric, logarithmic, integration and differentiation
- filters, including Butterworth, Chebyshev, Elliptic, Bessel, and user defined filters.
- vector functions, such as inner products, serial-to-parallel and parallel-to-serial conversions
- signal sources / sinks, including binary sources, white noise generators, pseudo-random number generators, and user defined sources.

In addition to these blocks, the user may define new blocks, either through a hierarchical combination of existing blocks or by designing custom coded blocks in Fortran or the C Programming Language (C).

The SDE can be used to generate signals for use in the BDE, or to examine the simulation results from a system that has been successfully modeled and simulated in the BDE. The major strength of the SDE lies in its signal analysis capabilities. In particular, the following

functions are available: Fast Fourier Transforms (FFTs), histograms, autocorrelation and cross-correlation analysis, and spectral density evaluation. Also, signals may be directly modified by a host of operations. For example, addition, scaling, inversion, differentiation, integration, and trigonometric functions may be performed on a signal or group of signals. In addition, several nonlinear filtering operations are provided, including quantizing, clipping, and limiting.

The FDS allows the designer to model and study many different types of digital filters for use in communication systems. Any Finite Impulse Response (FIR) or Infinite Impulse Response (IIR) filter can be designed. Butterworth, Chebyshev, Elliptic, Equiripple, and Bessel filters may be easily implemented with the aid of pre-defined "methods". In addition, the user can define methods for any other type of filter. Once a filter is modeled with the FDS it can be used in the BDE or SDE.

The CGS is able to convert the BDE simulations to C code. This code can then be downloaded to any of the digital signal processing boards or computers supported by SPW.

3.1.1 Classification of Blocks

The blocks in the BDE may be classified into three categories: SPW primitive and hierarchical library blocks, user custom coded primitive blocks, and user hierarchical blocks. Library blocks are the blocks supplied as a part of the SPW environment. Some library blocks are *primitive*, in that their specification is directly linked to the underlying software code (e.g C). Others are *hierarchical*, meaning that they are composed of other SPW library blocks which may be either primitive or hierarchical. A hierarchical block is specified by means of a "detail"[1] which displays the interconnection of its constituent blocks. User custom coded

[1] Words enclosed in quotes ("") refer to SPW terminology.

primitive blocks are written by the user in C or Fortran and linked to a graphical symbol. User hierarchical blocks are made up of library, custom coded, or other user hierarchical blocks. As may be seen, the capacity to create multiple levels of hierarchy provides an extremely powerful and flexible simulation environment.

Figure (3-1a) shows the symbol for a user custom coded primitive bubble sort block, and Fig. (3-1b) shows its detail. The detail of this block is a list of parameters that are passed to the C or Fortran code when the system is simulated. Once the block is complete, the SPW user need not be concerned with the actual C or Fortran code.

Figure (3-2a) shows the symbol for a user hierarchical MNT block, the detail of which is displayed in Fig. (3-2b). The inputs and outputs of the symbol in Fig. (3-2a) correspond to "ports" in the detail in Fig. (3-2b). The ports must have the same names as the inputs and outputs, but need not be in the same position. Note that in addition to the parameter list, other blocks are included in the detail. This is the characteristic difference between hierarchical and primitive blocks.

The concept of hierarchy is very useful in system design, and is an integral part of the BDE. On the top level of the hierarchy is the system to be simulated. The system consists of several blocks. These blocks may contain sub-systems (hierarchical blocks), which are a lower level of hierarchy. At the lowest level of the hierarchy are blocks that point directly to C or Fortran code, i.e. primitive blocks. One useful aspect of hierarchy is that a system can be easily transformed into a hierarchical block. This block may then be used as a component of a larger system, and the process continued until the overall system is completed.

Experience has shown that judicious use of all three types of blocks provides the most efficient simulations, both in terms of system complexity and simulation execution time. By taking advantage of the hierarchical nature of SPW, systems can be modularized, greatly simplifying their analysis.

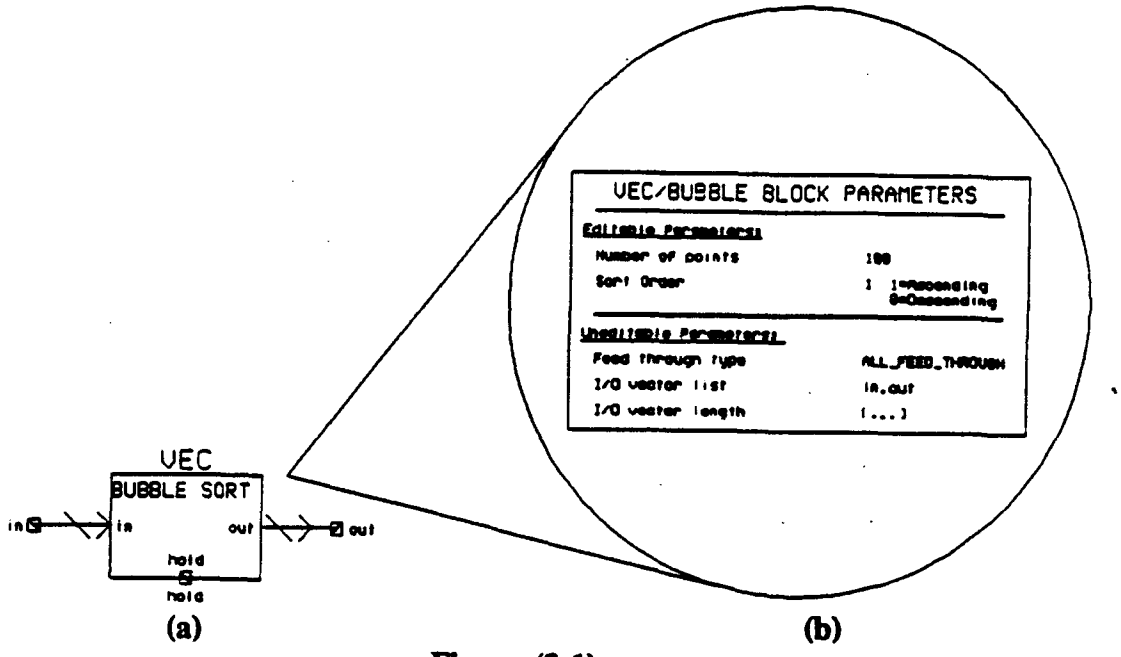

(a) (b)

Figure (3-1)

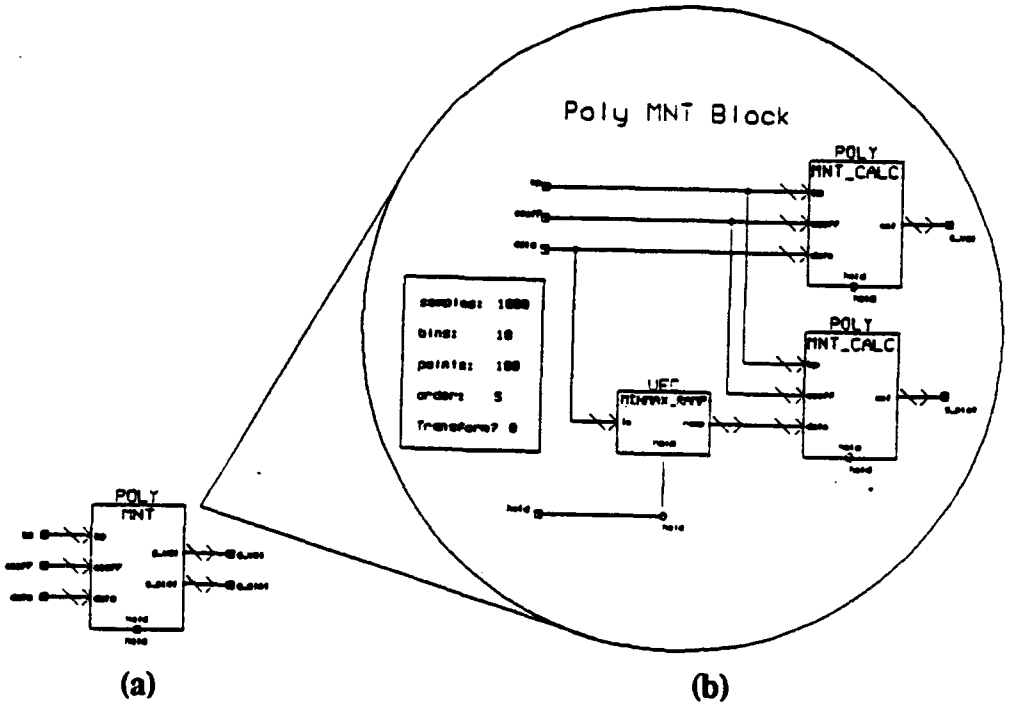

(a) (b)

Figure (3-2)

3.1.2 Exported Parameters

A very useful feature of the BDE is the exportation of parameters. This enables the designer to set the value of a parameter equal to a function of other parameters. Often, several different blocks have a common parameter, and this allows all common parameters to be exported to a single parameter on the top level of hierarchy. Rather than "pushing" into each block and changing each parameter, the designer need only change the parameter on the top level and all of the exported parameters will assume that value.

3.1.3 On-Line Documentation

On-line help may be obtained in the BDE by selecting HELP on the EZ-Menu [Comd91] and then pointing to the desired object. A text message containing the required documentation appears in a "viewport." This documentation is available for all SPW library blocks in three forms: 1) help on the block usage, 2) help on the block's input and output, and 3) help on the block's parameters. The first type of help is obtained by pointing to the block itself after selecting HELP on the EZ-Menu. The second type is obtained by pointing to any input or output port of the block. The third type is obtained by pushing into the block and pointing to any parameter. On-line help has also been provided for all blocks designed and implemented for use in the two simulations presented in the following sections[2].

[2] A complete listing of the help screens for each user block used to implement the simulations discussed herein is provided in Volume II of this report. For these SPW blocks all three types of help screens described above have been combined into the block usage help screen.

3.2 The Conventional QPSK Simulation

The purpose of this section is to provide an overview of the SPW simulation of a conventional QPSK communications system. An overview of the conventional QPSK baseband simulation is shown in Fig. (3-3). The simulation contains: a) a standard QPSK modulator which transmits a two-dimensional (I and Q) signal, b) a channel which contains multiple Continuous Wave (CW) jammers, a Gaussian Partial Band (PB) jammer, and background thermal (Gaussian) noise, and c) either the standard linear receiver implemented via a two-dimensional correlator or one of the memoryless LO processor implementations followed by the correlator.

The components of a typical memoryless LO processor block are shown in Fig. (3-4). The first operation performed in the LO processor block is rectangular to polar conversion which provides the magnitude and phase of the received signal. Next, the corresponding approximation (eg. traditional Histogram, EBH, FSA, etc.) of the received magnitude PDF is constructed. Through the use of the PDF approximation, in conjunction with the received magnitude, the LO nonlinearity is computed. Finally, the values for the LO nonlinear transform and the phase of the received signal are converted back to rectangular form. Thus, the output of the LO processor block is $(\hat{g}_{I_i},\hat{g}_{Q_i}) = (\hat{g}(r_k)\cos\theta_k, \hat{g}(r_k)\sin\theta_k)$, where $\hat{g}(\cdot)$ is the LO MNT estimate.

Using $(\hat{g}_{I_i},\hat{g}_{Q_i})$, the two-dimensional correlator generates the LO decision statistic of Eq. (1-5) discussed in Section 1.1, repeated here for convenience:

$$l_m = \sum_{k=1}^{N} \left\{ s_{I_{mk}} g(r_k)\cos\theta_k + s_{Q_{mk}} g(r_k)\sin\theta_k \right\} \qquad (3\text{-}1)$$

Conventional QPSK Communications System

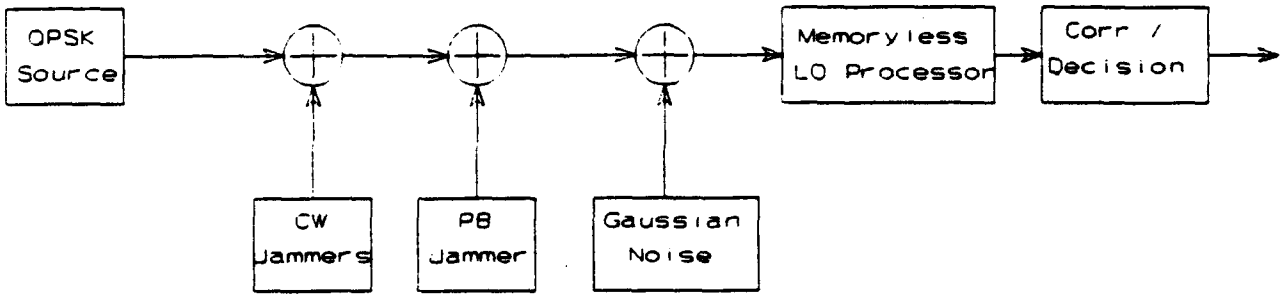

Figure (3-3)

LO Transform Block

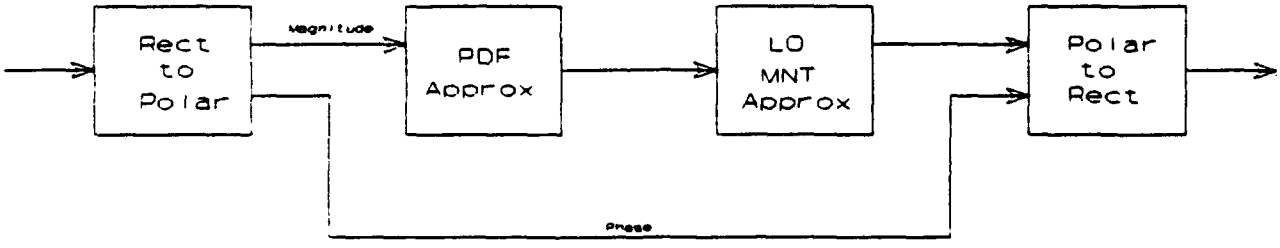

Figure (3-4)

3.3 The QPSK DSSS Simulation

The simulation of a baseband QPSK DSSS communication system with LO processing has been implemented using the SPW software package. An overview of the entire system is provided in Fig. (3-5). It consists of: a) a transmitter, with output $(\overline{\lambda}_I, \overline{\lambda}_Q)$, containing a QPSK source, whose output is given by $(\overline{s}_I, \overline{s}_Q)$, modulated by a Pseudo-Noise (PN) sequence generator producing a code sequence vector $\overline{c}$, b) a channel consisting of additive thermal (white Gaussian) noise, multiple CW jammers, and a Gaussian PB jammer, and c) a receiver, with input $(\overline{r}_I, \overline{r}_Q)$, that includes the LO MNT which outputs the signal vector $(\overline{g}_I, \overline{g}_Q)$, the PN sequence despreading source (perfect synchronization of transmitter and receiver is assumed) which when multiplied with the output of the LO MNT produces the ordered vector pair $(\overline{\gamma}_I, \overline{\gamma}_Q)$, and a two-dimensional correlator.

LO QPSK DSSS Simulation

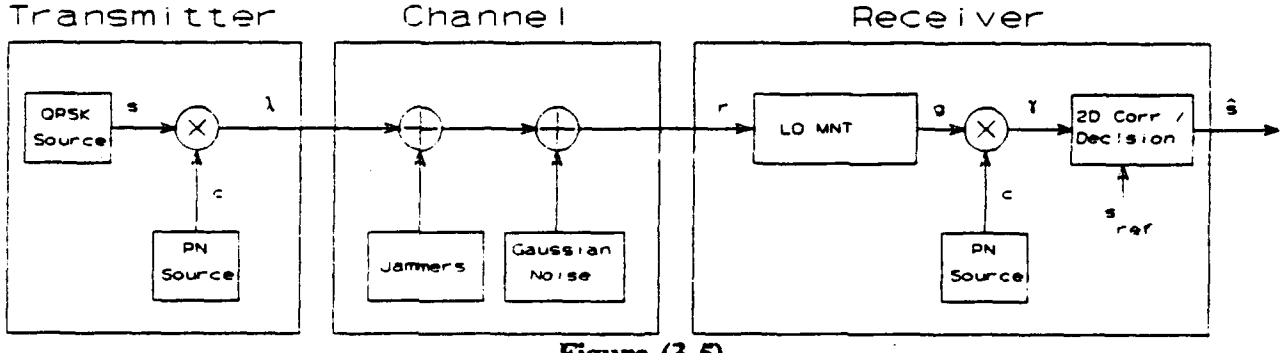

Figure (3-5)

3.3.1 Theoretical Justification

To construct the LO receiver for the QPSK DSSS system it is necessary to implement the LO decision statistic of Eq. (1-5), repeated here for convenience

$$l_m=\sum_{k=1}^{N}\left\{s_{I_m}\,g(r_k)\cos\theta_k+s_{Q_m}\,g(r_k)\sin\theta_k\right\} \tag{3-2}$$

Referring to Fig. (3-5), the kth sample of the baseband output of the QPSK DSSS transmitter is given by $(\lambda_{I_m},\lambda_{Q_m})=(c_k s_{I_m},c_k s_{Q_m})$, where $\overline{c}=[c_1,c_2,\ldots,c_k,\ldots,c_N]^T$ is the PN sequence which is fixed for a given signal period, and (s_{I_m},s_{Q_m}) is the kth sample of the mth possible transmitted signal pair. Since $c_k\cdot(c_k s_{I_m},c_k s_{Q_m})=(s_{I_m},s_{Q_m})$ for the DSSS system, there is a one-to-one and invertible mapping of s_{I_m} to λ_{I_m}. The process of memoryless LO detection of the received signal can be implemented by correlating the output of the LO MNT, $(\overline{g}_I,\overline{g}_Q)$, over the set of $\left\{(\overline{\lambda}_{I_m},\overline{\lambda}_{Q_m})\right\}$, $m=1,\ldots,M$, choosing the one corresponding to the largest decision statistic, l_m, and mapping the signal vector $(\overline{\lambda}_{I_m},\overline{\lambda}_{Q_m})$ to the possible information signal vector $(\overline{s}_{I_m},\overline{s}_{Q_m})$. This procedure may be stated more concisely as:

Choose the information signal $(\overline{s}_{I_m},\overline{s}_{Q_m})$ corresponding to the signal vector $(\overline{\lambda}_{I_m},\overline{\lambda}_{Q_m})$ which maximizes:

$$l_m=\sum_{k=1}^{N}\left\{\lambda_{I_m}\,g(r_k)\cos\theta_k+\lambda_{Q_m}\,g(r_k)\sin\theta_k\right\} \tag{3-3}$$

The receiver implementation of Eq. (3-3) is termed the *canonical form* LO receiver since it has the same form as Eq. (3-2). The block diagram for the LO QPSK DSSS receiver implementation given by Eq. (3-3) is shown in Fig. (3-6).

Canonical Form of the LO QPSK DSSS System

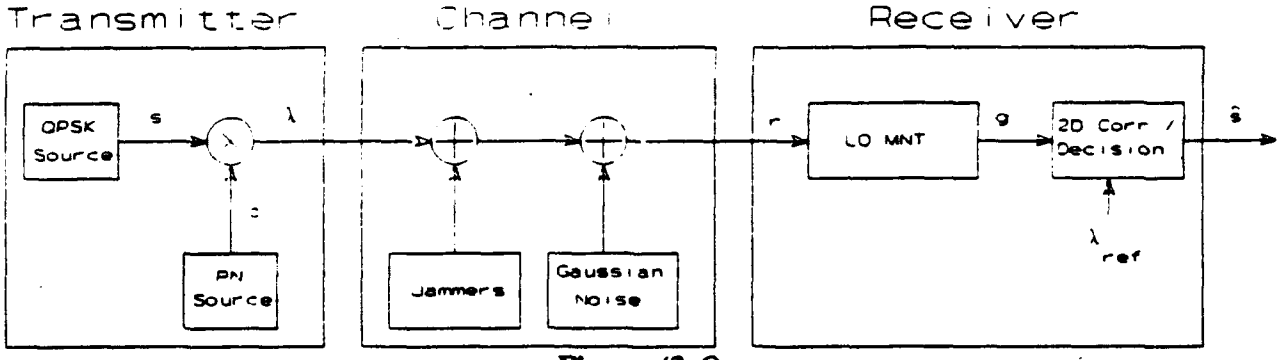

Figure (3-6)

An alternate LO receiver implementation requiring only a slight modification to the standard correlator-based linear receiver can be developed by noting that Eq. (3-3) may be written as

$$\begin{aligned} l_m &= \sum_{k=1}^{N} \left\{ \lambda_{I_m} g(r_k) \cos\theta_k + \lambda_{Q_m} g(r_k) \sin\theta_k \right\} \\ &= \sum_{k=1}^{N} \left\{ c_k s_{I_m} g(r_k) \cos\theta_k + c_k s_{Q_m} g(r_k) \sin\theta_k \right\} \\ &= \sum_{k=1}^{N} \left\{ s_{I_m} \left[c_k g(r_k) \cos\theta_k \right] + s_{Q_m} \left[c_k g(r_k) \sin\theta_k \right] \right\} \end{aligned} \tag{3-4}$$

Thus, the LO QPSK DSSS receiver can be implemented by first multiplying the output of the LO MNT by the PN sequence, and then correlating over the set of possible information signals $\left\{ (\overline{s}_{I_m}, \overline{s}_{Q_m}) \right\}$, $m=1,\ldots,M$. Note that this LO receiver may be easily implemented by placing the LO MNT before the despreading in a linear QPSK DSSS receiver. The resulting alternate, or *non-canonical form*, LO QPSK DSSS receiver implementation can be summarized in the following algorithm:

Choose the information signal $(\overline{s}_{I_m}, \overline{s}_{Q_m})$ which maximizes

$$l_m = \sum_{k=1}^{N} \left\{ s_{I_m} c_k g(r_k) \cos\theta_k + s_{Q_m} c_k g(r_k) \sin\theta_k \right\} \qquad (3\text{-}5)$$

Due to its modular nature, the LO receiver algorithm given by Eq. (3-5) was implemented in the SPW QPSK DSSS simulation shown in Fig. (3-5).

The non-canonical form LO receiver algorithm of Eq. (3-5) has two major advantages over the canonical form algorithm of Eq. (3-3). First, it has a more modular structure than the canonical algorithm and can be easily implemented by inserting the LO MNT into a standard correlator based QPSK DSSS linear receiver. Second, it is more flexible than the canonical algorithm in the sense that the PN spreading sequence can be modified without requiring new reference signals to be stored for use by the correlator. However, the canonical algorithm of Eq. (3-3) has the advantage of being a potentially faster implementation than the non-canonical algorithm, since only one multiplication is required (i.e. multiplying the output of the LO MNT by the stored reference signals), whereas the non-canonical algorithm requires two multiplications (i.e. multiplication of the output of the LO MNT by the PN sequence, and then multiplying the result by the stored reference signals). System requirements, e.g. speed versus flexibility, will dictate which LO receiver implementation is more desirable.

4. SIMULATION RESULTS FOR THE MEMORYLESS LOCALLY OPTIMAL PROCESSING ALGORITHMS

This section presents the simulation results for the conventional QPSK and DSSS QPSK systems with memoryless LO processing discussed in Sections 3.2 and 3.3. The following memoryless LO algorithms were examined in each system: Histogram, EBH, and FSA. In addition, the second order M-Interval Polynomial Approximation (MIPA) algorithm [Illi91, Illi93] was used in conjunction with the DSSS QPSK system. The probability of bit error, P_b, performance of each system and LO algorithm combination was computed for a multitude of jamming scenarios. When useful, the P_b for a standard linear system was also calculated for the purpose of comparison. By examining the operation of the LO algorithms in many different environments, it is possible to determine basic characteristics which govern performance, and ultimately which system/LO algorithm configuration is optimal for a given jamming scenario. This section is organized in the following manner. First, the simulation results for each LO algorithm in the conventional QPSK system are addressed. Next, the results are presented for the QPSK DSSS system when subjected to three different types of jammers, namely a single CW jammer, two CW jammers, and a PB jammer. Finally, the performance of both systems are compared to determine the effects of the SS system's processing gain on the LO processor.

4.1 Results for the Conventional QPSK System - The Single CW Jammer Scenario

The results for the conventional QPSK system when subjected to a single CW jammer are presented in this section. The user-definable parameters for each LO algorithm are shown in Table 4-1. As may be seen, the parameters B (number of bins), R_s (Symbol Rate)[1], N_s (Samples per Symbol), and N (Samples per Correlation) are common to all the memoryless LO algorithms.

[1] All other simulation parameters of interest are normalized to R_s. Thus, the value chosen for R_s is arbitrary.

Parameters for the LO Algorithms

LO Algorithm	User-Definable Parameters
1) Histogram 2) EBH 3) MIPA (2nd Order)	R_s - Symbol Rate B - Number of Bins N_s - Samples per Symbol N - Samples per Correlation (equivalent to samples per PDF approximation)
4) FSA	R_s - Symbol Rate P - Order of Approximation B - Number of Bins N_s - Samples per Symbol N - Samples per Correlation (equivalent to samples per PDF approximation)

Table 4-1

Before it is possible to thoroughly test each LO algorithm for a variety of Jammer-to-Signal power ratio (J/S), CW jammer frequency relative to the symbol rate (f_j/R_s), and bit energy to signal thermal (Gaussian) background noise power ratio (E_b/N_0) values[2], it was necessary to determine values for B, N_s, and N. In addition, P (Order of Approximation) must be chosen for the FSA LO algorithm. To determine a value of N_s that would be used in all subsequent analyses, the P_b for both the Histogram and EBH methods were computed using the system settings shown in Table 4-2, and the results are presented in Fig. (4-1), with the region $15 \leq N_s \leq 50$ emphasized in Fig. (4-2). Note that the rows are reversed in Fig. (4-2) for clarity. As may be seen from the figures, P_b for the conventional QPSK system with LO processing *decreases* as N_s *increases*. Using these results, and accounting for processing limitations, ***N_s = 20 was used for all subsequent simulations.***

[2] In this report, the values for J/S and E_b/N_0 are specified *per channel*.

Simulation Parameters

Parameter	Value
N_s	5 to 50
R_s	0.1
B	64
N	50,400
E_b/N_0	10 dB
N_0	0 dB
J/S	30 dB
f_j/R_s	0.496
Symbols per P_b Calculation	7,056

Table 4-2

To choose values for B and N, the P_b was computed for the Histogram and EBH methods for a range of B and N values when the system was subjected to a single CW jammer with J/S = 30 dB. The values for the system parameters used in this analysis are given in Table 4-3, and the results for the Histogram and EBH methods are displayed in Figs. (4-3) and (4-4), respectively. The P_b plots indicate that there is a critical relationship between B and N for both methods. If the chosen value of B is too large for a given value of N the P_b suffers. Conversely, if the chosen value of N is too small for a given value of B, the P_b also increases.

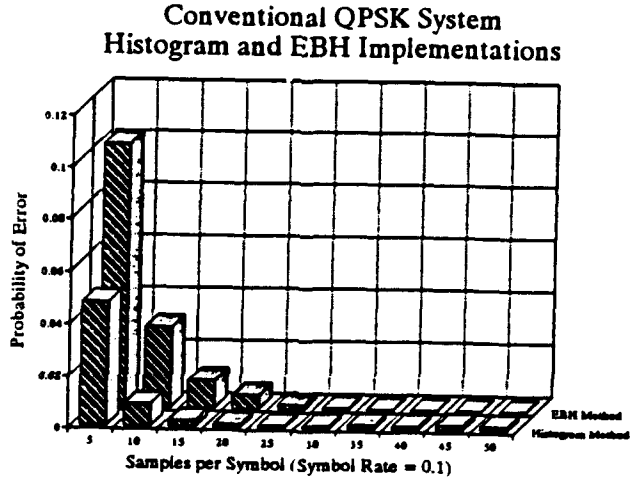

Figure (4-1)

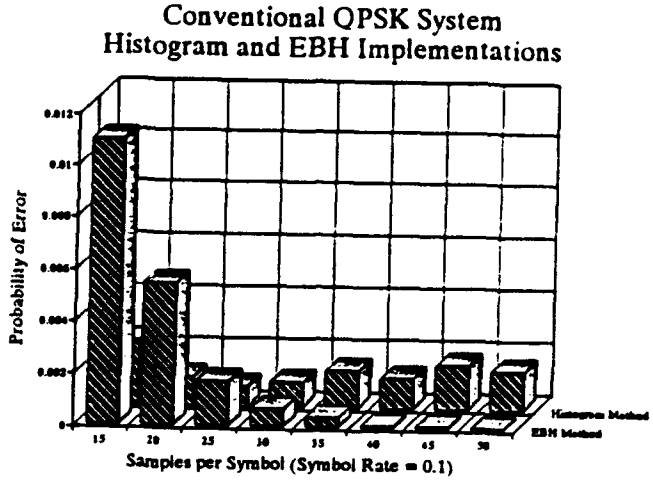

Figure (4-2)

Simulation Parameters

Parameter	Value
B	8 to 128
N	5,000 to 50,000
R_s	0.05
N_s	20
E_b/N_0	10 dB
N_0	0 dB
J/S	30 dB
f_j/R_s	0.496
Symbols per P_b Calculation	5,000

Table 4-3

Conventional QPSK System
Histogram Implementation

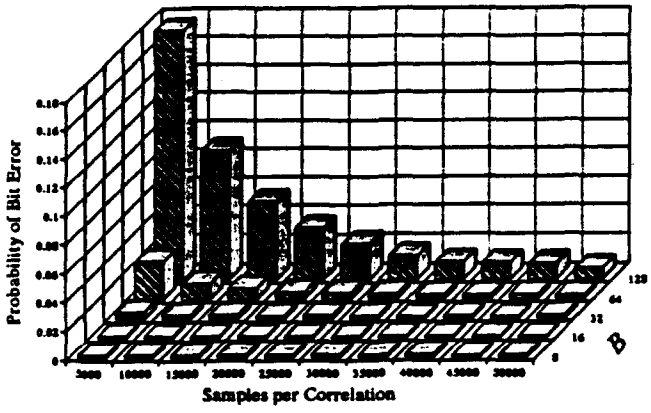

Figure (4-3)

Conventional QPSK System
EBH Implementation

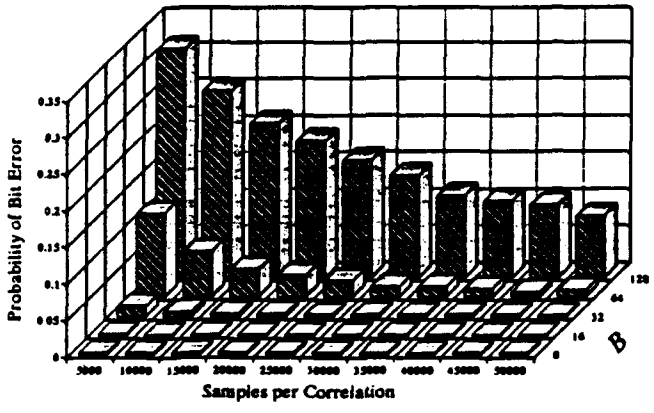

Figure (4-4)

The main reason for these relationships is that in both the Histogram and EBH methods, the total number of samples, N, is separated into B bins. As B increases for a given N, the average number of samples in each bin decreases. If this average number becomes too small, the PDF approximation will not be a good estimate of the actual PDF, and the resulting MNT will be inaccurate. ***For all subsequent analyses, the value of N was set to N = 50,000*** and the effect of varying B on the P_b was examined.

With the basic analysis of the LO processor parameters completed, it was possible to examine its performance relative to a variety of channel parameters, including: J/S, f_j/R_s, and E_b/N_0. In the first simulation, the relationships between these three parameters and B were examined for the Histogram and EBH methods. For the system parameters in Table 4-4, the following analyses are plotted: 1) for E_b/N_0 = 0 dB, Figs. (4-5) and (4-6) show the P_b relative to J/S and f_j/R_s [3] for B = 8, Figs. (4-7) and (4-8) show the P_b relative to J/S and f_j/R_s for B = 32, and Figs. (4-9) and (4-10) show P_b relative to J/S and f_j/R_s for B = 128; 2) for E_b/N_0 = 10 dB, Figs. (4-11) and (4-12) show the P_b relative to J/S and f_j/R_s for B = 8, Figs. (4-13) and (4-14) show the P_b relative to J/S and f_j/R_s for B = 32, and Figs. (4-15) and (4-16) show P_b relative to J/S and f_j/R_s for B = 128. For a baseline measurement, a plot of P_b for a conventional linear QPSK system with E_b/N_0 = 10 dB is provided in Fig. (4-17).

The first observation that can be made from these figures is that there is a clearly defined region in which the LO processor improves performance. In all the figures, this region begins around $J/S \geq 20$ dB and $f_j/R_s > 0.2$. Note that the relationship between P_b and f_j/R_s implies that the performance of the LO processor improves as the CW jammer moves farther away from the center of the main lobe bandwidth of the information signal, and only a slight performance improvement is seen as the CW jammer moves towards the center of the main lobe. The next

[3] The range of f_j/R_s was chosen to be 0.00496 to 0.496, rather than 0.005 to 0.5, so that samples of the CW jammer taken in successive periods would not have the same value. This produces a histogram that has a relatively "smooth" shape, rather than one that has a few bins of high probability, and a majority with zero probability.

observation is that increasing B only decreases P_b up to a point, after which the P_b increases. Furthermore, the effects of varying B seem to be more pronounced at low E_b/N_0 than at high E_b/N_0. This can be seen more clearly in Fig. (4-18) to (4-21) where P_b is shown for B and f_j/R_s varying.

Another interesting phenomenon that can be observed is that while J/S must be large for good performance, the LO processor is able to reduce the P_b more substantially in a high E_b/N_0 environment (e.g. 10 dB) than in a low E_b/N_0 environment (e.g. 0 dB). This indicates that for the best LO processor performance, the signal must be much weaker than the CW jammer, but at the same time larger than the background thermal (white Gaussian) noise.

Simulation Parameters

Parameter	Value
J/S	0 to 50 dB
f_j/R_s	0.00496 to 0.496
E_b/N_0	0 to 10 dB
B	8 to 128
R_s	0.05
N_s	20
N	50,000
N_0	0 dB
Symbols per P_b Calculation	5,000

Table 4-4

Finally, in comparing the results for the Histogram method to the EBH method for the parameters in Table 4-4, it may be observed that the Histogram method has a slightly lower P_b than the EBH method for most cases in the region of interest. It must be stressed, however, that the value of N_s was $N_s = 20$ for all simulation runs in Figs. (4-5) to (4-16). But from Fig. (4-2) it may be seen that while the Histogram method performs better than the EBH method for low values of N_s, the EBH method produces a lower P_b for higher values of N_s. Thus, by increasing N_s to a value larger than 20, it may be possible to improve the performance of the EBH method such that it will have a lower P_b than the Histogram method for most cases in the region of interest.

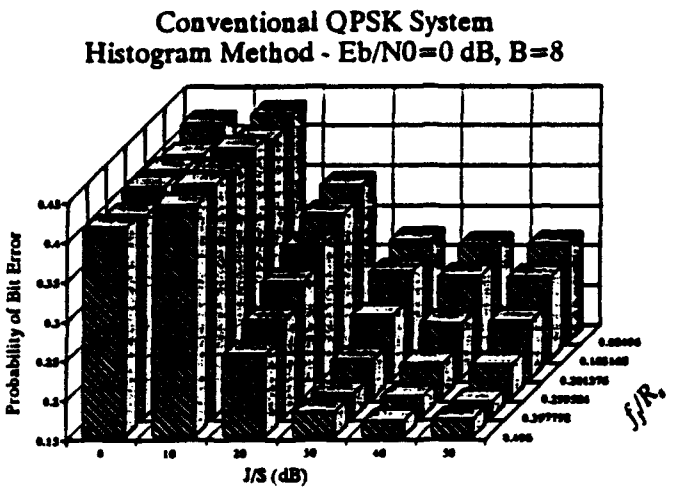

Figure (4-5)

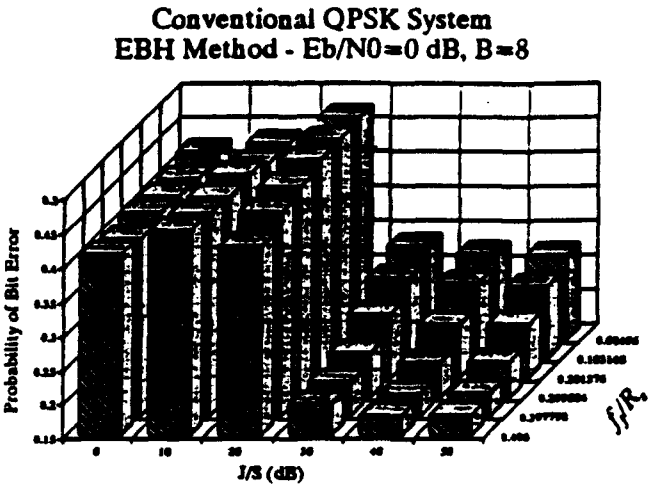

Figure (4-6)

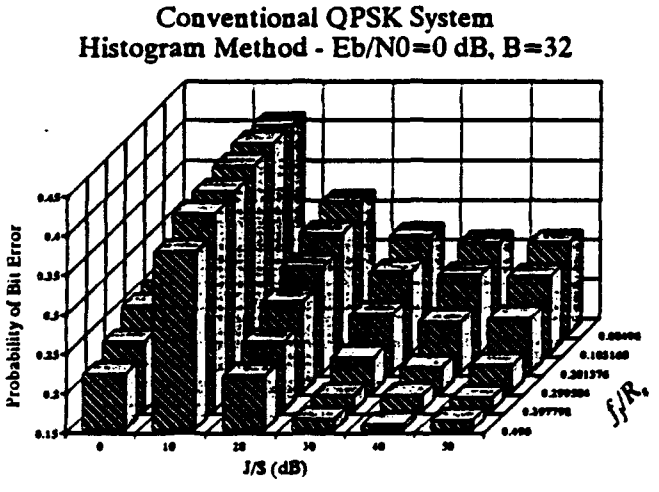

Figure (4-7)

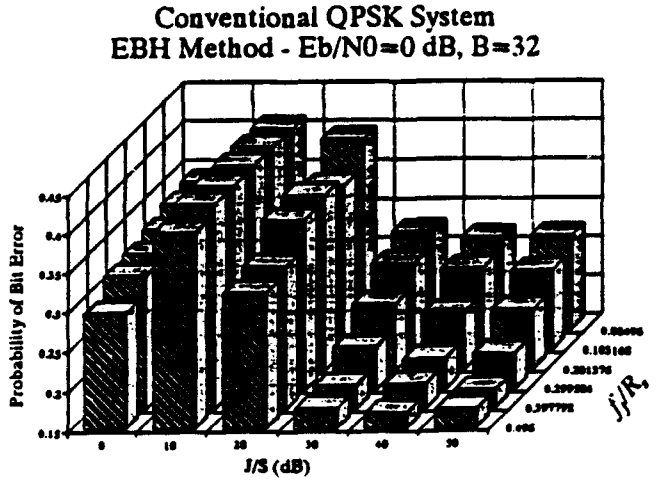

Figure (4-8)

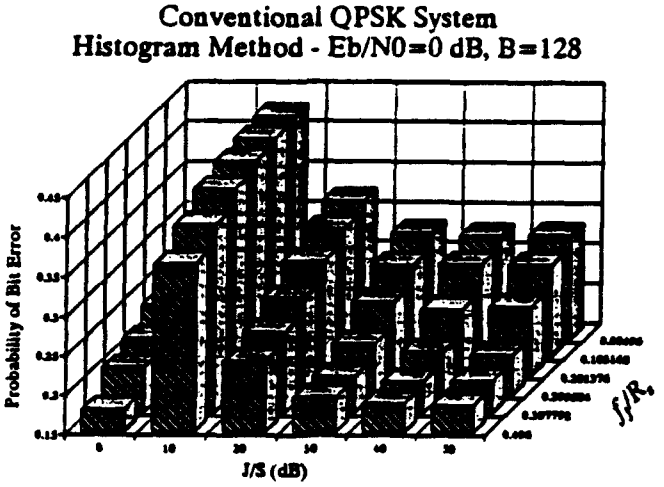

Figure (4-9)

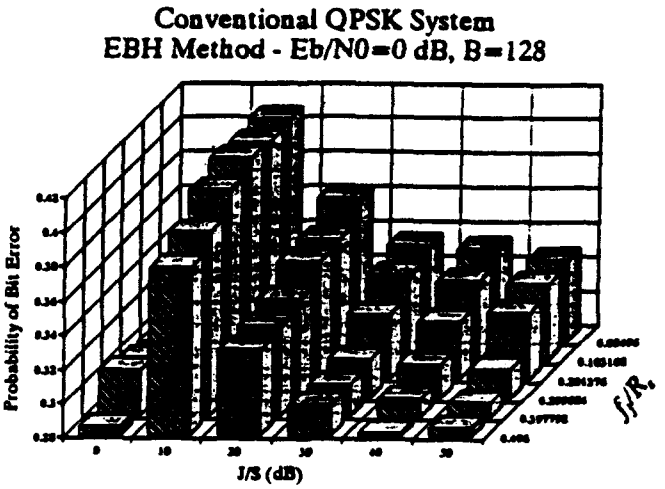

Figure (4-10)

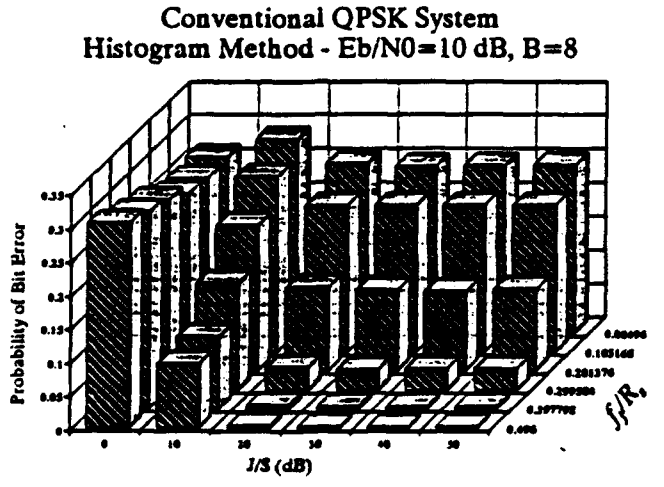

Figure (4-11)

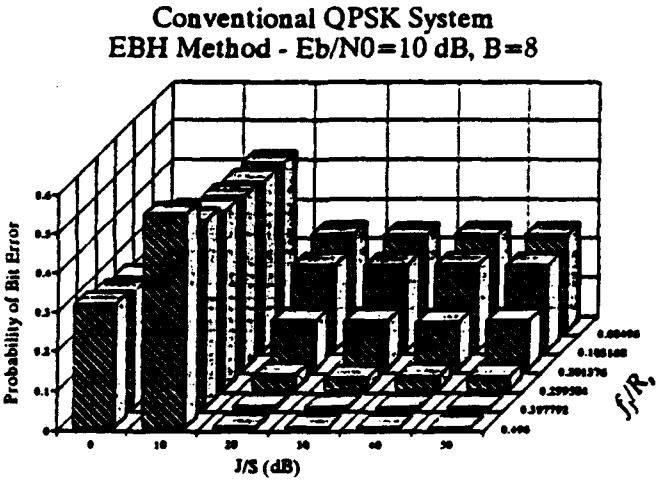

Figure (4-12)

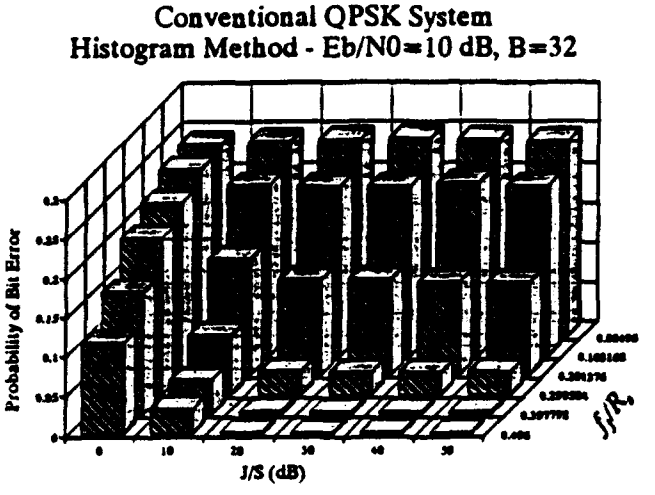

Figure (4-13)

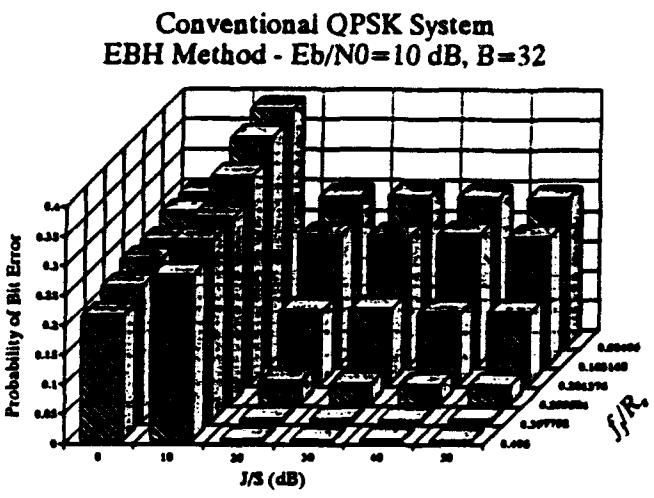

Figure (4-14)

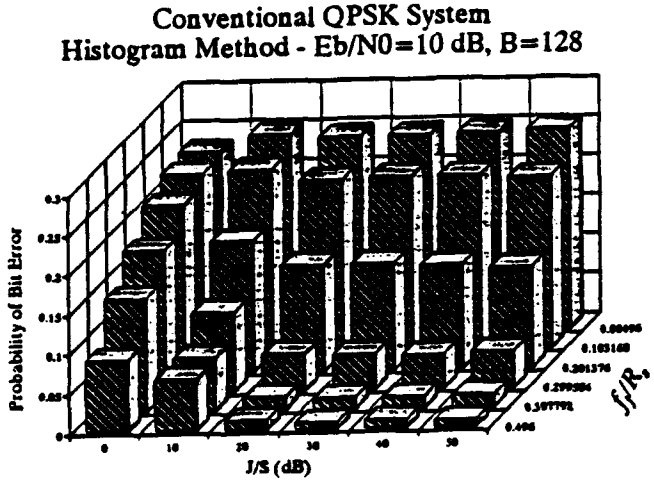

Figure (4-15)

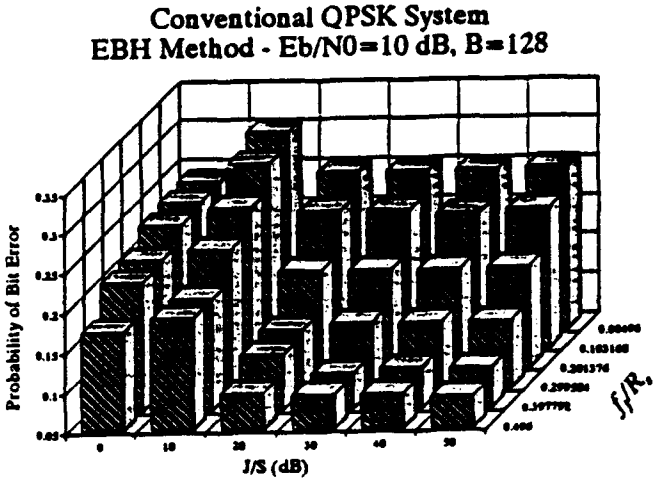

Figure (4-16)

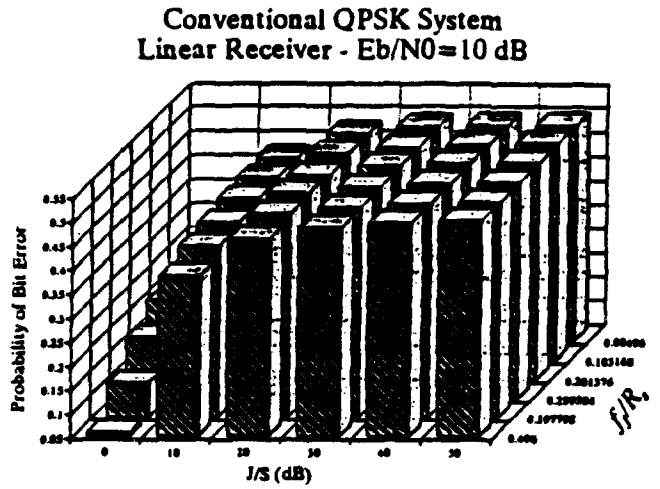

Figure (4-17)

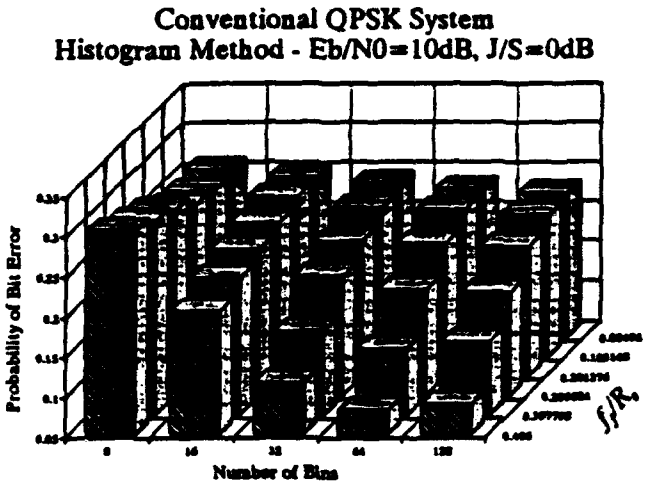

Figure (4-18)

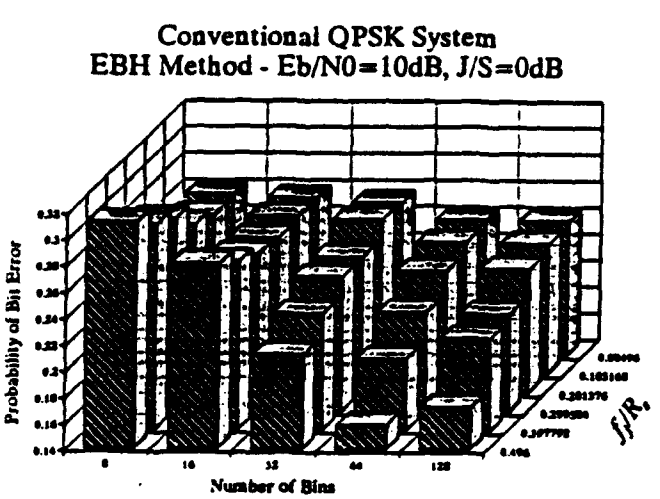

Figure (4-19)

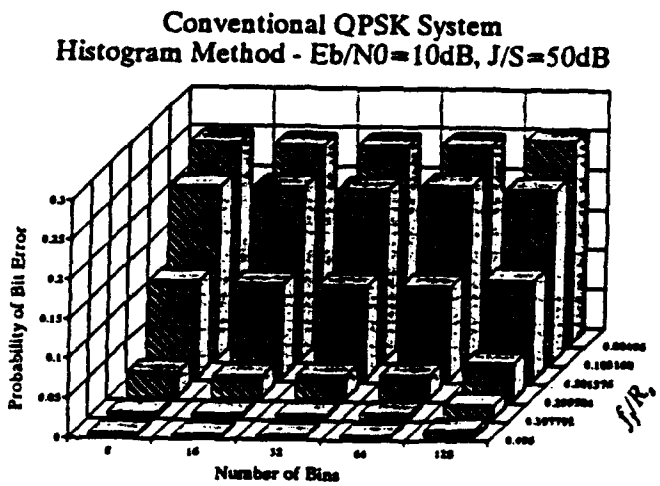

Figure (4-20)

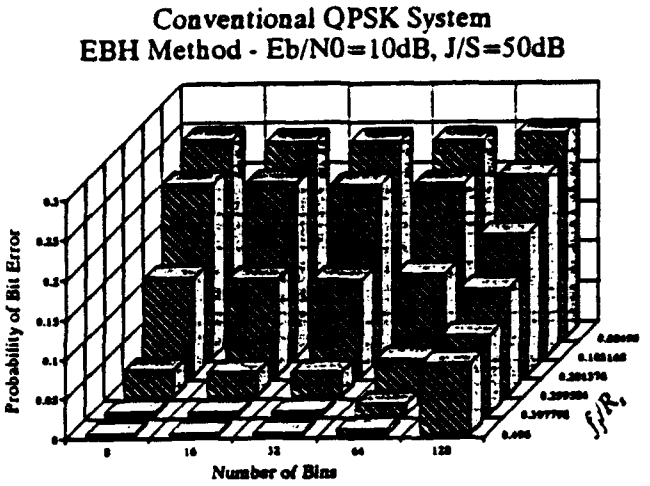

Figure (4-21)

The P_b performance for the histogram implementation of the FSA LO algorithm in conjunction with the conventional QPSK system was also investigated. Before examining the P_b performance with respect to J/S, f_j/R_s, and E_b/N_0, it was necessary to determine "good" values for P and B. Figure (4-22) shows the P_b performance of the FSA method relative to P and B for a single CW jammer having J/S = 30 dB and f_j/R_s = 0.496. The system parameters are displayed in Table 4-5. As may be seen from Fig. (4-22), there is a definite region where the FSA order, P, exceeds the histogram resolution, or B. Using these results, and after further investigation, the values P = 8 and B = 64 were chosen for the subsequent analysis.

Using the knowledge gained in the preceding analysis, the P_b for the histogram implementation of the FSA method was computed relative to J/S, f_j/R_s, and E_b/N_0. The results are displayed in Figs. (4-23) to (4-25) for the simulation parameters shown in Table 4-6. The first major observation is that the FSA method is governed by the same region of interest as the Histogram and EBH methods, namely $J/S \geq 20$ dB and $f_j/R_s > 0.2$, and the P_b decreases as f_j/R_s increases as before. Since these two observations are the same as those seen in the Histogram and EBH methods, it may be assumed they are characteristic of the basic LO processor algorithm and *not* the result of a specific implementation. One final observation of interest is that P_b decreases as E_b/N_0 increases. Thus, while it is critical that J/S be large enough for the small-signal assumption to be valid, it is also important that the information signal be larger than the background thermal (white Gaussian) noise.

Simulation Parameters

Parameter	Value
P	2 to 20
B	8 to 128
f_j/R_s	0.00496 to 0.496
R_s	0.05
N_s	20
N	50,000
E_b/N_0	10 dB
J/S	30 dB
N_0	0 dB
Symbols per P_b Calculation	5,000

Table 4-5

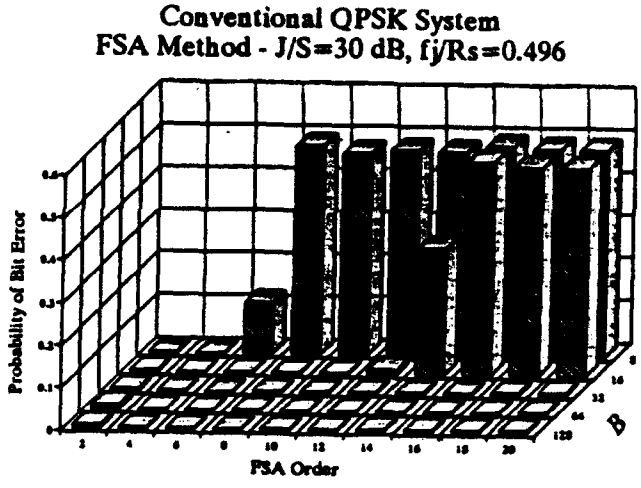

Figure (4-22)

In comparing all three methods, the Histogram, EBH, and the histogram implementation of the FSA, it may be observed that all three have approximately the same P_b performance. This is most likely a result of each method being based on a histogram approximation of the PDF. Because the parametric implementation of the FSA is not based on an initial histogram approximation, it is believed that this method will have a lower P_b in the region of interest than the other LO processor algorithms. This claim will be examined further in future research.

Simulation Parameters

Parameter	Value
J/S	0 to 50 dB
f_j/R_s	0.201376 to 0.496
E_b/N_0	0 to 10 dB
P	8
R_s	0.05
N_s	20
B	64
N	50,000
N_0	0 dB
Symbols per P_b Calculation	5,000

Table 4-6

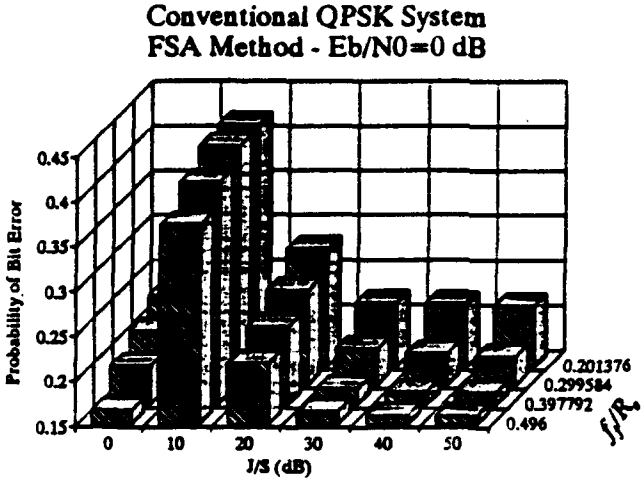

Figure (4-23)

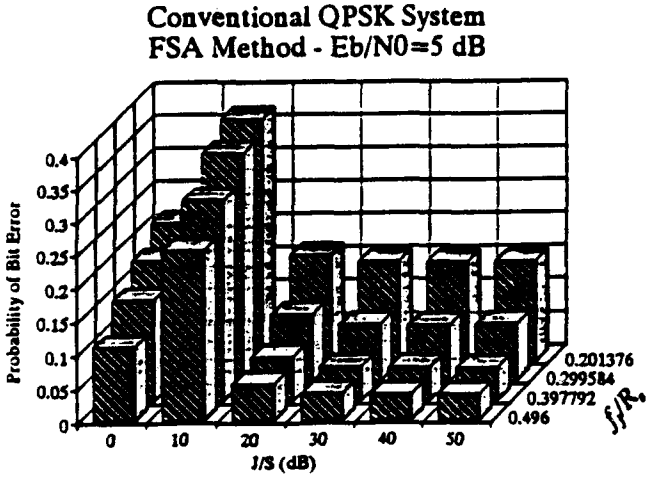

Figure (4-24)

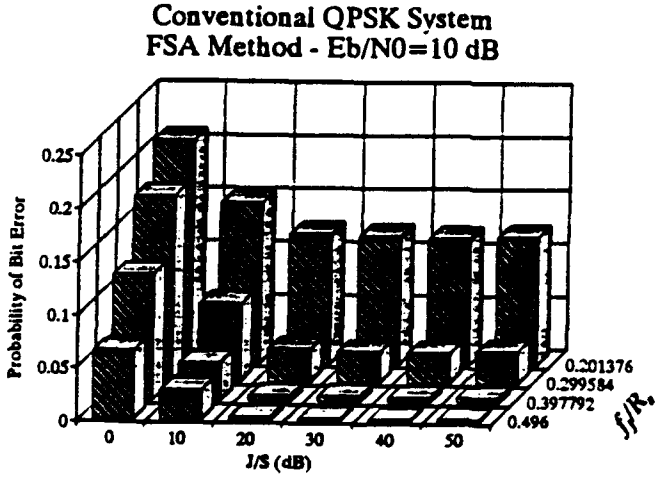

Figure (4-25)

4.2 Results for the QPSK DSSS System

The performance of the QPSK DSSS system was examined for the following overall jamming scenarios: 1) a single CW jammer, 2) two CW jammers, and 3) a single PB jammer.

4.2.1 The Single CW Jammer Scenario

The results for the QPSK DSSS system when subjected to a single CW jammer are presented in this section. Except for the addition of a new LO processor parameter, the Processing Gain (PG), the channel parameters (J/S, f_j/R_s, and E_b/N_0) and the LO processor parameters (R_s, N_s, N, B, and P) of interest are the same as for the conventional QPSK system. In this report, PG is defined as the number of chips per information symbol, or in terms of the other LO parameters:

$$PG = \frac{N_s}{N_c} \tag{4-1}$$

where N_c is the number of samples per chip.

The P_b performance of the QPSK DSSS system with LO processing relative to J/S, f_j/R_s, and PG was examined using the system parameters given in Table 4-7. The values for N_s, N, B, and P were chosen using the knowledge gained through the analysis of the conventional QPSK system. The organization of the P_b plots is as follows. For the Histogram method, Figs. (4-26) and (4-27) show the P_b with respect to J/S and f_j/R_s [4] and Figs. (4-28) and (4-29) show the P_b with respect to PG and f_j/R_s. Similarly, Figs. (4-30) to (4-33), (4-34) to (4-37), and

[4] Note that in these analyses P_b is plotted versus f_j/R_s for f_j/R_s in the range 0.201376 to 0.496, not 0.00496 to 0.496 as in the results for the conventional QPSK system. Values of f_j/R_s less than 0.2 are outside the region of interest because the P_b is large there.

(4-38) to (4-41) depict P_b with respect to J/S, PG, and f_j/R_s for the EBH, FSA, and second-order MIPA (MIPA2) methods, respectively. Comparable results for a standard linear QPSK DSSS system are provided in Figs. (4-42) to (4-45). From a cursory examination of the P_b plots, three observations can be made: 1) for $f_j/R_s > 0.2$ and a given PG, the P_b for almost all LO processor methods decreases as J/S increases; 2) for $J/S \geq 10$ dB and a given PG, the P_b decreases as f_j/R_s increases; and 3) for a given J/S and f_j/R_s, the P_b for almost all LO processor methods decreases as PG increases. These results are consistent with those for the conventional QPSK system.

Simulation Parameters

Parameter	Value
J/S	0 to 50 dB
f_j/R_s	0.201376 to 0.496
PG	5 to 20
R_s	0.1
N_c	2
N_s	PG * N_c
N	50,400
B (histogram and EBH)	32
(FSA)	64
(MIPA2)	8
P (FSA)	8
E_b/N_0	10 dB
N_0	0 dB
Symbols per P_b Calculation	5,040

Table 4-7

In comparing across LO processor methods, the following observations can be made. In the region of interest, $J/S \geq 20$ dB and $f_j/R_s > 0.2$, all the LO processor methods have roughly the same P_b performance characteristics with the following exceptions: 1) the FSA and MIPA2 methods perform better than the Histogram and EBH methods for low J/S ($J/S < 10$ dB), and 2) the Histogram, FSA, and MIPA2 methods perform better than the EBH method when PG and J/S are both low ($PG \leq 10$, $J/S < 10$ dB). The second exception is consistent with the results observed for the conventional QPSK system, namely that for low N_s the Histogram method has a smaller P_b than the EBH method, but the converse is true for high N_s. Future research is required to determine the reason(s) for the first exception.

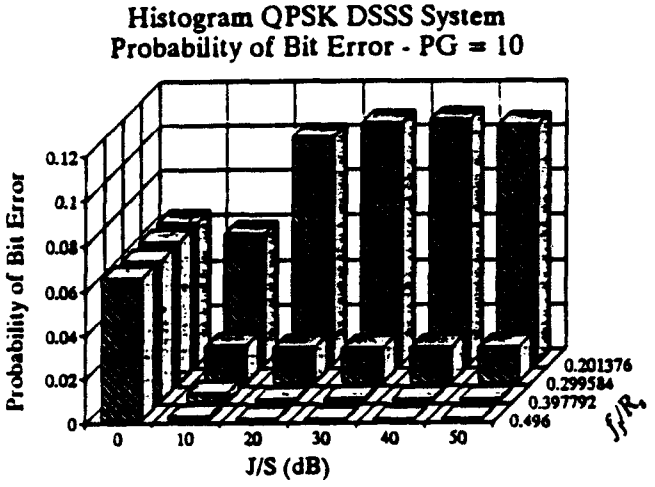

Figure (4-26)

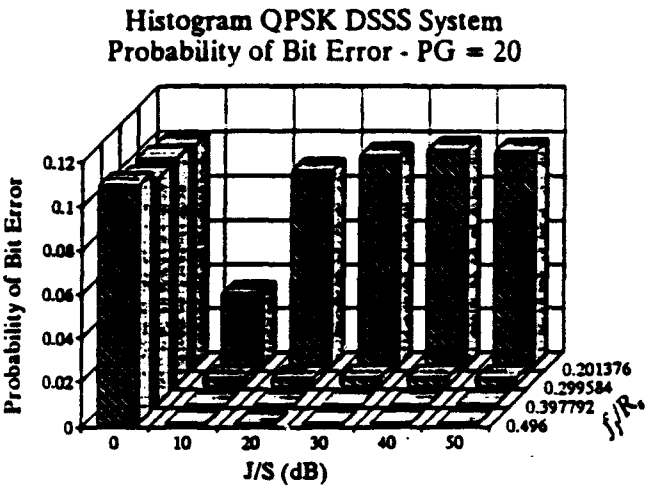

Figure (4-27)

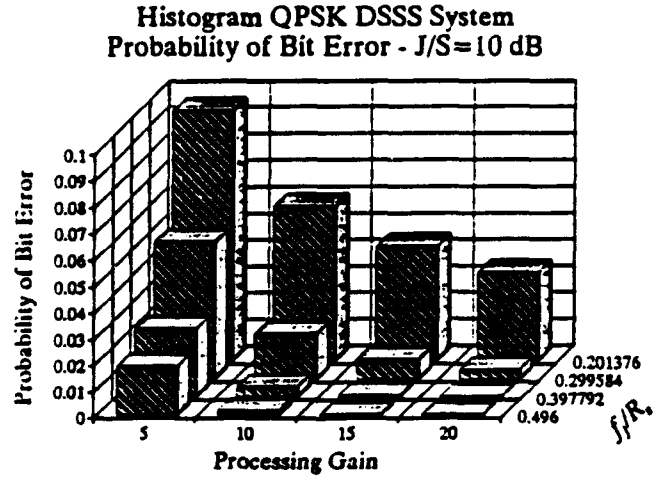

Figure (4-28)

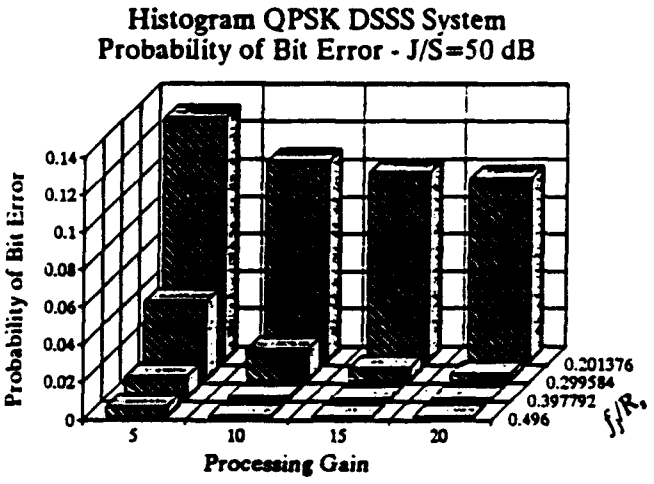

Figure (4-29)

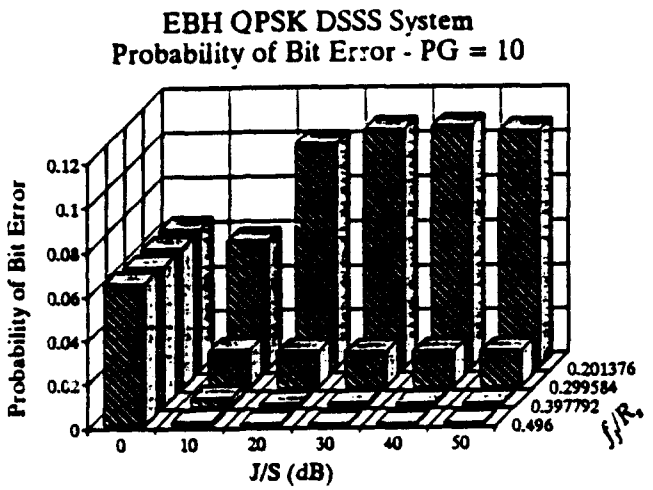

Figure (4-30)

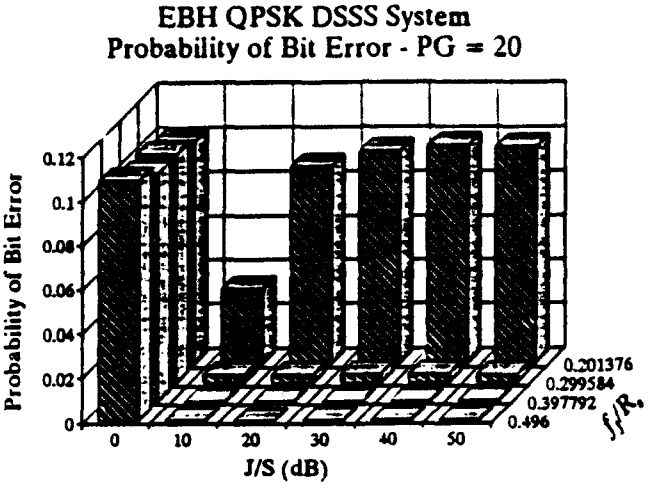

Figure (4-31)

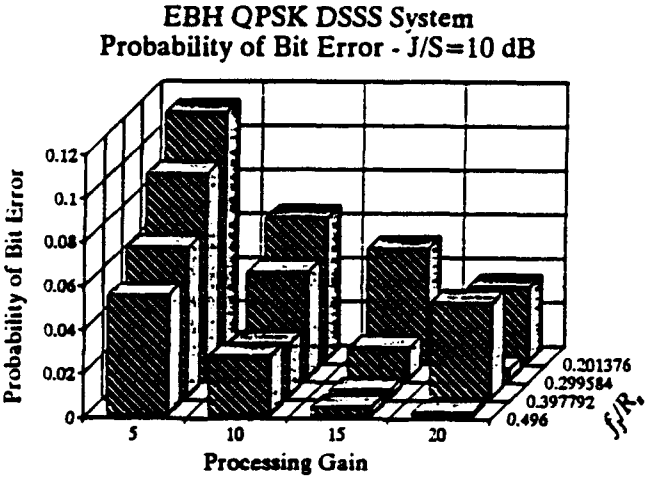

Figure (4-32)

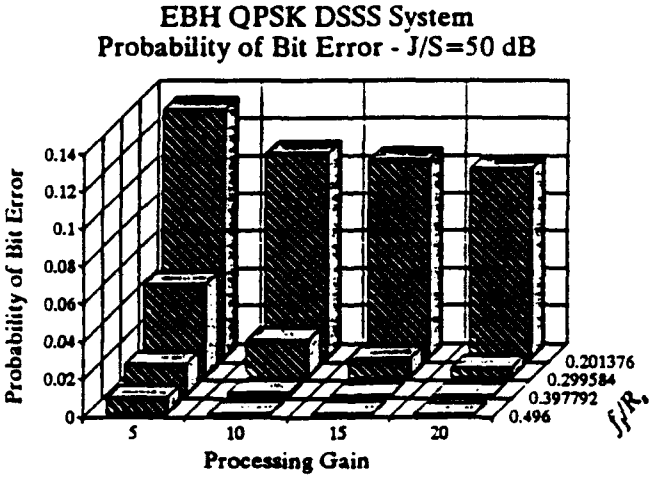

Figure (4-33)

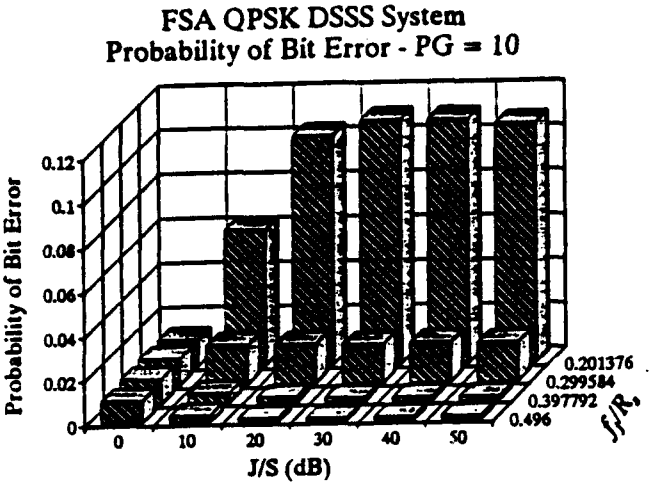

Figure (4-34)

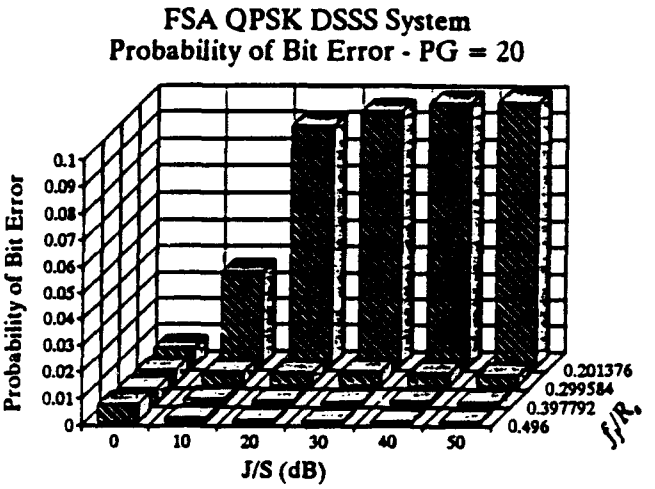

Figure (4-35)

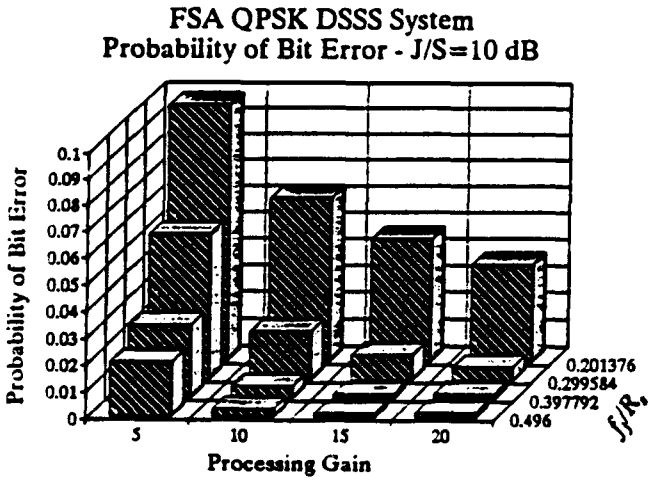

Figure (4-36)

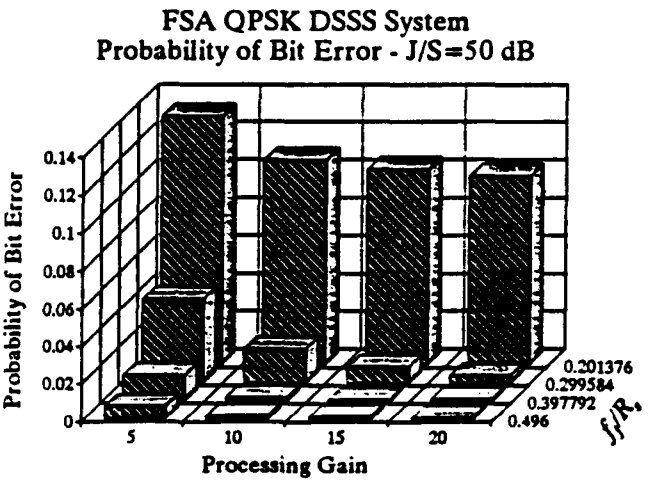

Figure (4-37)

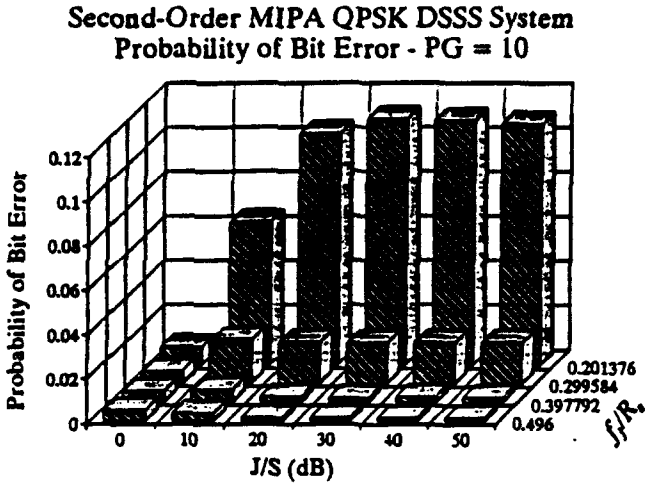

Figure (4-38)

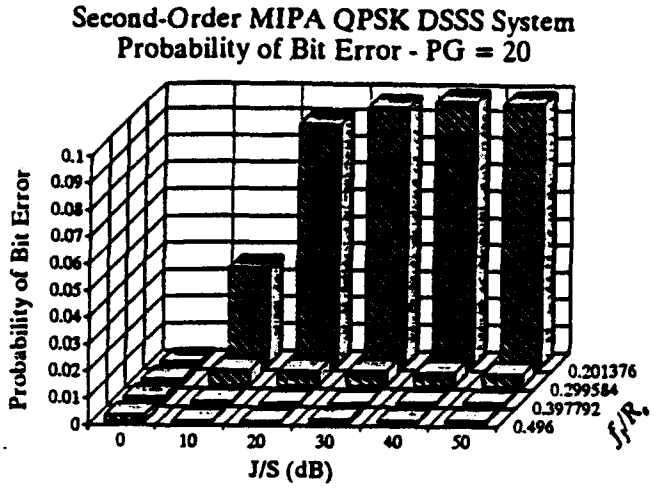

Figure (4-39)

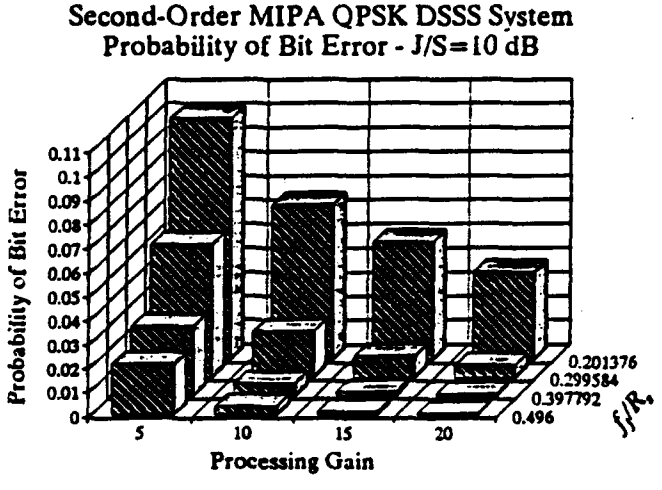

Figure (4-40)

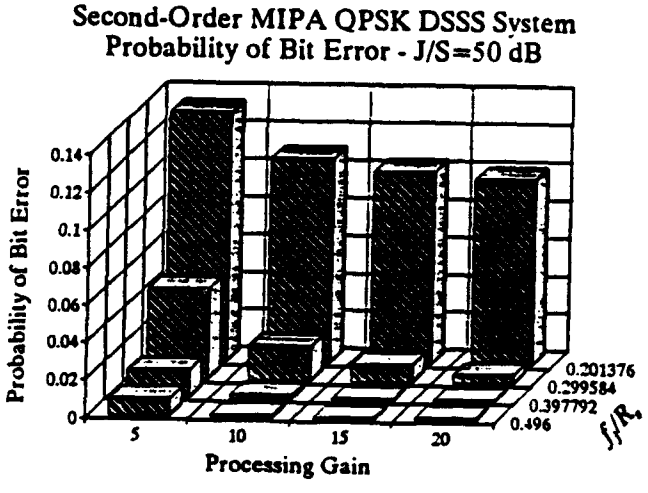

Figure (4-41)

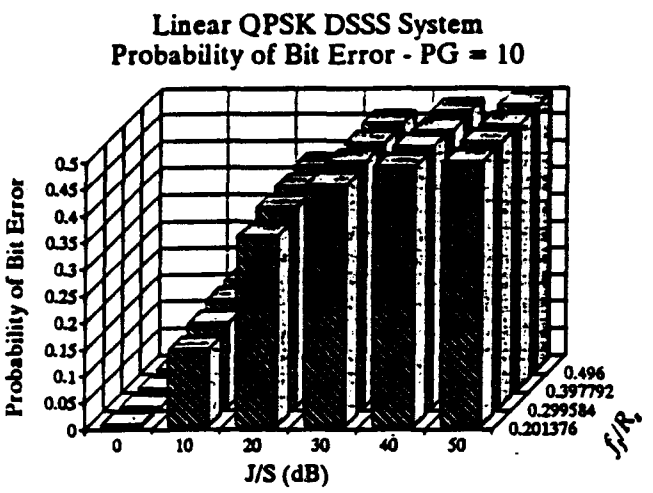

Figure (4-42)

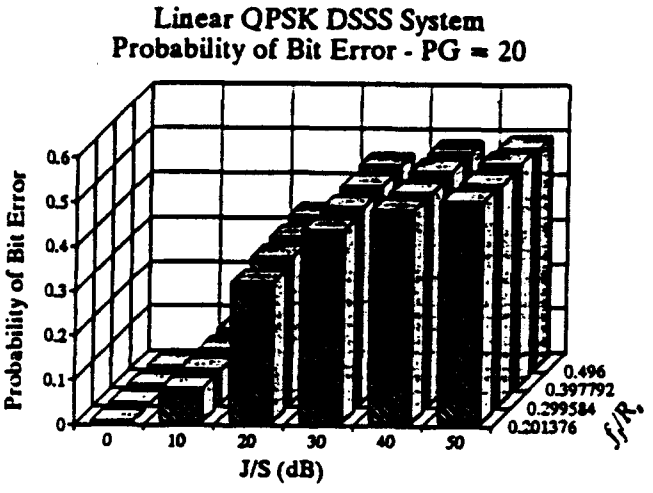

Figure (4-43)

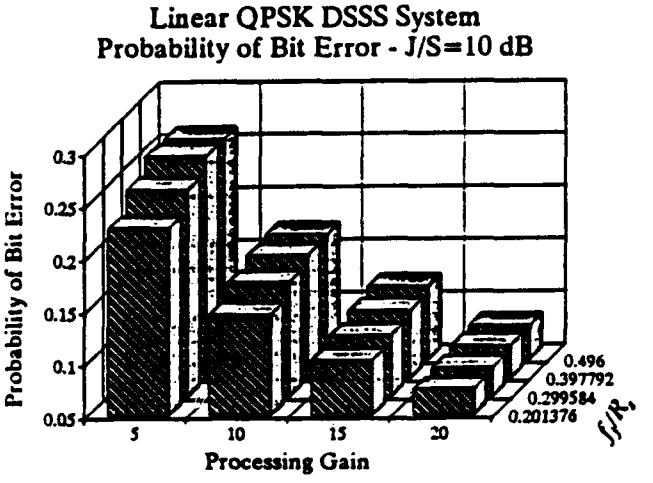

Figure (4-44)

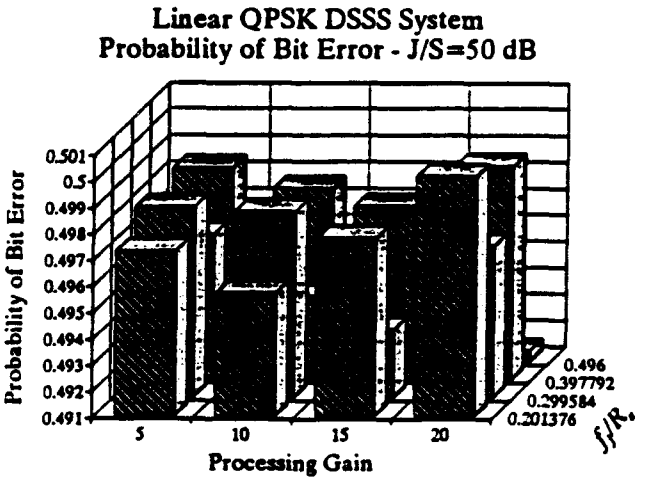

Figure (4-45)

4.2.2 The Two CW Jammers Scenario

This section presents the results for the QPSK DSSS system using the Histogram and EBH implementations of the LO nonlinear processor when subjected to two CW jammers. In this analysis, the first CW jammer was held fixed at J/S (1st CW) = 30 dB and f_j/R_s (1st CW) = 0.496. The second CW jammer was then varied over the range J/S (2nd CW) = -20 to 50 dB and f_j/R_s (2nd CW) = 0.00406 to 0.406. The remaining system parameters are given in Table 4-8. The P_b performance curves are plotted in Figs. (4-46) and (4-47) for the Histogram and EBH methods, respectively. As can be seen from the figures, the P_b is small when J/S (2nd CW) is low, and increases as J/S (2nd CW) increases. Note however, as J/S (2nd CW) grows larger than J/S (1st CW), i.e. as the second jammer becomes the dominant interferer, the P_b remains at a high value. This indicates that the absolute values of the J/S for both CWs, as well as the difference in their magnitudes, determines the P_b performance.

Another observation that can be made in this scenario is that as f_j/R_s (2nd CW) decreases, the P_b actually *decreases*. This would seem to contradict the results of the previous sections. However, a possible reason for this seemingly anomalous case is that as f_j/R_s (2nd CW) decreases, the second CW jammer's frequency spectrum moves farther away from that of the first CW jammer. Under this hypothesis it appears that the increased frequency spacing between interferers is not as detrimental to the system as are closely spaced interferers.

Simulation Parameters

Parameter	Value
J/S (2nd CW)	-20 to 50 dB
f_j/R_s (2nd CW)	0.00406 to 0.406
R_s	0.1
N_c	2
N_s	N_c * PG
PG	20
N	50,400
B	32
E_b/N_0	10 dB
N_0	0 dB
J/S (1st CW)	30 dB
f_j/R_s (1st CW)	0.496
Symbols per P_b Calculation	5,040

Table 4-8

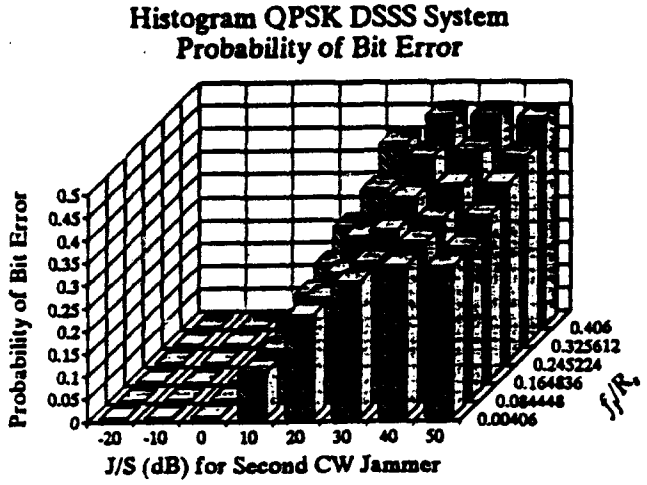

Figure (4-46)

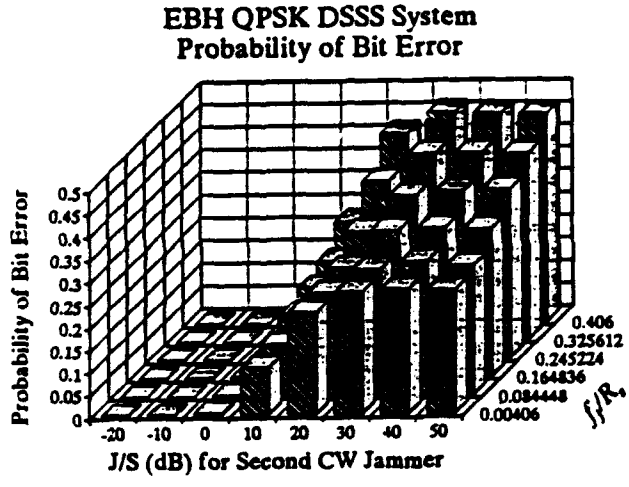

Figure (4-47)

4.2.3 The PB Jammer Scenario

This section discusses the P_b performance of the QPSK DSSS system when the channel interference is a single PB jammer, implemented by passing white Gaussian noise through a lowpass filter, and white Gaussian background noise. The results shown are for the LO processor implemented via the Histogram method. Two parameters govern the PB jammer: J/S and f_c/R_s, where f_c is the lowpass bandwidth (cutoff frequency) of the PB jammer (recall that the simulation is performed at baseband). The simulation results for $f_c/R_s < 1$, with the simulation parameters in Table 4-9, are shown in Figs. (4-48) to (4-50). Figure (4-48) illustrates the relationship of P_b to J/S and f_c/R_s,[5] for $PG = 20$ (similar results were observed for $PG = 5$ to 15 but are not shown here). The plots of P_b with respect to PG and f_c/R_s for $J/S = -10$ and 30 dB are shown in Figs. (4-49) and (4-50), respectively. As may be seen, P_b is small for low values of J/S ($J/S \leq 0$ dB) and increases as J/S increases. In addition, it may be observed that P_b decreases as PG increases for high J/S, but for low J/S P_b actually *increases* as PG increases. Future analysis is required to determine the reason(s) behind this trend. Finally, for a given PG and J/S, the P_b is seen to increase as f_c/R_s increases. This indicates that the LO processor performs well for narrowband interference and worse for wideband interference.

Figures (4-51) to (4-53) depict the P_b plots for $f_c/R_s > 1$ with the system parameters given in Table 4-10. These results confirm that the performance of the LO processor degrades as the power spectrum of the PB jammer becomes more wideband.

---

[5] Unlike the CW jammer, the values for f_c/R_s for the PB jammer may be chosen to be "nice" values, such as 0.2, 0.8, 1.2, etc. Since the PB jammer is implemented by passing white Gaussian noise through a lowpass filter, the probability of successive samples being identical is small. Thus, any reasonable value of f_c/R_s will produce a histogram that is relatively "smooth."

Simulation Parameters

Parameter	Value
J/S	-10 to 30 dB
f_c/R_s	0.2 to 0.8
R_s	0.1
N_c	2
N_s	N_c * PG
PG	20
N	50,400
B	32
E_b/N_0	10 dB
N_0	0 dB
Symbols per P_b Calculation	5,040

Table 4-9

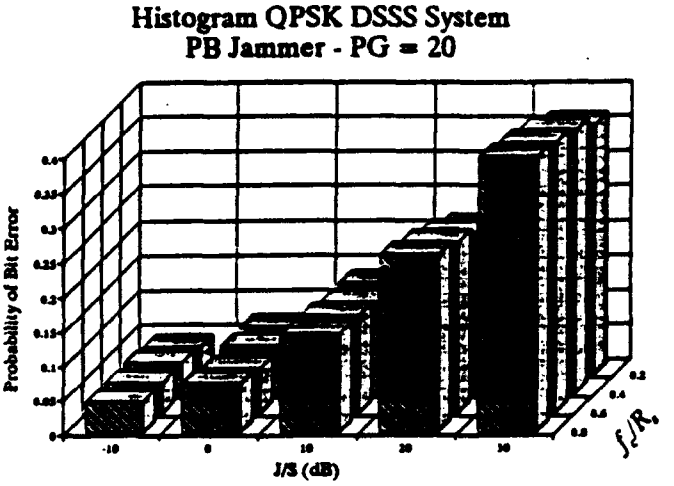

Figure (4-48)

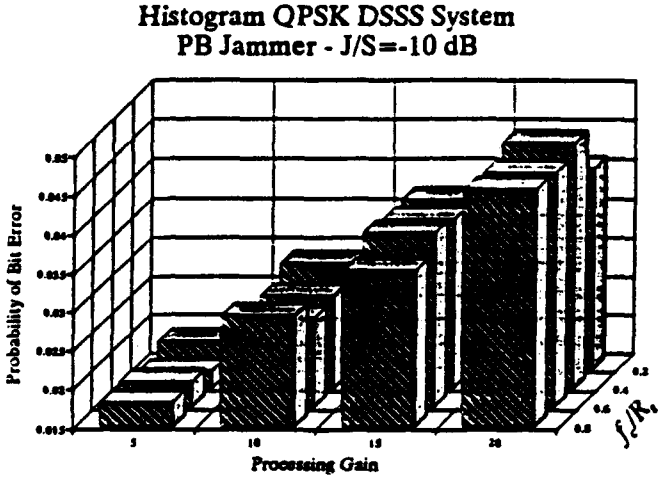

Figure (4-49)

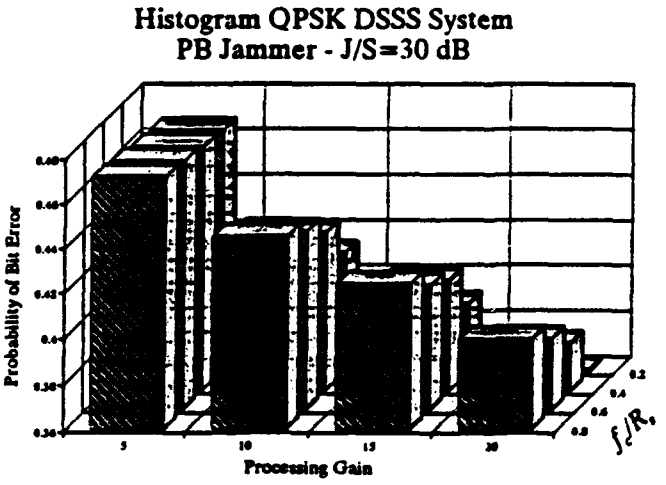

Figure (4-50)

Simulation Parameters

Parameter	Value
J/S	-10 to 30 dB
f_c/R_s	1 to 3.5
R_s	0.1
N_c	2
N_s	N_c * PG
PG	20
N	50,400
B	32
E_b/N_0	10 dB
N_0	0 dB
Symbols per P_b Calculation	5,040

Table 4-10

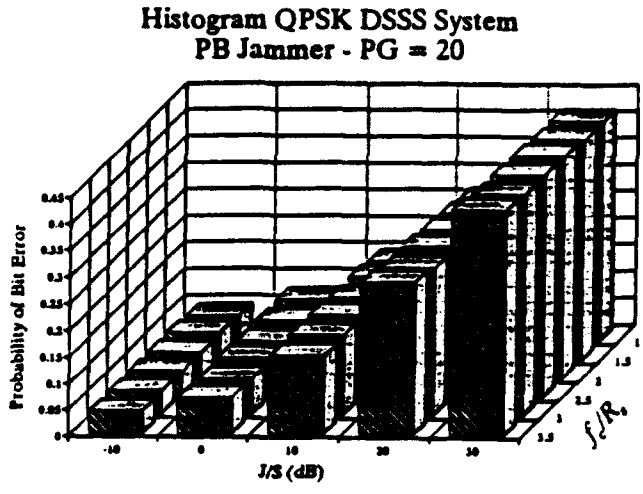

Figure (4-51)

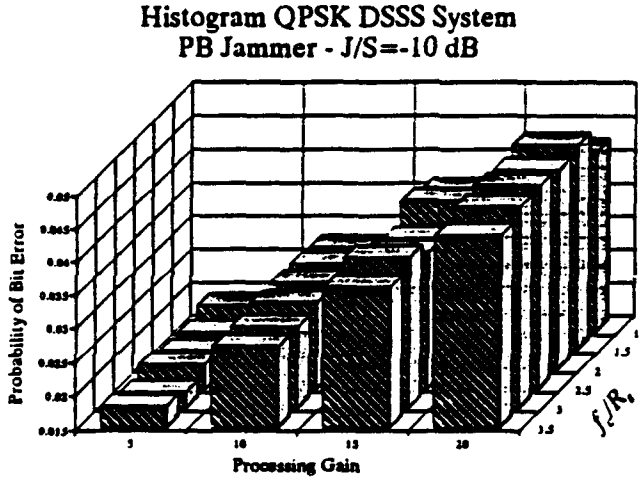

Figure (4-52)

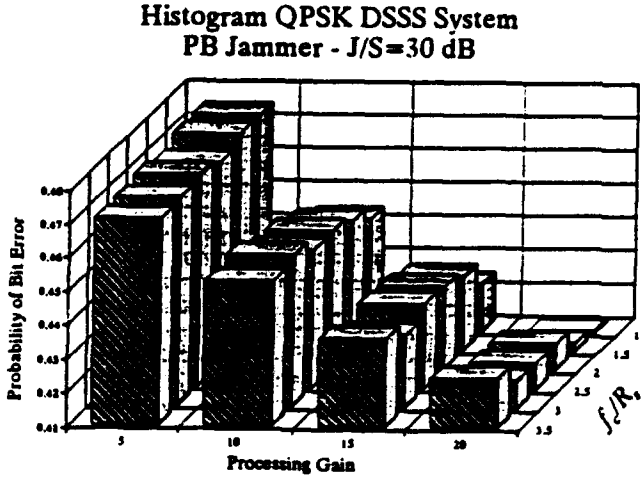

Figure (4-53)

4.3 Comparison of the Conventional QPSK and QPSK DSSS Systems

To compare the effects of spread spectrum on the LO processor, the P_b performance of the conventional QPSK and QPSK DSSS systems using the Histogram, EBH, and FSA LO implementation methods were compared for the single CW jammer scenario. As in previous simulations, N_s for the conventional QPSK system was fixed at $N_s = 20$, and $PG = 10$ and $N_c = 2$ were used for the QPSK DSSS system. Figs. (4-54) through (4-59) illustrate the P_b versus J/S results with $f_j/R_s = 0.397792$ and 0.496 for each of the three LO processor methods. The corresponding system parameters are provided in Table 4-11.

Simulation Parameters

Parameter	Value
J/S	0 to 50 dB
f_j/R_s	0.397792 and 0.496
R_s	0.1
N_s (conv. QPSK)	20
N_c (QPSK DSSS)	2
PG (QPSK DSSS)	10
N	50,400
B (histogram and EBH)	32
(FSA)	64
P (FSA)	8
E_b/N_0	10 dB
N_0	0 dB
Symbols per P_b Calculation	5,040

Table 4-11

As may be seen in the figures, the P_b for the QPSK DSSS system is smaller than that of the conventional QPSK system for low values of J/S. However, for larger values of J/S the P_b for the two systems is approximately the same. Thus, for high values of J/S, the LO processor dominates the improvement in performance. In addition, spread spectrum can be used to improve performance, and provide robustness, at lower values of J/S.

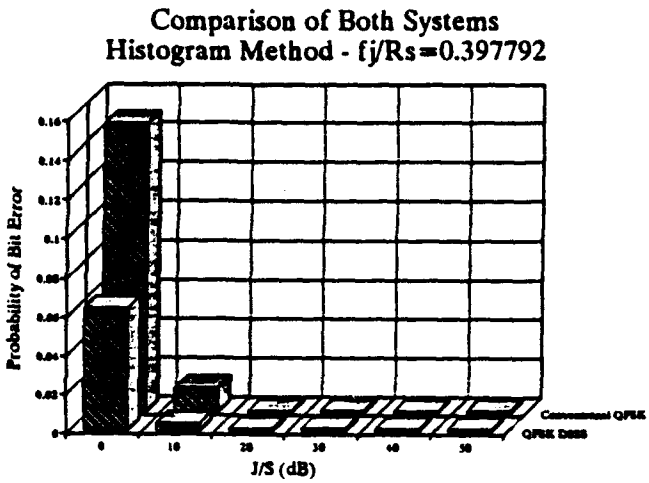

Figure (4-54)

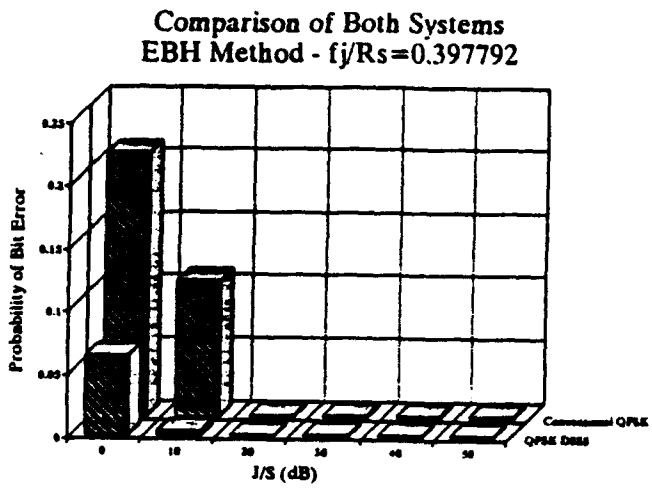

Figure (4-55)

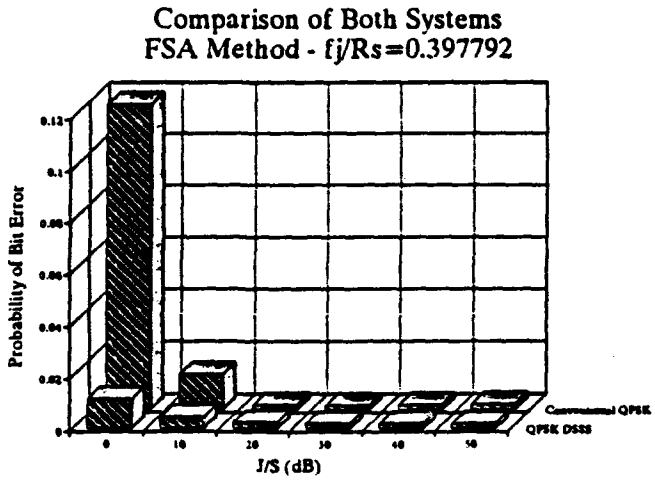

Figure (4-56)

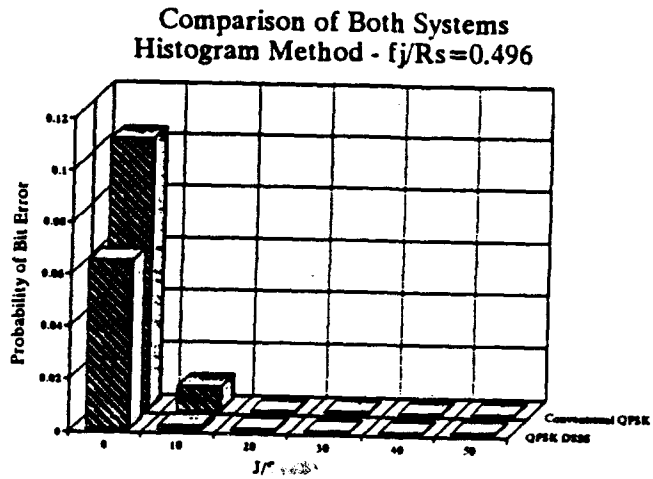

Figure (4-57)

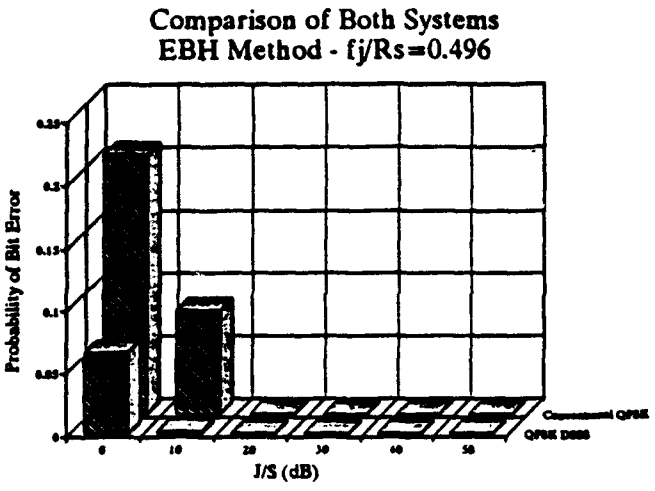

Figure (4-58)

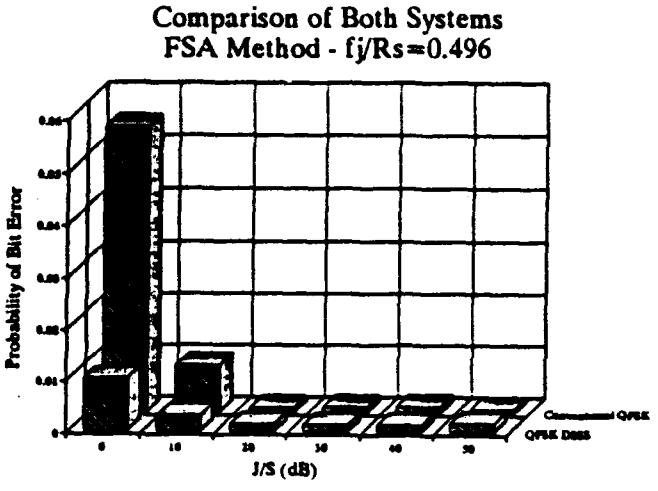

Figure (4-59)

4.4 Conclusions

Using the previous analyses, a number of conclusions can be drawn concerning the optimum use of the memoryless LO processor. When the channel interference consists of a single CW jammer:

- the *memoryless* LO processor is only effective in high J/S and high f_j/R_s environments
- the performance of the LO processor improves as the E_b/N_0 increases
- large values of N_s should be used
- regarding the LO processor implementation methods, for a given value of N, the value for B should be chosen judiciously such that the average number of samples in each histogram bin remains large enough so that an accurate approximation of the PDF is obtained

In the case of two CW jammers, the *memoryless* LO processor should be used only if one of the jammers has a relatively low J/S. In addition, the P_b performance improves as the spectral separation of the CW jammers increases.

If the channel contains a single PB jammer, the *memoryless* LO processor should only be used in moderate J/S environments. Also, the PG of the DSSS system must be modified as the J/S changes.

Finally, it should be noted that all of the results in this section are for the memoryless LO processor only. Future research should examine the use of LO processors *with* memory, and their ability to improve P_b performance, particularly in regions where the memoryless LO processor is insufficient.

5. LOCALLY OPTIMAL PROCESSING WITH MEMORY

The LO processors discussed in the previous sections assumed that adjacent samples of the total channel interference were Independent and Identically Distributed (IID). Using this assumption, it is possible to obtain the joint PDF of the interference samples as the product of the individual marginal PDFs. However, the resulting memoryless LO processor does not take advantage of the wealth of information contained in the interrelationships between adjacent samples. Thus, a more robust LO processor, of which the memoryless processor is a subset, can be derived by removing the IID assumption. This results in a processor with *memory*. Of particular interest during the contract effort was the derivation of the LO processor with memory presented in the Robust Digital Adaptive Transceiver (RDAT) report by Charles Stark Draper Laboratories, Inc. [Drap89]. The following sections present the RDAT theory and methodology, focusing on the development of the LO detector for one-dimensional (1D) and two-dimensional (2D) signalling environments. In addition, a particular interference scenario was simulated to provide further insight into, and a means of verifying, the research presented in the RDAT report.

5.1 Derivation of the LO Processor with Memory for 1D Signalling[1]

The LO processor with memory for the case of 1D signalling is derived in [Drap89] as the solution to the following radar problem: After translation to baseband, consider the following two hypotheses:

[1] The notation for all of Section 5 follows the symbology introduced in [Drap89]. When necessary to clarify the meaning of an equation or expression, notation consistent with this report is also included.

$$H_1: \quad \bar{z}_N = \bar{s}_N + \bar{n}_N$$
$$H_0: \quad \bar{z}_N = \bar{n}_N \tag{5-1}$$

where $\bar{z}_N=[z_1,\ldots,z_N]^T$ is the vector of received signal samples, $\bar{s}_N=[s_1,\ldots,s_N]^T$ is the vector of transmitted signal samples and may be written as $\bar{s}_N = s\bar{c}_N = s[c_1,\ldots,c_N]^T$ with the set of $\{c_i\}$'s having amplitudes equal to ± 1 and where s is a constant, $\bar{n}_N=[n_1,\ldots,n_N]^T$ is the vector of total channel noise (thermal noise and jammer) samples, and N is the number of samples per symbol period. The N-point joint PDF of the channel noise is given by $f_n(\bar{n}_N)$. The following assumptions are made in the derivation:

- $\bar{c}_N$ and $\bar{n}_N$ (and thus $\bar{s}_N$ and $\bar{n}_N$) are statistically independent
- the signal of interest is much weaker than the total channel noise.

The LO processor is derived by considering the standard likelihood ratio test [VanT68]:

$$l \triangleq \frac{f_{z|H_1}(\bar{z}_N|H_1)}{f_{z|H_0}(z_N|H_0)} \underset{H_0}{\overset{H_1}{\gtrless}} \eta \tag{5-2}$$

or equivalently

$$\ln(l) = \ln\left[\frac{f_{z|H_1}(\bar{z}_N|H_1)}{f_{z|H_0}(z_N|H_0)}\right] \underset{H_0}{\overset{H_1}{\gtrless}} \ln(\eta) \tag{5-3}$$

since the natural logarithm is a monotonic function. Using the assumption that the signal and interference are statistically independent, l becomes

$$l = \frac{f_n(\bar{z}_N - \bar{s}_N)}{f_n(\bar{z}_N)} \tag{5-4}$$

Taking the natural logarithm of l and using the first order N-dimensional Taylor series expansion gives the expression

$$\begin{aligned} \ln(l) &= \ln(f_n(\bar{z}_N - \bar{s}_N)) - \ln(f_n(\bar{z}_N)) \\ &\approx \ln(f_n(\bar{z}_N)) - \left[\frac{d}{d\bar{z}_N}\ln(f_n(\bar{z}_N))\right]^T \bar{s}_N - \ln(f_n(\bar{z}_N)) \\ &\approx -\left[\frac{d}{d\bar{z}_N}\ln(f_n(\bar{z}_N))\right]^T \bar{s}_N \end{aligned} \tag{5-5}$$

where $\frac{d}{d\bar{z}_N}h(\bar{z}_N) = \left[\frac{\partial}{\partial z_1}h(\bar{z}_N),\ldots,\frac{\partial}{\partial z_N}h(\bar{z}_N)\right]^T$ is the gradient of $h(\bar{z}_N)$. The expression of Eq. (5-5) is a valid approximation due to the weak signal assumption. Substituting Eq. (5-5) into Eq. (5-3) results in the following form for the *LO detector with memory*:

$$L \triangleq \bar{G}_N^T \bar{s}_N = s\bar{G}_N^T \bar{c}_N \underset{H_0}{\overset{H_1}{\gtrless}} \ln(\eta) \tag{5-6}$$

or equivalently

$$L \triangleq \bar{G}_N^T \bar{c}_N \underset{H_0}{\overset{H_1}{\gtrless}} \frac{\ln(\eta)}{s} = \gamma \tag{5-7}$$

where $\bar{G}_N=[g_1,\ldots,g_N]^T$ with the nonlinearity at the ith instant, $g_i(\bar{z}_N)$, given by

$$g_i(\overline{z}_N) = -\frac{\partial}{\partial z_i}\ln(f_n(\overline{z}_N)) \tag{5-8}$$

5.1.1 Simplification of the LO Processor using Markov Processes

The LO processor of Eq. (5-7) requires the N-point joint PDF of the baseband channel noise. In practice, it is usually difficult to obtain this PDF either theoretically or through estimation techniques. However, if it is possible to model the channel noise using Markov random vectors, then generation of the joint PDF can be greatly simplified.

Recall that by using Bayes rule, an N-point joint PDF, $f_n(\overline{z}_N)$, of a random vector $\overline{n}$ may be written as [Woze65]:

$$\begin{aligned} f_n(\overline{z}_N) &= f_n(z_1, z_2, \ldots, z_N) = f_n(z_N \mid z_1, \ldots, z_{N-1}) f(z_1, \ldots, z_{N-1}) \\ &= f_n(z_N \mid z_1, \ldots, z_{N-1}) f_n(z_{N-1} \mid z_1, \ldots, z_{N-2}) f_n(z_1, \ldots, z_{N-2}) \\ &= \ldots \\ &= f_n(z_N \mid z_1, \ldots, z_{N-1}) f_n(z_{N-1} \mid z_1, \ldots, z_{N-2}) \cdots f_n(z_2 \mid z_1) f_n(z_1) \end{aligned} \tag{5-9}$$

However, if the vector $\overline{n}_N$ is an M^{th} order Markov random vector, then

$$f_n(z_j \mid z_1, \ldots, z_{j-1}) = f_n(z_j \mid z_{j-M}, \ldots, z_{j-1}) \tag{5-10}$$

In particular, if $\overline{n}_N$ is a first order Markov random vector, then $f_n(z_j \mid z_1, \ldots, z_{j-1}) = f_n(z_j \mid z_{j-1})$ and Eq. (5-9) reduces to

$$f_n(\overline{z}_N) = \prod_{j=1}^{N} f_n(z_j \mid z_{j-1}) \tag{5-11}$$

with $f_n(z_1 \mid z_0) \triangleq f_n(z_1)$.

Using Eq. (5-11) and assuming $\overline{n}_N$ is a first order Markov random vector, the nonlinearity at the i^{th} instant in Eq. (5-8) becomes

$$\begin{aligned} g_i(\overline{z}_N) &= -\frac{\partial}{\partial z_i}\ln(f_n(\overline{z}_N)) = -\frac{\partial}{\partial z_i}\ln\left[\prod_{j=1}^{N} f_n(z_j|z_{j-1})\right] \\ &= -\frac{\partial}{\partial z_i}\sum_{j=1}^{N}\ln(f_n(z_j|z_{j-1})) \\ &= -\frac{\partial}{\partial z_i}f_n(z_i|z_{i-1}) - \frac{\partial}{\partial z_i}f_n(z_{i+1}|z_i) \end{aligned} \tag{5-12}$$

or equivalently,

$$g_i(\overline{z}_N) = g_i(z_i|z_{i-1}) + g_i(z_{i+1}|z_i) \equiv g_i(z_{i-1},z_i,z_{i+1}) \tag{5-13}$$

where

$$g_i(z_i|z_{i-1}) \triangleq -\frac{\partial}{\partial z_i}\ln(f_n(z_i|z_{i-1})) \tag{5-14}$$

and

$$g_i(z_{i+1}|z_i) \triangleq -\frac{\partial}{\partial z_i}\ln(f_n(z_{i+1}|z_i)) \tag{5-15}$$

Thus, for the first order Markov case the general N-point nonlinear processor, $g_i(\overline{z}_N)$, becomes the simplified three point processor, $g_i(z_{i-1},z_i,z_{i+1})$, of Eq. (5-13). Finally, by incorporating the first order Markov nonlinearity of Eq. (5-13) into Eq. (5-7), the LO processor with memory reduces to the following expression:

$$L=\sum_{i=1}^{N} c_i g_i(z_{i-1},z_i,z_{i+1}) \underset{H_0}{\overset{H_1}{\gtrless}} \gamma \tag{5-16}$$

where $g_1(z_0,z_1,z_2) \triangleq g_1(z_1,z_2)$ and $g_N(z_{N-1},z_N,z_{N+1}) \triangleq g_N(z_{N-1},z_N)$.

The LO processor given in Eq. (5-16) for the first order Markov case may be further simplified to include only two point nonlinearities, $g_i(z_i,z_{i-1})$, by modifying the correlation sequence $\overline{c_N}$ in the following manner. Using Eq. (5-13) in Eq. (5-16), L becomes

$$L=\sum_{i=1}^{N} c_i[g_i(z_i|z_{i-1})+g_i(z_{i+1}|z_i)] \tag{5-17}$$

Manipulation of the summation indices provides the following system of equations:

$$\begin{aligned}
L&=\sum_{i=1}^{N} c_i g_i(z_i|z_{i-1})+\sum_{i=1}^{N} c_i g_i(z_{i+1}|z_i)\\
&=\sum_{i=1}^{N} c_i g_i(z_i|z_{i-1})+\sum_{i=2}^{N+1} c_{i-1} g_{i-1}(z_i|z_{i-1})\\
&=\sum_{i=1}^{N}[c_i g_i(z_i|z_{i-1})+c_{i-1} g_{i-1}(z_i|z_{i-1})]\\
&\qquad +c_N g_N(z_{N+1}|z_N)-c_0 g_0(z_1|z_0)\\
&=\sum_{i=1}^{N}\left[c_i+c_{i-1}\frac{g_{i-1}(z_i|z_{i-1})}{g_i(z_i|z_{i-1})}\right] g_i(z_i|z_{i-1})\\
&\qquad +c_N g_N(Z_{N+1}|z_N)-c_0 g_0(z_1|z_0)
\end{aligned} \tag{5-18}$$

Using Eq. (5-14) and noting that $f_n(z_i|z_{i-1}) \triangleq \frac{f_n(z_i,z_{i-1})}{f_n(z_{i-1})}$ [Woze65], $g_i(z_i|z_{i-1})$ may be written as:

$$g_i(z_i|z_{i-1}) = -\frac{\partial}{\partial z_i}\ln\left[\frac{f_n(z_i,z_{i-1})}{f_n(z_{i-1})}\right]$$

$$= -\frac{\partial}{\partial z_i}\ln[f_n(z_i,z_{i-1})] + \frac{\partial}{\partial z_i}\ln[f_n(z_{i-1})] \qquad \textbf{(5-19)}$$

$$= -\frac{\partial}{\partial z_i}\ln[f_n(z_i,z_{i-1})]$$

or

$$g_i(z_i|z_{i-1}) = g_i(z_i,z_{i-1}) \qquad \textbf{(5-20)}$$

where $g_i(z_i,z_{i-1}) \triangleq -\frac{\partial}{\partial z_i}\ln[f_n(z_i,z_{i-1})]$. In addition, a new correlating sequence, $\tilde{c}$, may be defined as $\tilde{c}_i = c_i + c_{i-1}\frac{g_{i-1}(z_i|z_{i-1})}{g_i(z_i|z_{i-1})}$. Thus, the 3-point test statistic of Eq. (5-16) reduces to the following 2-point test statistic [2]:

$$L = \sum_{i=1}^{N} \tilde{c}_i g_i(z_i,z_{i-1}) \qquad \textbf{(5-21)}$$

The resulting expression in Eq. (5-21) is the 2-point equivalent processor discussed in [Drap89][3].

---

[2] The processor given by Eq. (5-21) is derived from results presented in [Drap89] under the assumption that $c_N g_N(z_{N+1}|z_N) = 0$ and $c_0 g_0(z_1|z_0) = 0$. These conditions can be met by defining $c_0 = 0$ and $g_N(z_{N+1}|z_N) = 0$ since i = 1, ..., N. This was not explicitly stated in [Drap89].

[3] There is an error in Figure 2-4 of [Drap89]. The second processor in this figure is the equivalent 2-point processor. However, the block diagram indicates that three points are necessary. Thus, $g_i(z_{i+1},z_i,z_{i-1})$ should be replaced with $g_i(z_i,z_{i-1})$.

5.1.2 Derivation of the Theoretical LO Gain for 1D Signalling

It is possible to derive analytical expressions for the performance gain associated with the LO processor with memory if, under the central limit theorem [Woze65], the statistics of L are assumed to be Gaussian. Then, the probability of detection, P_D, and the probability of false alarm, P_F, for the nonlinear receiver are given by [Drap89]:

$$P_D = \mathrm{Erf}\left[\frac{\gamma - \langle L_1 \rangle}{\sigma_{L_1}}\right] \tag{5-22}$$

and

$$P_F = \mathrm{Erf}\left[\frac{\gamma - \langle L_0 \rangle}{\sigma_{L_0}}\right] \tag{5-23}$$

where $\langle L_1 \rangle$ and σ_{L_1} are the mean and standard deviation, respectively, of L under hypothesis H_1, $\langle L_0 \rangle$ and σ_{L_0} are the mean and standard deviation, respectively, of L under H_0, and $\mathrm{Erf}(x) = \frac{1}{\sqrt{2\pi}} \int_x^\infty e^{-\frac{x^2}{2}} dx$ [Drap85]. It can be shown [Drap85,Drap89] that Eqs. (5-22) and (5-23) are a function of the Signal-to-Noise Ratio (SNR) at the output of the LO processor, SNR_{TAP} [4], which is given by

[4] The term SNR_{TAP} is used here to be consistent with [Drap89]. In [Drap89], the LO processor with memory is called the *Time Amplitude Processor* (TAP), with corresponding output SNR equal to SNR_{TAP}.

$$SNR_{TAP_1} = \left[\frac{<L_1> - <L_0>}{\sigma_{L_1}} \right]^2$$

$$SNR_{TAP_0} = \left[\frac{<L_1> - <L_0>}{\sigma_{L_0}} \right]^2 \qquad \textbf{(5-24)}$$

under hypotheses H_1 and H_0, respectively. Since it is assumed that $\sigma_{L_0} \approx \sigma_{L_1}$, Eq. (5-24) becomes

$$SNR_{TAP} = \left[\frac{<L_1> - <L_0>}{\sigma_{L_0}} \right]^2 = SNR_{TAP_0} \approx SNR_{TAP_1} \qquad \textbf{(5-25)}$$

Thus, it is necessary to evaluate the quantities $(<L_1> - <L_0>)$ and σ_{L_0} in order to analytically specify the performance of the LO receiver.

The following is a sketch of the derivation presented in [Drap89] for the quantity $(<L_1> - <L_0>)$. The decision statistic, L, is given by [5]

$$L = \frac{1}{N} \overline{c_N}^T \hat{G}_N(\overline{z_N}) \qquad \textbf{(5-26)}$$

where $\hat{G}$ is used instead of $\overline{G}$ to indicate that this is the *actual* LO processor implementation, not the theoretically optimum one. The expression for $<L_l>$ is given by

---

[5] The $\frac{1}{N}$ scale factor is introduced in this equation in [Drap89] as a result of implementing the required summation for the LO receiver with a standard linear correlator. The effects of this scale factor can be removed by appropriately modifying the decision threshold.

$$<L_1> = \int_{\bar{z}_N} \int_{\bar{c}_N} \frac{1}{N} \bar{c}_N \hat{G}_N(\bar{z}_N) f_{z|H_1}(\bar{z}_N|H_1) f_c(\bar{c}_N) d\bar{z}_N d\bar{c}_N \qquad \textbf{(5-27)}$$

where $f_{z|H_1}(\cdot)$ is equivalent to $f_{z|c}(\cdot)$ since under hypothesis H_1 it is assumed that the vector $\bar{c}_N$ is transmitted. Assuming that the signal is much weaker than the channel interference, $f_{z|H_1}(\cdot)$ can be approximated using a Taylor series expansion as

$$\begin{aligned} f_{z|H_1}(\bar{z}_N|H_1) &= f_n(\bar{z}_N - \bar{s}_N) \\ &\approx (1 + \bar{s}_N^T \bar{G}_N(\bar{z}_N)) f_n(\bar{z}_N) \end{aligned} \qquad \textbf{(5-28)}$$

where $\bar{G}_N(\bar{z}_N)$ is given by Eqs. (5-7) and (5-8). Substituting Eq. (5-28) into Eq. (5-27) and identifying terms, it can be shown that

$$<L_1> - <L_0> \approx \frac{S}{N} \int_{\bar{z}_N} \int_{\bar{c}_N} \left[\bar{c}_N^T \hat{G}_N(\bar{z}_N) \bar{G}_N^T(\bar{z}_N) \bar{c}_N \right] f_n(\bar{z}_N) f_c(\bar{c}_N) d\bar{z}_N d\bar{c}_N \qquad \textbf{(5-29)}$$

or

$$<L_1> - <L_0> \approx \frac{S}{N} <\bar{c}_N^T \hat{G}_N(\bar{z}_N) \bar{G}_N^T(\bar{z}_N) \bar{c}_N>_{\bar{z}_N \bar{c}_N} \qquad \textbf{(5-30)}$$

where $<\cdot>_{\bar{z}_N \bar{c}_N}$ indicates expectation with respect to $\bar{z}_N$ (under H_0) and $\bar{c}_N$. Next, by assuming that the correlation matrix of $\bar{c}_N$ is the identity matrix [Drap89], and by using the identity $\overline{x^T y} = \mathrm{Tr}(\bar{x}\,\bar{y}^T)$, Eq. (5-30) becomes

$$<L_1> - <L_0> \approx \frac{s}{N}\mathrm{Tr}\left(<\hat{G}_N \overline{G}_N^T>_{\overline{z}_N}\right) \approx s K_m \tag{5-31}$$

where

$$K_m \triangleq \frac{1}{N}\mathrm{Tr}\left(<\hat{G}_N \overline{G}_N^T>_{\overline{z}_N}\right) = \frac{1}{N}\sum_{i=1}^{N} <\hat{g}_i g_i>_{\overline{z}_N} \tag{5-32}$$

The expression for σ_{L_0} can be derived as follows. Assuming that $<L_0> \approx 0$ because $\overline{z}_N = \overline{n}_N$ under H_0, then $\sigma_{L_0}^2 \approx <L_0^2>$. Using Eq. (5-26) and noting that $\overline{z}_N$ and $\overline{c}_N$ are statistically independent under H_0, the expression for $<L_0^2>$ is

$$<L_0^2> = \int_{\overline{z}_N}\int_{\overline{c}_N} \frac{1}{N^2}\left[\overline{c}_N^T \hat{G}_N \hat{G}_N^T \overline{c}_N\right] f_n(\overline{z}_N) f_c(\overline{c}_N)\, d\overline{z}_N d\overline{c}_N \tag{5-33}$$

Again assuming that the correlation matrix of $\overline{c}_N$ is the identity matrix, Eq. (5-33) reduces to

$$<L_0^2> = \frac{1}{N^2}\mathrm{Tr}<\hat{G}_N \hat{G}_N^T>_{\overline{z}_N} = \frac{K_v}{N} \tag{5-34}$$

where

$$K_v \triangleq \frac{1}{N}\mathrm{Tr}<\hat{G}_N\hat{G}_N^T>_{\bar{z}_w}$$
$$= \frac{1}{N}\sum_{i=1}^{N}<\hat{g}_i^2>_{\bar{z}_w} \tag{5-35}$$

Finally, by substituting Eqs. (5-32) and (5-35) into Eq. (5-25), the output SNR for the LO receiver becomes

$$SNR_{TAP} = s^2 N\frac{K_m^2}{K_v} = s^2 Nk \tag{5-36}$$

where

$$k \triangleq \frac{K_m^2}{K_v} \tag{5-37}$$

The expressions for K_m and K_v of Eqs. (5-32) and (5-35) may be simplified if the noise PDF, $f_n(\cdot)$, is spherically symmetric[6]. In this case, $<\hat{g}_i g_i> = <\hat{g}_j g_j> \triangleq <\hat{g}g>$ and $<\hat{g}_i^2> = <\hat{g}_j^2> \triangleq <\hat{g}^2>$ for all i and j, and Eqs. (5-32) and (5-35) reduce to

$$K_m = <\hat{g}g> \tag{5-38}$$

and

$$K_v = <\hat{g}^2> \tag{5-39}$$

---

[6] In [Drap89], the assumption of stationarity, not spherical symmetry, is used to obtain the results in Eqs. (5-38) and (5-39). However, stationarity does not guarantee that $<\hat{g}_i g_i> = <\hat{g}_j g_j>$ and $<\hat{g}_i^2> = <\hat{g}_j^2>$ for all i and j, as will be shown through simulation in Section 5.3.

The gain of the LO receiver relative to a linear receiver may be calculated by dividing Eq. (5-36) by the output SNR for a linear receiver. The output SNR for a linear receiver, SNR_{LR}, may be computed by substituting $\overline{z}_N$ for $\hat{G}_N(\overline{z}_N)$ in Eqs. (5-32) and (5-35), and using the result in Eq. (5-36). This gives the expression

$$SNR_{LR} = \frac{s^2 N}{\sigma_n^2} \tag{5-40}$$

where σ_n^2 is the variance of the total channel noise. Dividing Eq. (5-36) by Eq. (5-40), the resulting gain of the LO receiver relative to a linear receiver is given by

$$G_{TAP} \triangleq \frac{SNR_{TAP}}{SNR_{LR}} = \sigma_n^2 \frac{K_m^2}{K_v} = k\sigma_n^2 \tag{5-41}$$

The following is a summary of the assumptions made in the derivation of SNR_{TAP} and G_{TAP} :

- the signal of interest is much weaker than the total channel noise
- the statistics of L are Gaussian
- $\sigma_{L_0} \approx \sigma_{L_1}$
- $<L_0> \approx 0$, and thus $\sigma_{L_0}^2 \approx <L_0^2>$
- the individual samples of $\overline{c}_N$ are uncorrelated
- the vectors $\overline{z}_N$ and $\overline{c}_N$ are independent under hypothesis H_0.

5.2 Derivation of the LO Processor with Memory for 2D Signalling

Similar to the case of 1D signalling, the LO processor with memory for 2D signalling is derived in [Drap89] as the solution to the following radar problem: After translation of the

I and Q channels to baseband, consider the following two hypotheses:

$$\begin{aligned} H_1: \quad & x_i = S\cos(\alpha_i+\theta) + n_{x_i} \\ & y_i = S\sin(\alpha_i+\theta) + n_{y_i} \\ H_0: \quad & x_i = n_{x_i} \\ & y_i = n_{y_i} \end{aligned} \tag{5-42}$$

where (x_i,y_i) is the sample pair of the I and Q channels at the i^{th} instant, α_i is the i^{th} sample of the information sequence (phase modulation is assumed), S and θ are unknown amplitude and phase components associated with the channel, and (n_{x_i},n_{y_i}) is the sample pair of the total noise in the I and Q channels at the i^{th} instant. The following assumptions are made in the derivation of the LO processor:

- α_i is independent of S and θ
- α_i is independent of n_{x_i} and n_{y_i}
- S and θ are independent of n_{x_i} and n_{y_i}
- the underlying random noise process, $n(t)$, which when sampled in the I and Q channels produces n_{x_i} and n_{y_i}, is stationary and has zero mean
- the signal of interest is much weaker than the total channel noise.

The received signal under hypothesis H_1 of Eq. (5-42) can be written in a more compact form:

$$\overline{R}_i = \overline{S}_i + \overline{n}_i \tag{5-43}$$

where $\overline{R}_i = [x_i \; y_i]^T$, $\overline{S}_i = T(\alpha_i)\,\overline{\delta}(S,\theta)$ with

$$\overline{\delta}(S,\theta) = S\,\overline{e}(\theta) = S[\cos(\theta) \; \sin(\theta)]^T \tag{5-44}$$

representing the unknown parameters, and

$$T(\alpha_i) = \begin{bmatrix} \cos(\alpha_i) & -\sin(\alpha_i) \\ \sin(\alpha_i) & \cos(\alpha_i) \end{bmatrix} \tag{5-45}$$

representing the known parameters. The matrix $T(\alpha_i)$ of Eq. (5-45) has the following useful properties:

- $T^{-1}(\alpha_i) = T^T(\alpha_i)$
- $T(-\alpha_i) = T^T(\alpha_i)$, and
- $T(\alpha_i)\,T(\alpha_j) = T(\alpha_i + \alpha_j)$

The LO processor is derived from the standard likelihood ratio test [VanT68]:

$$l \underset{H_0}{\overset{H_1}{\gtrless}} \gamma \quad \text{where} \quad l \triangleq \frac{f_{r|H_1}(\overline{R}_1,\ldots,\overline{R}_N|H_1)}{f_{r|H_0}(\overline{R}_1,\ldots,\overline{R}_N|H_0)} \tag{5-46}$$

where N is the number of samples per signal period. Using the assumptions outlined at the beginning of Section 5.2, the conditional PDF $f_{r|H_1}(\cdot)$ can be written as

$$f_{r|H_1}(\overline{R}_1,\ldots,\overline{R}_N) = \int_{\overline{\delta}} f_{n|\delta}(\overline{R}_1-\overline{S}_1,\ldots,\overline{R}_N-\overline{S}_N|\,\overline{\delta}) f_{\delta|H_1}(\overline{\delta}|H_1)\,d\overline{\delta} \tag{5-47}$$

where $f_n(\cdot)$ is the joint PDF of $\overline{n}_i$, $i=1,\ldots,N$, and conditioning on H_1 implies that α_i is known. Also, from Eq. (5-42), $f_{r|H_0}(\cdot)$ is given by

$$f_{r|H_0}(\overline{R}_1,\ldots,\overline{R}_N|H_0) = f_n(\overline{R}_1,\ldots,\overline{R}_N) \tag{5-48}$$

Using Eqs. (5-47) and (5-48) in Eq. (5-46), the likelihood ratio becomes

$$l = \int_{\bar{\delta}} \frac{f_{n|\delta}(\bar{R}_1 - \bar{S}_1, \ldots, \bar{R}_N - \bar{S}_N | \bar{\delta})}{f_n(\bar{R}_1, \ldots, \bar{R}_N)} f_{\delta|H_1}(\bar{\delta}|H_1) d\bar{\delta}$$
$$= \int_{\bar{\delta}} l(\bar{\delta}) f_{\delta|H_1}(\bar{\delta}|H_1) d\bar{\delta} \quad \textbf{(5-49)}$$

where

$$l(\bar{\delta}) \triangleq \frac{f_{n|\delta}(\bar{R}_1 - \bar{S}_1, \ldots, \bar{R}_N - \bar{S}_N | \bar{\delta})}{f_n(\bar{R}_1, \ldots, \bar{R}_N)} \quad \textbf{(5-50)}$$

indicates the dependence of the likelihood ratio on $\bar{\delta}$, i.e. on the unknown amplitude and phase terms. Assuming that the desired signal, $\bar{S}_i$, is much weaker than the channel noise, $\bar{n}_i$, the expression for $l(\bar{\delta})$ may be approximated via a multidimensional Taylor series expansion as

$$l(\bar{\delta}) \approx 1 + \bar{\delta}^T \bar{L} - \frac{1}{2} \bar{\delta}^T M \bar{\delta} \quad \textbf{(5-51)}$$

where $\bar{L}$ is a [2x1] vector defined as

$$\bar{L} \triangleq \frac{-1}{f_n(\bar{R}_1, \ldots, \bar{R}_N)} \sum_{i=1}^{N} T^T(\alpha_i) \frac{\partial f_n(\bar{R}_1, \ldots, \bar{R}_N)}{\partial \bar{R}_i} \quad \textbf{(5-52)}$$

and M is the [2x2] matrix defined as

$$M \triangleq \frac{-1}{f_n(\bar{R}_1, \ldots, \bar{R}_N)} \sum_{i=1}^{N} \sum_{j=1}^{N} T^T(\alpha_i) \frac{\partial^2 f_n(\bar{R}_1, \ldots, \bar{R}_N)}{\partial \bar{R}_i \partial \bar{R}_j} T(\alpha_j) \quad \textbf{(5-53)}$$

Since the second order term, $\frac{1}{2} \bar{\delta}^T M \bar{\delta}$, is on the order of $\| \bar{\delta} \|^2 \triangleq \bar{\delta}^T \bar{\delta}$, M is replaced by its

average value [Drap89], $\bar{M}$, given by

$$\bar{M} = \int M(\bar{R}_1,\ldots,\bar{R}_N) f_n(\bar{R}_1,\ldots,\bar{R}_N) d\bar{R}_1 \ldots d\bar{R}_N \tag{5-54}$$

resulting in the following approximation of Eq. (5-51):

$$l(\bar{\delta}) \approx 1 + \bar{\delta}^t \bar{L} - \frac{1}{2} \bar{\delta}^t \bar{M} \bar{\delta} \tag{5-55}$$

5.2.1 Statistics for the LO Likelihood Ratio Assuming Known Signal Amplitude and Phase Offset

An interesting result may be observed if the likelihood ratio of Eq. (5-55) is examined for a known $\bar{\delta}$. If $\bar{\delta}$ is known, then the likelihood ratio of Eq. (5-49) reduces to $l = l(\delta)$ and the likelihood ratio test becomes

$$l(\bar{\delta}) \underset{H_0}{\overset{H_1}{\gtrless}} \gamma \tag{5-56}$$

An equivalent test statistic, as discussed in [Drap89], is

$$e^{l(\bar{\delta})} \underset{H_0}{\overset{H_1}{\gtrless}} e^{\gamma} \tag{5-57}$$

Furthermore, the expression in Eq. (5-55) for $l(\bar{\delta})$ may be written in a slightly different fashion by "completing the square" to yield

$$l(\bar{\delta}) \approx 1 - \frac{1}{2}(\bar{L}-\bar{M}\bar{\delta})^T\bar{M}^{-1}(\bar{L}-\bar{M}\bar{\delta}) + \frac{1}{2}\bar{L}^T\bar{M}\bar{L} \tag{5-58}$$

In addition, if the threshold, γ, is assumed to small, the approximation

$$e^{\gamma} \approx 1 + \gamma \tag{5-59}$$

may be used in Eq. (5-57). Finally, substituting Eqs. (5-58) and (5-59) into Eq. (5-57), and rearranging terms, yields the equivalent likelihood ratio test

$$\frac{\exp\left[-\frac{1}{2}(\bar{L}-\bar{M}\bar{\delta})^T\bar{M}^{-1}(\bar{L}-\bar{M}\bar{\delta})\right]}{\exp\left[-\frac{1}{2}\bar{L}^T\bar{M}\bar{L}\right]} \begin{matrix} H_1 \\ > \\ < \\ H_0 \end{matrix} \gamma \tag{5-60}$$

As may be seen, the likelihood ratio is a function of $\bar{L}$. Since the likelihood ratio is defined as a ratio of two PDFs, Eq. (5-60) may be interpreted as

$$\frac{f_L(\bar{L}|H_1)}{f_L(\bar{L}|H_0)} \begin{matrix} H_1 \\ > \\ < \\ H_0 \end{matrix} \gamma \tag{5-61}$$

where, from Eq. (5-60), $f_L(\bar{L}|H_1)$ is a Gaussian PDF with mean equal to $\bar{M}\bar{\delta}$, $f_L(\bar{L}|H_0)$ is a Gaussian PDF with zero mean, and both have a covariance matrix equal to $\bar{M}$. In this context, the decision statistic $\bar{L}$ may be considered to be a Gaussian random vector under both the hypotheses, H_1 and H_0. Thus, the development of Eq. (5-60) provides another argument, in addition to the central limit theorem, that the statistics of $\bar{L}$ are Gaussian.

5.2.2 Development of the LO Likelihood Ratio Assuming an Unknown Nonrandom Signal Amplitude and a Random Phase Offset

The most useful scenario to examine is when the signal amplitude is unknown, but not necessarily random, and the phase offset is a random variable. In this case, H_1 becomes a *composite hypothesis* [VanT68] because the overall problem is still a binary detection problem, but the received signal under H_1 is a function of a random variable, θ, and an unknown albeit nonrandom parameter S. Assuming S is a known parameter for the moment, the likelihood ratio for this scenario is given by [VanT68]

$$l = \frac{f_{r|H_1}(\overline{R}_1,\ldots,\overline{R}_N|H_1)}{f_{r|H_0}(\overline{R}_1,\ldots,\overline{R}_0|H_0)} = \frac{\int f_{r|\theta H_1}(\overline{R}_1,\ldots,\overline{R}_N|\theta,H_1) f_{\theta|H_1}(\theta|H_1)\,d\theta}{f_{r|H_0}(\overline{R}_1,\ldots,\overline{R}_N|H_0)} \qquad (5\text{-}62)$$

Now, for the case when S is unknown, it is intuitively obvious that the detector with the best performance will be one that is able to measure S perfectly and then use this value in the optimum likelihood ratio test. However, in most cases this type of detector is unrealizable due to errors caused by the channel noise. Thus. one logical method for constructing the likelihood ratio is to first estimate S and then use this estimate in the likelihood ratio test as if it were exact. One possible estimator for S is the Maximum Likelihood Estimate (MLE), denoted by $\hat{S}_{ml}$. The value of $\hat{S}_{ml}$ is equal to the value of S which maximizes $f_{r|s}(\overline{R}_1,\ldots,\overline{R}_N|S)$ [7], or in other words, $\hat{S}_{ml}$ is the value of S most likely to have produced the given value of the received signal vector. Using the above argument, one can construct the *Generalized Likelihood Ratio* (GLR) [VanT68], which in this case is

[7] This is the reason why one of the main focal points of Section 3.2.2.2.1 of [Drap89] is determining the value of S which maximizes the decision statistic, l.

$$l_g = \frac{f_{r|S,H_1}(\overline{R}_1,\ldots,\overline{R}_N|S,H_1)|_{S=\hat{S}_{ml}}}{f_{r|H_0}(\overline{R}_1,\ldots,\overline{R}_N|H_0)}$$

$$= \frac{\max\limits_{S} f_{r|S,H_1}(\overline{R}_1,\ldots\overline{R}_N|S,H_1)}{f_{r|H_0}(\overline{R}_1,\ldots,\overline{R}_N|H_0)} \qquad \textbf{(5-63)}$$

Using the development of Eq. (5-63), Eq. (5-62) can be modified to yield the GLR for the case of unknown nonrandom signal amplitude and random phase offset

$$l_g = \frac{\max\limits_{S} \int_\theta f_{r|\theta\, S\, H_1}(\overline{R}_1,\ldots,\overline{R}_N|\theta,S,H_1) f_{\theta|S\,H_1}(\theta|S,H_1)\,d\theta}{f_{r|H_0}(\overline{R}_1,\ldots,\overline{R}_N|H_0)} \qquad \textbf{(5-64)}$$

But $f_{r|\theta SH_1}(\overline{R}_1,\ldots,\overline{R}_N|\theta,S,H_1) = f_{n|\delta}(\overline{R}_1-\overline{S}_1,\ldots,\overline{R}_N-\overline{S}_N|\overline{\delta})$ and $f_{r|H_0}(\overline{R}_1,\ldots,\overline{R}_0|H_0) = f_n(\overline{R}_1,\ldots,\overline{R}_N)$.

Also, $f_{\theta|SH_1}(\cdot) = f_{\theta|H_1}(\cdot)$ since S and θ are assumed to be statistically independent. Thus

$$l_g = \max_S \int \frac{f_{n|\delta}(\overline{R}_1-\overline{S}_1,\ldots,\overline{R}_N-\overline{S}_N|\overline{\delta})}{f_n(\overline{R}_1,\ldots,\overline{R}_N)} f_{\theta|H_1}(\theta|H_1)\,d\theta$$

$$= \max_S \int_\theta l(\overline{\delta})\, f_{\theta|H_1}(\theta|H_1)\,d\theta \qquad \textbf{(5-65)}$$

$$= <\max_S\ l(S,\theta)>_\theta$$

where $<\cdot>_\theta$ indicates expectation with respect to θ.

Substituting Eq. (5-44) into Eq. (5-51) yields the following LO expression for $l(\overline{\delta})$:

$$l(\bar{\delta}) = l(S,\theta) = 1 + S\,\bar{e}(\theta)^T\bar{L} - \frac{1}{2}S^2\bar{e}(\theta)^T\bar{M}\,\bar{e}(\theta) \tag{5-66}$$

Provided that $\bar{M} > 0$, the maximum of $l(S,\theta)$ with respect to S occurs when

$$S = S^*(\theta) = \frac{\bar{e}(\theta)^T\bar{L}}{\bar{e}(\theta)^T\bar{M}\,\bar{e}(\theta)} \tag{5-67}$$

Substituting Eq. (5-67) into Eq. (5-66) produces the expression

$$\max_S l(S,\theta) = l(S^*,\theta) = 1 + \frac{1}{2}\frac{(\bar{e}(\theta)^T\bar{L})^2}{\bar{e}(\theta)^T\bar{M}\,\bar{e}(\theta)} \tag{5-68}$$

Using Eq. (5-68) in Eq. (5-65) yields the generalized likelihood ratio test

$$<\frac{1}{2}(\bar{e}(\theta)^T\bar{L})^2>_\theta \underset{H_0}{\overset{H_1}{\gtrless}} \tilde{\gamma} < \bar{e}(\theta)^T\bar{M}\,\bar{e}(\theta)>_\theta \tag{5-69}$$

where $\tilde{\gamma} = \gamma - 1$. Using the identity

$$<\bar{e}(\theta)^T\bar{M}\,\bar{e}(\theta)>_\theta = \mathrm{Tr}\left[\bar{M} < \bar{e}(\theta)\,\bar{e}(\theta)^T>_\theta\right] \tag{5-70}$$

and assuming that θ is uniformly distributed over the interval $[0,2\pi)$ yields the result

$$\begin{aligned} <\bar{e}(\theta)^T\bar{M}\,\bar{e}(\theta)>_\theta &= \mathrm{Tr}\left[\bar{M} < \bar{e}(\theta)\,\bar{e}(\theta)^T>_\theta\right] \\ &= \frac{1}{2}\mathrm{Tr}[\bar{M}] \end{aligned} \tag{5-71}$$

since $<\bar{e}(\theta)\,\bar{e}(\theta)^T>_\theta$ is a two dimensional identity matrix. Similarly, it can be shown that

$$<(\bar{e}(\theta)^T\bar{L})^2>_\theta = \bar{L}^T\bar{L} \triangleq \|\bar{L}\|^2 \tag{5-72}$$

Substituting Eqs. (5-71) and (5-72) in Eq. (5-69) gives the expression

$$\frac{1}{2}\frac{\|\bar{L}\|^2}{\mathrm{Tr}[\bar{M}]} \underset{H_0}{\overset{H_1}{\gtrless}} \tilde{\gamma} \tag{5-73}$$

Finally, recalling the discussion in Section 5.2.1, $\bar{M}$ may be though of as the covariance matrix of $\bar{L}$, and as such

$$\begin{aligned} \mathrm{Tr}[\bar{M}] &= \mathrm{Tr} < \bar{L}\bar{L}^T >_{\bar{R}} \\ &= < \bar{L}^T \bar{L} >_{\bar{R}} \\ &\triangleq < \|\bar{L}_0\|^2 >_{\bar{R}} \end{aligned} \tag{5-74}$$

where $< \cdot >_{\bar{R}}$ indicates expectation with respect to the received signal under H_0 (the channel noise) [8]. Thus, the resulting LO likelihood ratio test for the case of an unknown nonrandom signal amplitude and a random phase offset is

$$\frac{1}{2}\frac{\|\bar{L}\|^2}{< \|\bar{L}_0\|^2 >} \underset{H_0}{\overset{H_1}{\gtrless}} \gamma \tag{5-75}$$

5.2.3 Derivation of the Theoretical LO Gain for 2D Signalling

The performance measures of interest, as in the case for 1D signalling, are P_D and P_F. Similar to the 1D signalling case, and discussed in [Drap85], the output signal to noise ratio,

---

[8] This result is presented in [Drap89]. Note that for Eq. (5-74) to be true, the covariance matrix of $\bar{L}$ under H_1 must be approximately equal to the covariance matrix of $\bar{L}$ under H_0, and the mean of $\bar{L}$ under H_0 must be approximately equal to the zero vector. These assumptions were not explicitly stated in [Drap89].

SNR_{TAP}, of the LO processor determines the performance. SNR_{TAP} is given by the expression [Drap89][9]

$$SNR_{TAP} = E\left\{ \frac{\| <\overline{L}_1 | \overline{\delta}> - <\overline{L}_0 | \overline{\delta}> \|^2}{<\| \overline{L}_0 \|^2>} \right\}_{\overline{\delta}} \tag{5-76}$$

where $< \cdot >$ represents expectation with respect to the information sequence and the received signal under hypothesis H_0 or H_1 as required, and $E\{\cdot\}_{\overline{\delta}}$ indicates expectation with respect to $\overline{\delta}$.

As indicated in Eq. (5-76), the terms required to evaluate SNR_{TAP} are calculated given $\overline{\delta}$, and then the result is averaged with respect to S, or θ, or both depending on the given scenario. Recalling Eq. (5-52), the expression for $\overline{L}$ may be written as

$$\overline{L} = \sum_{i=1}^{N} T^T(\alpha_i)\, \hat{G}_i(\overline{R}_1, \ldots, \overline{R}_N) \tag{5-77}$$

where $\hat{G}_i(\overline{R}_1, \ldots, \overline{R}_N)$ represents the implemented/approximated version of

$$\overline{G}_i(\overline{R}_1, \ldots, \overline{R}_N) = -\frac{1}{f_n(\overline{R}_1, \ldots, \overline{R}_N)} \frac{\partial f_n(\overline{R}_1, \ldots, \overline{R}_N)}{\partial \overline{R}_i} \tag{5-78}$$

in Eq. (5-52). Since α_i, $\overline{\delta}$, and $\overline{n}_i$ are independent, and since the received signal under hypothesis H_1 is a function of all three of these variables, the expression for $<\overline{L}|\overline{\delta}>$ may be written as

---

[9] Note that in [Drap89] the required conditioning on $\overline{\delta}$ was omitted.

$$<\bar{L}_1|\bar{\delta}> = \int_{\bar{\alpha}_N}\int_{\bar{R}} \bar{L} f_{R,\alpha}(\bar{R}_1,\ldots,\bar{R}_N,\bar{\alpha}_N|\bar{\delta})\,d\bar{R}_1\ldots d\bar{R}_N d\bar{\alpha}_N$$
$$= \int_{\bar{\alpha}_N}\int_{\bar{R}} \bar{L} f_n(\bar{R}_1-\bar{S}_1,\ldots,\bar{R}_N-\bar{S}_N) f_\alpha(\bar{\alpha}_N)\,d\bar{R}_1\ldots d\bar{R}_N d\bar{\alpha}_N \quad \textbf{(5-79)}$$

where $\bar{\alpha}_N = [\alpha_1,\ldots,\alpha_N]^T$. Assuming that the signal is much weaker than the channel noise, a first order multidimensional Taylor series expansion of $f_n(\cdot)$ may be used, resulting in the expression

$$f_n(\bar{R}_1-\bar{S}_1,\ldots,\bar{R}_N-\bar{S}_N) \approx f_n(\bar{R}_1,\ldots,\bar{R}_N)\left[1+S\sum_{j=1}^{N}\bar{G}_j^T(\bar{R}_1,\ldots,\bar{R}_N)\,T(\alpha_j)\,\bar{e}(\theta)\right] \quad \textbf{(5-80)}$$

where

$$\bar{G}_j = -\frac{\partial}{\partial \bar{R}_j}\ln\left[f_n(\bar{R}_1,\ldots,\bar{R}_N)\right] \quad \textbf{(5-81)}$$

Using Eqs. (5-77) and (5-80) in Eq. (5-79), and identifying the term that represents $<\bar{L}_0|\bar{\delta}> = <\bar{L}_0>$, yields the following result

$$<\bar{L}_1|\bar{\delta}> - <\bar{L}_0|\bar{\delta}> = SNK_m\,\bar{e}(\theta) \quad \textbf{(5-82)}$$

where K_m is the [2x2] matrix defined as

$$K_m \triangleq \frac{1}{N}\sum_{i=1}^{N}\sum_{j=1}^{N} <T^T(\alpha_i)\,\hat{G}_i\bar{G}_j^T\,T(\alpha_j)>_{\bar{R},\bar{\alpha}_N} \quad \textbf{(5-83)}$$

where $<\cdot>_{\bar{R},\bar{\alpha}_N}$ indicates expectation with respect to the received signal and $\bar{\alpha}_N$. Since in the approximation of Eq. (5-80), the received signal is assumed to be nearly equal to the noise, and $\bar{n}_i$ and α_i are assumed to be independent, Eq. (5-83) may be written as

$$K_m \approx \frac{1}{N}\sum_{i=1}^{N}\sum_{j=1}^{N} < T^T(\alpha_i) < \hat{G}_i \overline{G}_j^T >_{\overline{R}} T(\alpha_j) >_{\overline{\alpha}_N} \quad \textbf{(5-84)}$$

Finally, if it is assumed that α_i is independent of α_j, and that α_i is uniformly distributed over the region $[0,2\pi)$, then the expression for K_m simplifies to

$$K_m \approx \frac{1}{N}\sum_{i=1}^{N} < T^T(\alpha_i) < \hat{G}_i \overline{G}_i^T >_{\overline{R}} T(\alpha_i) >_{\overline{\alpha}_N} \quad \textbf{(5-85)}$$

The expression for $< \| \overline{L}_0 \|^2 >$ is given by:

$$< \| \overline{L}_0 \|^2 > = < \| \overline{L}_0 \|^2 | \overline{\delta} > = \int_{\overline{\alpha}_N} \int_{\overline{R}} \| \overline{L} \|^2 f_n(\overline{R}_1,\ldots,\overline{R}_N) f_\alpha(\overline{\alpha}_N)\, d\overline{R}_1 \ldots d\overline{R}_N d\overline{\alpha}_N \quad \textbf{(5-86)}$$

Substituting Eq. (5-77) into Eq. (5-86) yields the following expression for $< \| \overline{L}_0 \|^2 >$

$$< \| \overline{L}_0 \|^2 > = N K_v \quad \textbf{(5-87)}$$

where K_v is the scalar parameter defined as

$$K_v \triangleq \frac{1}{N}\sum_{i=1}^{N}\sum_{j=1}^{N} < \hat{G}_i^T T(\alpha_i) T^T(\alpha_j) \hat{G}_j >_{\overline{R},\overline{\alpha}_N} \quad \textbf{(5-88)}$$

Again, since $\overline{n}_i$ is independent of α_i, and if it is assumed that α_i is independent of α_j, with α_i uniformly distributed over the region $[0,2\pi)$, the Eq. (5-88) reduces to

$$K_v = \frac{1}{N}\sum_{i=1}^{N} < \hat{G}_i^T \hat{G}_i >_{\overline{R}} \quad \textbf{(5-89)}$$

The expressions for K_m and K_v of Eqs. (5-85) and (5-89) may be simplified if the noise

PDF, $f_n(\cdot)$ is spherically symmetric [10]. In this case, $<\hat{G}_i\overline{G}_i^T> = <\hat{G}_j\overline{G}_j^T> \triangleq <\hat{G}\overline{G}^T>$ and $<\hat{G}_i^T\hat{G}_i> = <\hat{G}_j^T\hat{G}_j> \triangleq <\hat{G}^T\hat{G}>$ for all i and j, and Eqs. (5-85) and (5-89) reduce to

$$K_m = <\hat{G}\overline{G}^T> \tag{5-90}$$

and

$$K_v = <\hat{G}^T\hat{G}> \tag{5-91}$$

Finally, substituting Eqs. (5-82) and (5-87) into Eq. (5-76) yields the following expression for SNR_{TAP}:

$$SNR_{TAP} = \frac{N}{K_v} E\left\{S^2 \| K_m \overline{e}(\theta) \|^2\right\}_{\overline{\delta}} \tag{5-92}$$

For the case when S is deterministic and θ is uniform over $[0,2\pi)$, Eq. (5-92) becomes

$$SNR_{TAP} = \frac{S^2 N}{K_v} \frac{1}{2\pi} \int_0^{2\pi} \overline{e}^T K_m^T K_m \overline{e}\, d\theta \tag{5-93}$$

or

$$SNR_{TAP} = \frac{S^2 N}{K_v} \mathrm{Tr}\left[K_m K_m^T \frac{1}{2\pi} \int_0^{2\pi} \overline{e}\overline{e}^T d\theta \right] \tag{5-94}$$

However, since θ is uniform over $[0,2\pi)$

---

[10] In [Drap89], the assumption of stationarity, not spherical symmetry, is used to obtain the results in Eqs. (5-90) and (5-91). However, stationarity does not guarantee that $<\hat{G}_i\overline{G}_i^T> = <\hat{G}_j\overline{G}_j^T>$ and $<\hat{G}_i^T\hat{G}_i> = <\hat{G}_j^T\hat{G}_j>$ for all i and j, as will be shown through simulation in Section 5.3.

$$\frac{1}{2\pi}\int_0^{2\pi} \overline{e}\,\overline{e}^T d\theta = \frac{1}{2}\begin{bmatrix} 1 & 0 \\ 0 & 1 \end{bmatrix} \tag{5-95}$$

Thus, Eq. (5-94) reduces to

$$SNR_{TAP} = S^2 N \frac{\mathrm{Tr}\left[K_m K_m^T\right]}{2K_v} \tag{5-96}$$

The theoretical gain of the LO processor relative to a linear receiver, G_{TAP}, may be computed by taking the ratio of SNR_{TAP} to the output SNR of a linear receiver, SNR_{LR}. The expression for SNR_{LR} is calculated by using $\hat{G}_i = [x_i \; y_i]^T$ to evaluate K_m and K_v in Eq. (5-96). Evaluating $<\hat{G}_i \overline{G}_j^T>_{\overline{R}}$ in Eq. (5-84) for $\hat{G}_i = [x_i, y_i]^T$ yields

$$<\hat{G}_i \overline{G}_j^T>_{\overline{R}} = -\int_{\overline{R}} Q(\overline{R}_1,\ldots,\overline{R}_N)\, d\overline{R}_1,\ldots,d\overline{R}_N \tag{5-97}$$

where

$$Q(\overline{R}_1,\ldots,\overline{R}_N) = \begin{bmatrix} x_i \dfrac{\partial f_n(\overline{R}_1,\ldots,\overline{R}_N)}{\partial x_j} & x_i \dfrac{\partial f_n(\overline{R}_1,\ldots,\overline{R}_N)}{\partial y_j} \\ y_i \dfrac{\partial f_n(\overline{R}_1,\ldots,\overline{R}_N)}{\partial x_j} & y_i \dfrac{\partial f_n(\overline{R}_1,\ldots,\overline{R}_N)}{\partial y_j} \end{bmatrix} \tag{5-98}$$

Evaluating the two off-diagonal terms, and assuming that the tails of $f_n(\cdot)$ approach zero as x_j and y_j approach $\pm\infty$, yields

$$-\int_{\overline{R}} x_i \frac{\partial f_n(\overline{R}_1,\ldots,\overline{R}_N)}{\partial y_j} d\overline{R}_1 \ldots d\overline{R}_N = -\int_{\substack{\overline{R} \\ \text{except } y_j}} x_i f_n(\overline{R}_1,\ldots,\overline{R}_N)\Big|_{y_j=-\infty}^{y_j=\infty} d\overline{R}_1 .. d\overline{R}_{j-1} dx_j d\overline{R}_{j+1} .. d\overline{R}_N = 0 \tag{5-99}$$

and

$$-\int_{\overline{R}} y_i \frac{\partial f_n(\overline{R}_1,\ldots,\overline{R}_N)}{\partial y_j} d\overline{R}_1 \ldots d\overline{R}_N = -\int_{\substack{\overline{R} \\ \text{except } x_j}} y_i f_n(\overline{R}_1,\ldots,\overline{R}_N)\Big|_{x_j=-\infty}^{x_j=\infty} d\overline{R}_1 .. d\overline{R}_{j-1} dy_j d\overline{R}_{j+1} .. d\overline{R}_N = 0 \tag{5-100}$$

For $i=j$, using integration by parts the diagonal terms of Eq. (5-97) reduce to

$$-\int_{\overline{R}} x_i \frac{\partial f_n}{\partial x_i} d\overline{R}_1 \ldots d\overline{R}_N = -\int_{\substack{y_1,\ldots,y_N \\ \text{except } y_i}} x_i f_n(\overline{R}_1,\ldots,\overline{R}_N)\Big|_{x_i=-\infty}^{x_i=+\infty} dy_1 .. dy_{i-1} dy_{i+1} .. dy_N + \int_{\overline{R}} f_n(\overline{R}_1 \ldots \overline{R}_N) d\overline{R}_1 \ldots d\overline{R}_N$$

$$= \int_{\overline{R}} f_n(\overline{R}_1,\ldots,\overline{R}_N) d\overline{R}_1 \ldots d\overline{R}_N$$

$$= 1 \tag{5-101}$$

and

$$-\int_{\overline{R}} y_i \frac{\partial f_n}{\partial y_i} d\overline{R}_1 \ldots d\overline{R}_N = -\int_{\substack{x_1,\ldots,x_N \\ \text{except } x_i}} y_i f_n(\overline{R}_1,\ldots,\overline{R}_N)\Big|_{y_i=-\infty}^{y_i=+\infty} dx_1 \ldots dx_{i-1} dx_{i+1} \ldots dx_N + \int_{\overline{R}} f_n(\overline{R}_1 \ldots \overline{R}_N) d\overline{R}_1 \ldots d\overline{R}_N$$

$$= \int_{\overline{R}} f_n(\overline{R}_1,\ldots,\overline{R}_N) d\overline{R}_1 \ldots d\overline{R}_N$$

$$= 1 \qquad \textbf{(5-102)}$$

Note in the above the tails of $f_n(\cdot)$ are assumed to decay to zero as x_i and y_i approach $\pm\infty$. For $i \neq j$, the diagonal terms of Eq. (5-97) reduce to

$$-\int_{\overline{R}} x_i \frac{\partial f_n}{\partial x_j} d\overline{R}_1,\ldots,d\overline{R}_N = -\int_{\substack{\overline{R}_1,\ldots,\overline{R}_N \\ \text{except } x_j}} x_i f_n(\overline{R}_1,\ldots,\overline{R}_N)\Big|_{x_j=-\infty}^{x_j=+\infty} d\overline{R}_1 \ldots \overline{R}_{j-1} dy_j d\overline{R}_{j+1} \ldots d\overline{R}_N = 0 \qquad \textbf{(5-103)}$$

and

$$-\int_{\overline{R}} y_i \frac{\partial f_n}{\partial y_j} d\overline{R}_1,\ldots,d\overline{R}_N = -\int_{\substack{\overline{R}_1,\ldots,\overline{R}_N \\ \text{except } y_j}} y_i f_n(\overline{R}_1,\ldots,\overline{R}_N)\Big|_{y_j=-\infty}^{y_j=+\infty} d\overline{R}_1 \ldots \overline{R}_{j-1} dx_j d\overline{R}_{j+1} \ldots d\overline{R}_N = 0 \qquad \textbf{(5-104)}$$

again since the tails of the channel noise PDF are assumed to decay to zero. Substituting the results of Eqs. (5-99) through (5-104) into Eq. (5-84), and noting that $T^T(\alpha_i)T(\alpha_i)$ is the two dimensional identity matrix, $K_{m_{LS}}$ becomes

$$K_{m_{LR}} = I_{2x2} \tag{5-105}$$

where

$$I_{2x2} \triangleq \begin{bmatrix} 1 & 0 \\ 0 & 1 \end{bmatrix} \tag{5-106}$$

To evaluate $K_{v_{LR}}$, $\hat{G}_i = [x_i, y_i]^T$ is substituted into Eq. (5-88) which yields the expression

$$K_{v_{LR}} = \sigma_n^2 \triangleq \sigma_x^2 + \sigma_y^2 \tag{5-107}$$

where

$$\begin{aligned} \sigma_x^2 = \sigma_{x_i}{}^2 &= \int_{\overline{R}} x_i^2 f_n(\overline{R}_1, \ldots, \overline{R}_N)\, d\overline{R}_1 \ldots d\overline{R}_N \;, \quad \text{for all } i \\ \sigma_y^2 = \sigma_{y_i}{}^2 &= \int_{\overline{R}} y_i^2 f_n(\overline{R}_1, \ldots, \overline{R}_N)\, d\overline{R}_1 \ldots d\overline{R}_N \;, \quad \text{for all } i \end{aligned} \tag{5-108}$$

Substituting Eq. (5-105) and (5-108) into Eq. (5-96) yields the following result for SNR_{LR} :

$$SNR_{LR} = \frac{S^2 N}{\sigma_n^2} \tag{5-109}$$

Finally, dividing Eq. (5-96) by (5-109) yields the expression for G_{TAP} :

$$G_{TAP} = \frac{\sigma_n^2 \mathrm{Tr}\left[K_m K_m^T\right]}{2 K_v} \tag{5-110}$$

5.2.4 Theoretical LO Output SNR and Gain for BPSK Modulation

The derivation of SNR_{TAP} and G_{TAP} for the case of BPSK modulation is examined in this section. For BPSK, $\alpha_i = 0°$ or $180°$ and $T(\alpha_i)$ is

$$T(\alpha_i) = \begin{cases} I_{2x2} & \text{for } \alpha_i = 0° \\ -I_{2x2} & \text{for } \alpha_i = 180° \end{cases} \tag{5-111}$$

Thus, K_m becomes

$$K_m = \frac{1}{N}\sum_{i=1}^{N} <\hat{G}_i \overline{G}_i^T>_{\overline{R}} \tag{5-112}$$

By defining $\overline{G}_i(\overline{R}_1,\ldots,\overline{R}_N)$ as

$$\overline{G}_i = \left[G_{x_i}(\overline{x}_N, \overline{y}_N) \quad G_{y_i}(\overline{x}_N, \overline{y}_N)\right]^T \tag{5-113}$$

where

$$\begin{aligned} G_{x_i} &\triangleq -\frac{\partial}{\partial x_i}\ln\left[f_n(\overline{R}_1,\ldots,\overline{R}_N)\right] \\ G_{y_i} &\triangleq -\frac{\partial}{\partial y_i}\ln\left[f_n(\overline{R}_1,\ldots,\overline{R}_N)\right] \end{aligned} \tag{5-114}$$

and $\hat{G}_i = [\hat{G}_{x_i} \ \hat{G}_{y_i}]^T$ as the implementation/approximation of $\overline{G}_i = [G_{x_i} \ G_{y_i}]^T$, K_m may be written as

$$K_m = \frac{1}{N}\sum_{i=1}^{N} \begin{bmatrix} K_{m_{xx_i}} & K_{m_{xy_i}} \\ K_{m_{yx_i}} & K_{m_{yy_i}} \end{bmatrix} \tag{5-115}$$

where

$$
\begin{aligned}
K_{m_{x_i}} &= \int \hat{G}_{x_i} G_{x_i} f_n(\bar{x}_N, \bar{y}_N) d\bar{x}_N d\bar{y}_N \\
K_{m_{y_i}} &= \int \hat{G}_{y_i} G_{y_i} f_n(\bar{x}_n, \bar{y}_N) d\bar{x}_N d\bar{y}_N \\
K_{m_{x_i}} &= \int \hat{G}_{y_i} G_{x_i} f_n(\bar{x}_N, \bar{y}_N) d\bar{x}_N d\bar{y}_N \\
K_{m_{y_i}} &= \int \hat{G}_{x_i} G_{y_i} f_n(\bar{x}_N, \bar{y}_N) d\bar{x}_N d\bar{y}_N
\end{aligned}
\tag{5-116}
$$

Also, K_v becomes

$$
K_v = \frac{1}{N} \sum_{i=1}^{N} \left(K_{v_{x_i}} + K_{v_{y_i}} \right) \tag{5-117}
$$

where

$$
\begin{aligned}
K_{v_{x_i}} &= \int \hat{G}_{x_i}^2 f_n(\bar{x}_N, \bar{y}_N) d\bar{x}_N d\bar{y}_N \\
K_{v_{y_i}} &= \int \hat{G}_{y_i}^2 f_n(\bar{x}_N, \bar{y}_N) d\bar{x}_N d\bar{y}_N
\end{aligned}
\tag{5-118}
$$

Substituting Eqs. (5-115) and (5-117) into Eq. (5-96) yields the resulting expression for SNR_{TAP} for BPSK:

$$
SNR_{TAP} = \frac{S^2 \left[\sum_{i=1}^{N} \sum_{j=1}^{N} K_{M_{x_i}} K_{m_{x_j}} + \sum_{i=1}^{N} \sum_{j=1}^{N} K_{m_{y_i}} K_{m_{y_j}} + \sum_{i=1}^{N} \sum_{j=1}^{N} K_{m_{x_i}} K_{m_{x_j}} + \sum_{i=1}^{N} \sum_{j=1}^{N} K_{m_{x_i}} K_{m_{x_j}} \right]}{2 \sum_{i=1}^{N} \left(K_{v_{x_i}} + K_{v_{y_i}} \right)} \tag{5-119}
$$

Similarly, G_{TAP} for the case of BPSK modulation is:

$$G_{TAP} = \frac{\sigma_n^2 \left[\sum_{i=1}^{N} \sum_{j=1}^{N} K_{M_{x_i}} K_{m_{x_j}} + \sum_{i=1}^{N} \sum_{j=1}^{N} K_{m_{y_i}} K_{m_{y_j}} + \sum_{i=1}^{N} \sum_{j=1}^{N} K_{m_{y_i}} K_{m_{y_j}} + \sum_{i=1}^{N} \sum_{j=1}^{N} K_{m_{x_i}} K_{m_{x_j}} \right]}{2N \sum_{i=1}^{N} \left(K_{v_{x_i}} + K_{v_{y_i}} \right)} \tag{5-120}$$

If the channel noise PDF, $f_n(\cdot)$, is spherically symmetric, the expressions for SNR_{TAP} and G_{TAP} may be greatly simplified. In this case, $K_{m_{x_i}} = K_{m_{x_j}} \triangleq K_{m_x}$, $K_{m_{y_i}} = K_{m_{y_j}} \triangleq K_{m_y}$, $K_{m_{y_i}} = K_{m_{y_j}} \triangleq K_{m_y}$, $K_{m_{x_i}} = K_{m_{x_j}} \triangleq K_{m_x}$, and also $K_{v_{x_i}} = K_{v_{x_j}} \triangleq K_{v_x}$ and $K_{v_{y_i}} = K_{v_{y_j}} \triangleq K_{v_y}$ for all i and j. Thus, Eqs. (5-119) and (5-120) simplify to

$$SNR_{TAP} = \frac{S^2 N \left(K_{m_x}^2 + K_{m_y}^2 + K_{m_y}^2 + K_{m_x}^2 \right)}{2 \left(K_{v_x}^2 + K_{v_y}^2 \right)} \tag{5-121}$$

and

$$G_{TAP} = \frac{\sigma_n^2 \left(K_{m_x}^2 + K_{m_y}^2 + K_{m_y}^2 + K_{m_x}^2 \right)}{2 \left(K_{v_x}^2 + K_{v_y}^2 \right)} \tag{5-122}$$

5.3 Simulation Results for the LO Processor with Memory

To provide insight into the RDAT theory and methodology, and to provide a means of verification, an interference scenario discussed in [Drap89] was simulated using the MATLAB™ software package by The Math Works, Inc. The scenario, depicted in Fig. (5-1), involves 1D

signalling and a channel interference consisting of: i) additive white Gaussian noise, *w(n)*, with variance given by σ_w^2, and ii) colored Gaussian noise, *j(n)*, with variance given by σ_c^2. The sequence *j(n)* is obtained as the output of an N-point Moving Average (MA) process, whose input is white Gaussian noise, *v(n)*, having variance equal to σ_c^2. Thus, the colored Gaussian noise sequence, *j(n)*, is given by the equation

$$j(n) = \frac{1}{\sqrt{N}} \sum_{k=0}^{N-1} v(n-k) \tag{5-123}$$

The autocorrelation sequence, $\lambda(k) = E\{n(n)\,n(n+k)\} = \langle n(n)\,n(n+k) \rangle$, of the total channel noise, $n(n) = j(n) + w(n)$, is given by

$$\lambda(k) = \begin{cases} \sigma_w^2 + \sigma_c^2 , & k=0 \\ \dfrac{N-|k|}{N}\,\sigma_c^2 , & 1 \le |k| < N \\ 0 , & k \ge N \end{cases} \tag{5-124}$$

Finally, the covariance matrix for the total channel noise is given by

$$\Lambda = \begin{bmatrix} \lambda(0) & \lambda(1) & \lambda(2) & \cdots & \lambda(p-1) \\ \lambda(1) & \lambda(0) & \lambda(1) & \cdots & \lambda(p-2) \\ \lambda(2) & \lambda(1) & \lambda(0) & \cdots & \lambda(p-3) \\ \vdots & & & \ddots & \vdots \\ \lambda(p-1) & \lambda(p-2) & \lambda(p-3) & \cdots & \lambda(0) \end{bmatrix} \tag{5-125}$$

where *p* is the number of received samples processed by the LO processor per signal period.

LO Processing with Memory

Colored Gaussian Noise Scenario

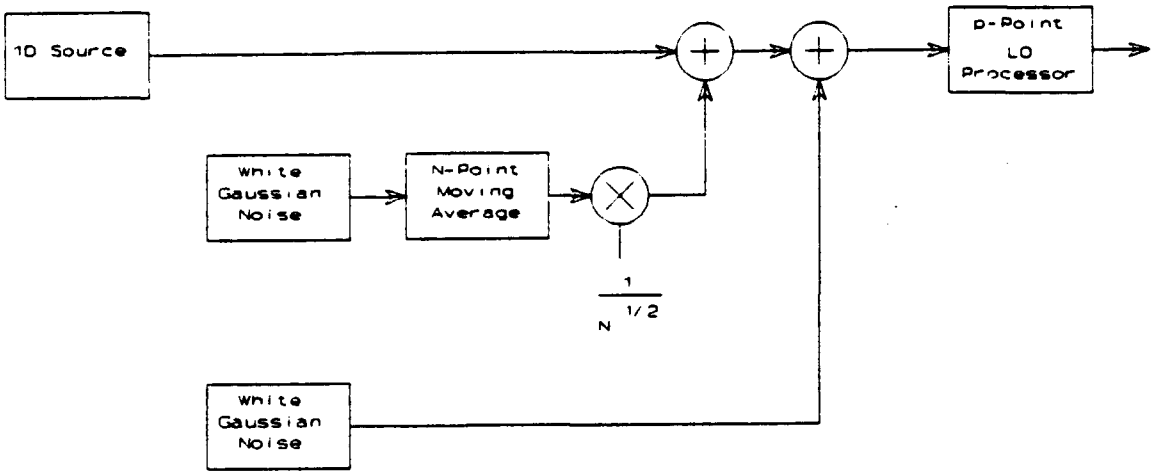

Figure (5-1)

Since the total channel noise is the sum of two zero mean Gaussian noise processes, its PDF is also Gaussian and is given by

$$f_n(\vec{n}) = \frac{1}{(2\pi)^{p/2}\,|\Lambda|^{-1/2}}\, e^{-\frac{1}{2}\vec{n}^T\Lambda^{-1}\vec{n}} \qquad \textbf{(5-126)}$$

where $\vec{n}=[n_1\ n_2\ \ldots\ n_p]^T$. Thus, the nonlinearity at the ith instant, g_i, is given by

$$g_i = -\frac{\partial}{\partial n_i}\ln(f_n(\vec{n})) = \vec{n}^T\Lambda^{-1}\vec{e}_i \qquad \textbf{(5-127)}$$

where $\vec{e}_i$ is a vector of length p whose elements are all zero except for the ith element which is equal to one. Recalling that for 1D signalling the gain of the LO processor relative to a linear receiver, G_{TAP}, is given by

$$G_{TAP} = k\sigma_n^2 \tag{5-128}$$

where $k = \frac{K_m^2}{K_v}$, K_m and K_v are given by Eqs. (5-32) and (5-35), $\sigma_n^2 = \sigma_c^2 + \sigma_w^2$ in this scenario, and that for the LO receiver $\hat{g}_i = g_i$. Thus, the value of k for the LO receiver may be computed as

$$k = \frac{1}{p}\sum_{i=1}^{p} < g_i^2 > \tag{5-129}$$

Substituting Eq. (5-127) into Eq. (5-129), and noting that $< \overline{n}\ \overline{n}^T > = \Lambda$, yields the following result for k:

$$k = \frac{1}{p}\sum_{i=1}^{p} \overline{e_i}^T \Lambda^{-1} \overline{e_i} \tag{5-130}$$

Finally, the expression for G_{TAP} is given by

$$G_{TAP} = \frac{\sigma_n^2}{p}\sum_{i=1}^{p} \overline{e_i}^T \Lambda^{-1} \overline{e_i} \tag{5-131}$$

Figures (5-2) to (5-5) illustrate the resulting values of G_{TAP} in relation to the LO processor length, p, and the length of the colored Gaussian MA process, N, for $\sigma_c^2 = \sigma_w^2 = 1$, $\sigma_c^2 = 10\sigma_w^2 = 10$, $\sigma_c^2 = 100\sigma_w^2 = 100$, and $\sigma_c^2 = 1000\sigma_w^2 = 1000$, respectively. As may be seen, the gain of the LO processor increases as its length increases. It is shown in [Drap89] that as the LO processor length increases, the gain relative to a standard linear receiver approaches that of the optimal filter for this scenario, the Wiener filter. Furthermore, for a given LO processor length, the gain increases as the value of N increases. This indicates that the LO processor is better able to remove the effects of the colored Gaussian noise as adjacent samples become more correlated.

In comparing the results shown in Figs. (5-2) through (5-5) to those in [Drap89] (see Figs. 2-8 to 2-11 on pp. 2-33 to 2-36), it was noticed that the results were not identical. The reason for this discrepancy is that the results in [Drap89] were generated using the assumption that since the channel noise process was stationary, the value for k could be calculated using just one g_i, i.e. using the equation

$$k = \langle g_i^2 \rangle \tag{5-132}$$

for any i. However, as discussed in Sections 5.1.2 and 5.2.3, stationarity is not a sufficient condition to ensure that $\langle g_i^2 \rangle = \langle g_j^2 \rangle$ for all i and j. Instead, the PDF of the channel noise must be spherically symmetric, which is not the case in this scenario. To show that stationarity is not a sufficient condition to give the result in Eq. (5-132), the values of G_{TAP} in relation to p and N were plotted for the case of $\sigma_c^2 = 100\sigma_w^2 = 100$ using Eq. (5-132) with $i=1$. The results of this experiment are shown in Fig. (5-6) and are almost identical to the results presented in [Drap89] [11]. It may be observed that Figs. (5-6) and (5-4) are not the same, but should be if stationarity is sufficient to ensure the validity of Eq. (5-132). Thus, stationarity is not a sufficient condition to warrant the simplification of the expression for k given in Eq. (5-129) to that given in Eq. (5-132).

[11] There are some slight differences in the plot shown in Fig. (5-6) and that of Fig. 2-10 of [Drap89]. These differences are most likely a result of differences in the resolution of the computer software used to generate and plot the results.

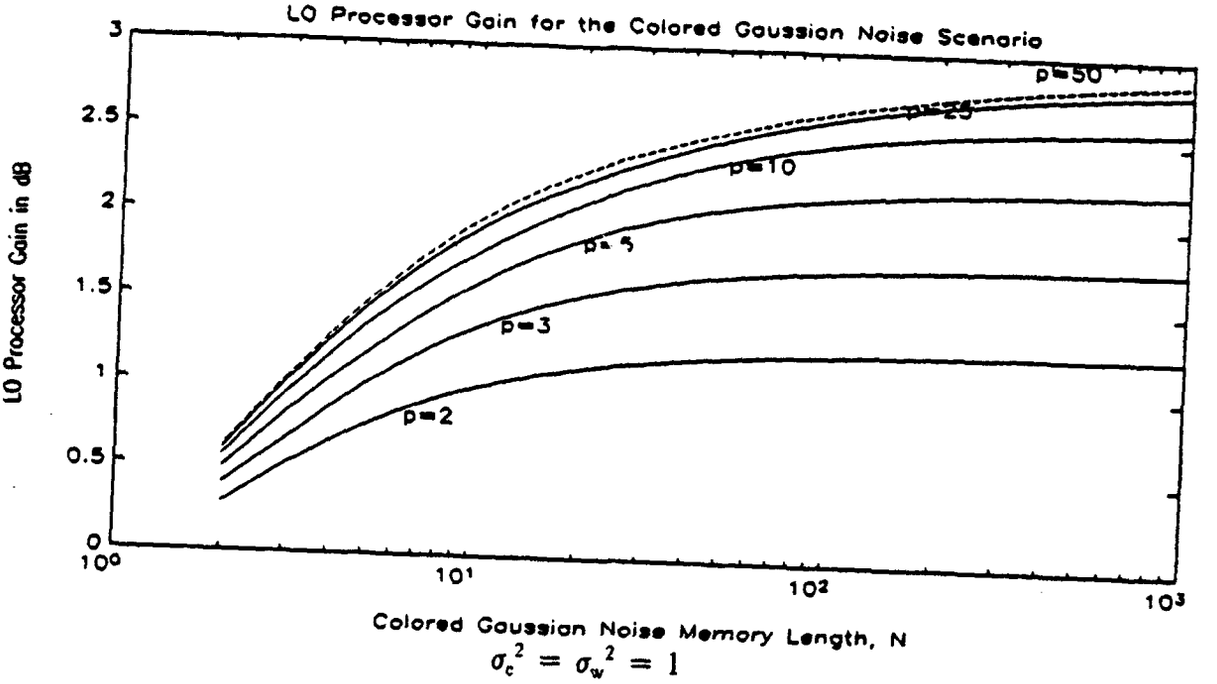

$\sigma_c^2 = \sigma_w^2 = 1$

Figure (5-2)

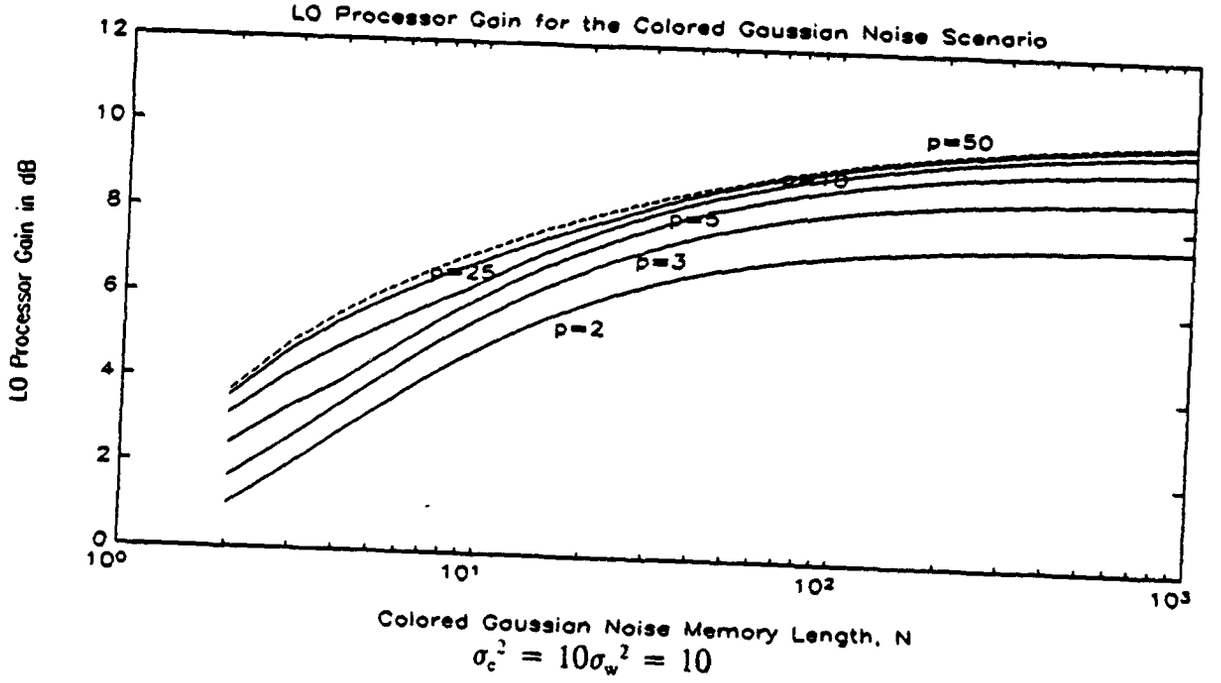

$\sigma_c^2 = 10\sigma_w^2 = 10$

Figure (5-3)

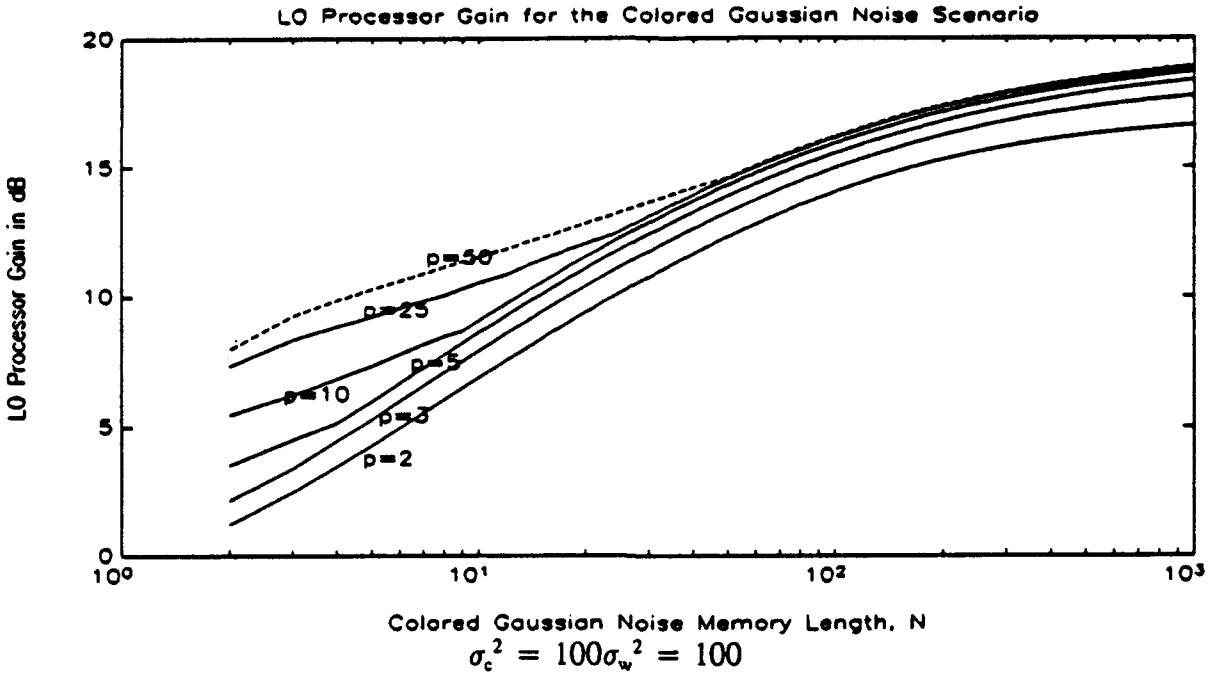

$\sigma_c^2 = 100\sigma_w^2 = 100$

Figure (5-4)

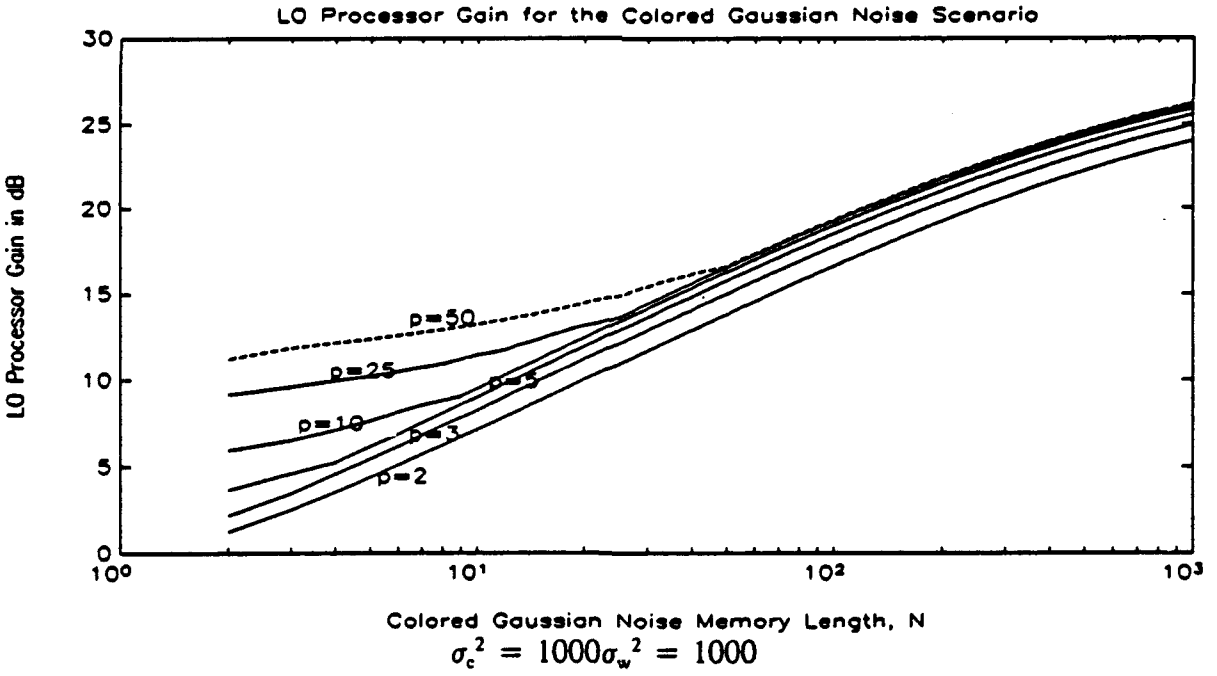

$\sigma_c^2 = 1000\sigma_w^2 = 1000$

Figure (5-5)

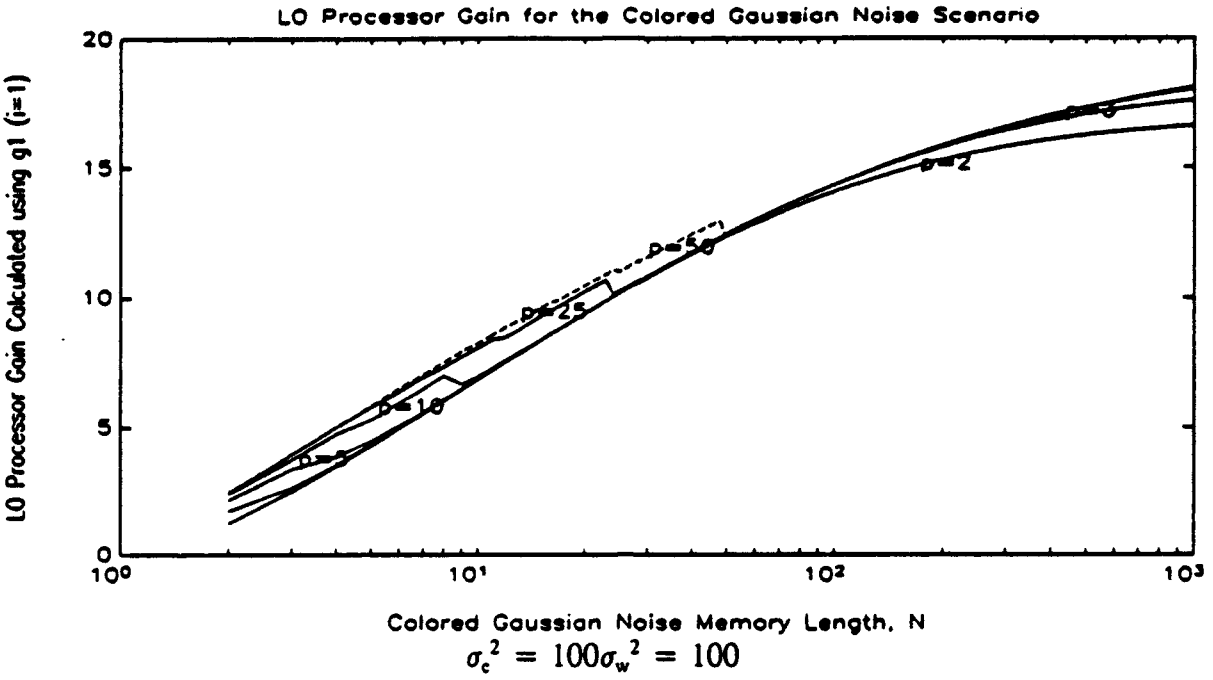

$\sigma_c^2 = 100\sigma_w^2 = 100$

Figure (5-6)

6. FUTURE OBJECTIVES

While the work presented herein provides an assortment of clues into the fundamental behavior of the LO processor, there is still much research to be done in this area. Previous sections of this report addressed the memoryless LO processor and the many algorithms used to implement it. Software simulation is the method of choice for characterizing the performance of this processor. Two simulations were presented which provided a means of investigating the P_b of the memoryless LO processor in a variety of jamming environments. The LO processor with memory was also discussed, with an emphasis placed on its derivation and the development of the theoretical expressions for the output SNR and gain relative to a linear receiver. A number of logical extensions of the research presented in this report may be identified. Some of these include:

- Simulation of the LO processor with memory and its incorporation into the QPSK DSSS system. By comparing the results of this simulation to the memoryless LO processor results, the performance enhancement gained through the use of memory can be quantified.

- Investigation of other modulation techniques, particularly Continuous Phase Frequency Shift Keying (CPFSK) [Leib93], a form of Minimum Shift Keying (MSK), and their effects on the performance of the LO processor.

- Simulation of the parametric implementation of the FSA algorithm. All of the LO processor implementation methods mentioned in this report employ a histogram approximation of the received signal PDF at some point in their respective algorithms. Since it was seen that all the methods had roughly the same performance results, one may conclude that the histogram is the limiting factor. By examining the parametric implementation of the FSA algorithm, it may be possible to determine if this hypothesis

is true, or if the method of LO processor implementation has relatively little effect on its overall performance.

- Adaptation of the Continuous Polynomial Approximation (CPA) algorithm [Grim93] for use as an LO processor implementation method. Through simulation the performance of this algorithm can be compared to the other methods (Histogram, EBH, FSA, and MIPA) previously discussed.

LO processing is a rich area of study. Intuitively, the LO processor with memory should be more robust than the memoryless processor and thus able to mitigate a wide array of different jammer types, including those for which the memoryless LO processor performed poorly. Also, whether or not different LO processor implementation algorithms have a strong influence on overall performance remains to be seen. The work presented in this report, along with the future tasks mentioned in this section, will lead to the definition of a communications system that is robust and able to provide a secure and reliable information exchange in a multitude of interference scenarios.

REFERENCES

[Comd91] Comdisco Systems, Inc., SPW Version 2.8 User's Guide, May 1991.

* [Drap85] Charles Stark Draper Laboratories, Inc. Report No. CSDL-R-1787, Digital Density Detector (D^3) Development Program, RADC Contract No. F30602-83-K-0160, RADC-TR-85-218, Nov 85, ADB100046.

* [Drap89] Charles Stark Draper Laboratories, Inc. Report No. CSDL-R-2167, Robust Digital Adaptive Transceiver (RDAT), RADC Contract No. F30602-87-C-0149, RADC-TR-89-332, Feb 90, ADB141829L.

[Grim93] Grimm, Jimm H. et. al., "Continuous Polynomial Approximation", to be published in *Proceedings of MILCOM '93*, October 1993.

* [Haze88] Hazeltine Report No. 6662, Adaptive Nonlinear Coherent Processor Design, Vols. I and II, RADC Contract No. F30602-86-C-0106, RADC-TR-89-387, Mar 90, Vol I - ADB142874L and Vol II - ADB142875L.

[Higb88] Higbie, J.H., "Adaptive Nonlinear Suppression of Interference," *IEEE Proceedings of MILCOM '88*, October 1988.

[Illi91] Illinois Institute of Technology Report, Continuation Study of a Communications Receiver for Spread Spectrum Signals, RADC Contract No. F49620-88-C-0053/SB5881-0378, January 31, 1991.

* [Illi93] Illinois Institute of Technology Report, A Spread Spectrum Communications Receiver with Nonlinear Processing, RL Contract No. F30602-91-C-0059, RL-TR-93-50, May 93, ADB174588.

[Krey88] Kreyszig, E., Advanced Engineering Mathematics, Sixth Edition, John Wiley & Sons, Inc., 1988.

[Leib93] Leib, Harry and Pasupathy, Subbarayan, "Error-Control Properties of Minimum Shift Keying," *IEEE Communications Magazine*, January 1993.

[Mels78] Melsa, James L. and Cohn, David L., Decision and Estimation Theory, McGraw-Hill, 1978.

[Midd66] Middleton, D., "Canonically Optimum Threshold Detection," *IEEE Transactions on Information Theory*, Vol. IT-12, No. 2, April 1966, pp. 230-243.

[Spau85] Spaulding, A.D., "Locally Optimum and Suboptimum Detector Performance in a Non-Gaussian Interference Environment," *IEEE Transactions on Communications*, VOL. COM-33, No. 6, June 1985, pp. 509-517.

[VanT68] Van Trees, H.L., Detection, Estimation and Modulation Theory, Part I, John Wiley and Sons, 1968.

[Woze65] Wozencraft, J. M. and Jacobs, I. M., Principles of Communication Engineering, John Wiley & Sons, Inc., 1965.